Aus dem
Max-Planck-Institut für Herz- und Lungenforschung, Bad Nauheim
am Fachbereich Biologie und Chemie
der Justus-Liebig-Universität Gießen

The role of pulmonary fibroblast subtypes in lung development.

Inaugural-Dissertation

zur Erlangung des Grades Doktor der Naturwissenschaften
-Dr. rer. nat.-
der naturwissenschaftlichen Fachbereiche (Fachbereich 08 Biologie und Chemie)
der Justus-Liebig-Universität Gießen
vorgelegt von
Dipl.-Biol. Aglaia Ntokou
aus Thessaloniki, Griechenland

Gießen 2017

Die vorliegende Arbeit wurde im Rahmen des Graduiertenkollegs Molecular Biology and Medicine of the Lung (MBML) am Max-Planck-Institut für Herz- und Lungenforschung in Bad Nauheim in der Zeit von Oktober 2013 bis December 2016 unter der Leitung von Prof. Dr. Adriaan Dorresteijn angefertigt. Das Thema und das Labor wurden von Prof. Dr. med. Werner Seeger bereitgestellt, unter dessen Betreuung diese Arbeit entstand.

Table of Contents

1 Introduction

1.1 Anatomy and physiology of the lung

The lung is a large organ in the human body, responsible for gas exchange and providing oxygen in the circulating blood for metabolic reactions. It was as early as in the Devonian Period (416 million to 359 million years ago) when, for the first time, spongy ventricle forms started appearing in Rhipidistian fishes, the ancestors of tetrapods. Moving from the aquatic environment to land, many changes took place in the respiratory system. Most essential for survival in the atmosphere of the Earth atmosphere was the loss of gills and the development of lungs, when lung formations became the dominant organs of respiration (30).

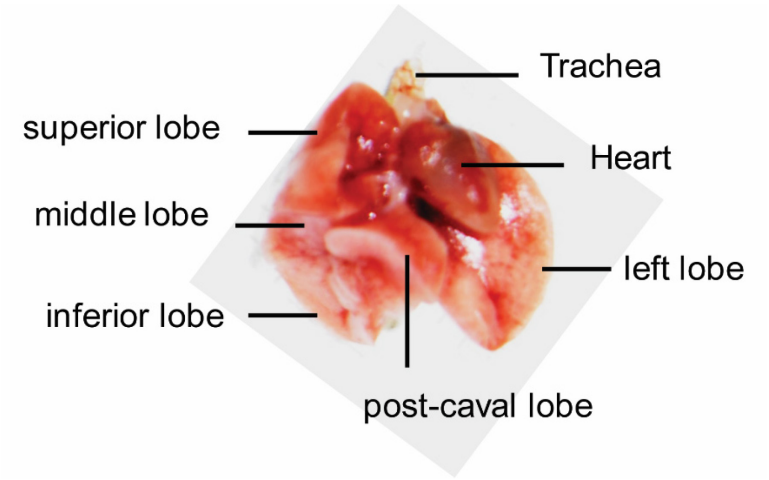

Figure 1 Anatomical compartments of the mouse lung.

Mouse lungs consist of right and left wings and five lobes; the superior, the middle, the inferior, the post-caval at the right wing and the left lobe being the only lobe of the left wing. Image of a wild type mouse (C57Bl/6) lung, at post-natal day 14, adapted from (23).

The particular structure of the lung is variable among vertebrates, and the position of the lung, which is along the anterior limb, ventral to the esophagus and between the thyroid gland and the stomach, is conserved (59). Mammalian lungs are embedded in the thoracic cavity as a sac-like organ, and are located above the diaphragm. The lung is separated from the thorax by the pleura and the pleural cavity (76). A pair of typical mammalian lungs consists of a right and a left lung wing (*pulmo dexter* and *pulmo sinister*) that are further divided into asymmetrically-arranged lung lobes (59, 116). Despite that both human and mouse lungs have five lobes in total, the arrangement at the left and the right lungs are not

the same. Human right lung wings consist of three lobes, the *superior,* the *medius*, and the *inferior*; and the left lung wings consist of the *lobus superior* and *lobus inferior*. The mouse lung, however, has four right wing lobes (*superior*, *middle*, *inferior* and *post-caval*) and the left wing has a single lobe (23) (Figure 1).

The respiratory structures can be separated into two general zones; the conducting zone that includes structures such as the nose, pharynx, larynx, trachea and bronchial tree and the respiratory zone that includes tissues contributing directly to gas exchange. The terminal bronchioles mark the beginning of the respiratory zone, followed by alveolar ducts that end in alveolar sacs (Figure 2A).

Alveolar ducts are the pipes formed by connective tissue, airway epithelial cells (peripheral squamous cells and proximal cuboidal cells), smooth muscle cells and extracellular matrix (ECM) leading to an alveoli cluster, the alveolar sac (23, 112). The smallest unit of respiration is the alveolus, which is where gas exchange takes place (112). The principal cells of the alveolar wall are type I cells that are highly permeable to gases, type II cells that secrete pulmonary surfactant (phospholipid rich substance that minimizes surface tension) and alveolar macrophages that remove pathogens in the alveoli (Figure 2B).

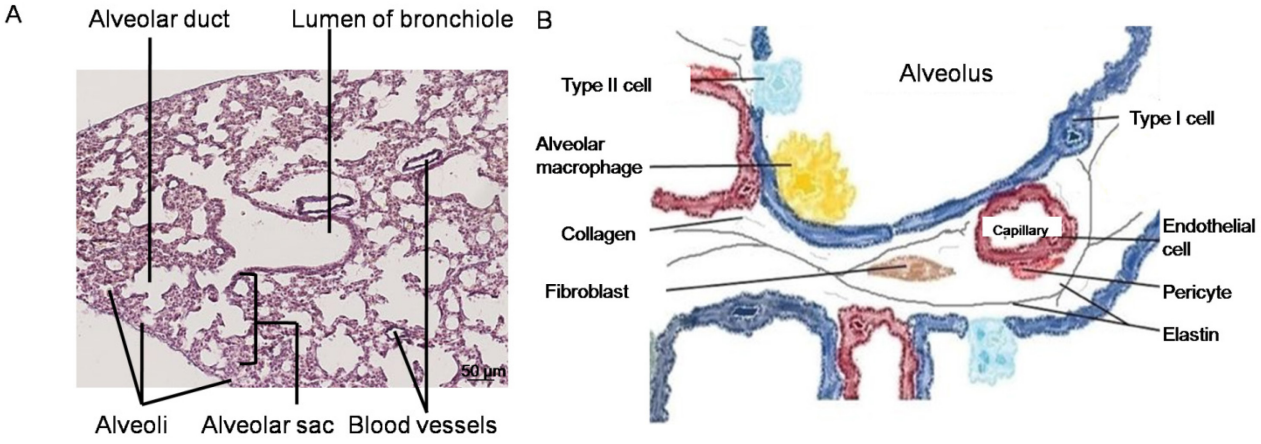

Figure 2 Respiratory structures.

(A) Structural compartments of the lung in histological section. Image of a wild type mouse (C57Bl/6), at post-natal day 14, indications as adapted from adapted from (114). (B) The principal structure of respiration, the alveolus, consists of type I and type II cells, fibroblasts, epithelial cells, as well as macrophages, adapted from (8).

1.2 Lung development in the pre-and post-natal periods

In human embryos, the lung starts developing with the tracheal bud, around the first 5-7 weeks after the zygote has formed and is completed in late childhood. The developmental stages are divided as pre- or postnatal and are defined by the structural changes occurring at each time-point (63). As depicted in Figure 3, the first steps of lung development are prenatal both in human and mouse, but alveolarization starts only postnatally in mice, suggesting that mice are ideal candidates for studies on the alveolar formation and associated diseases (63).

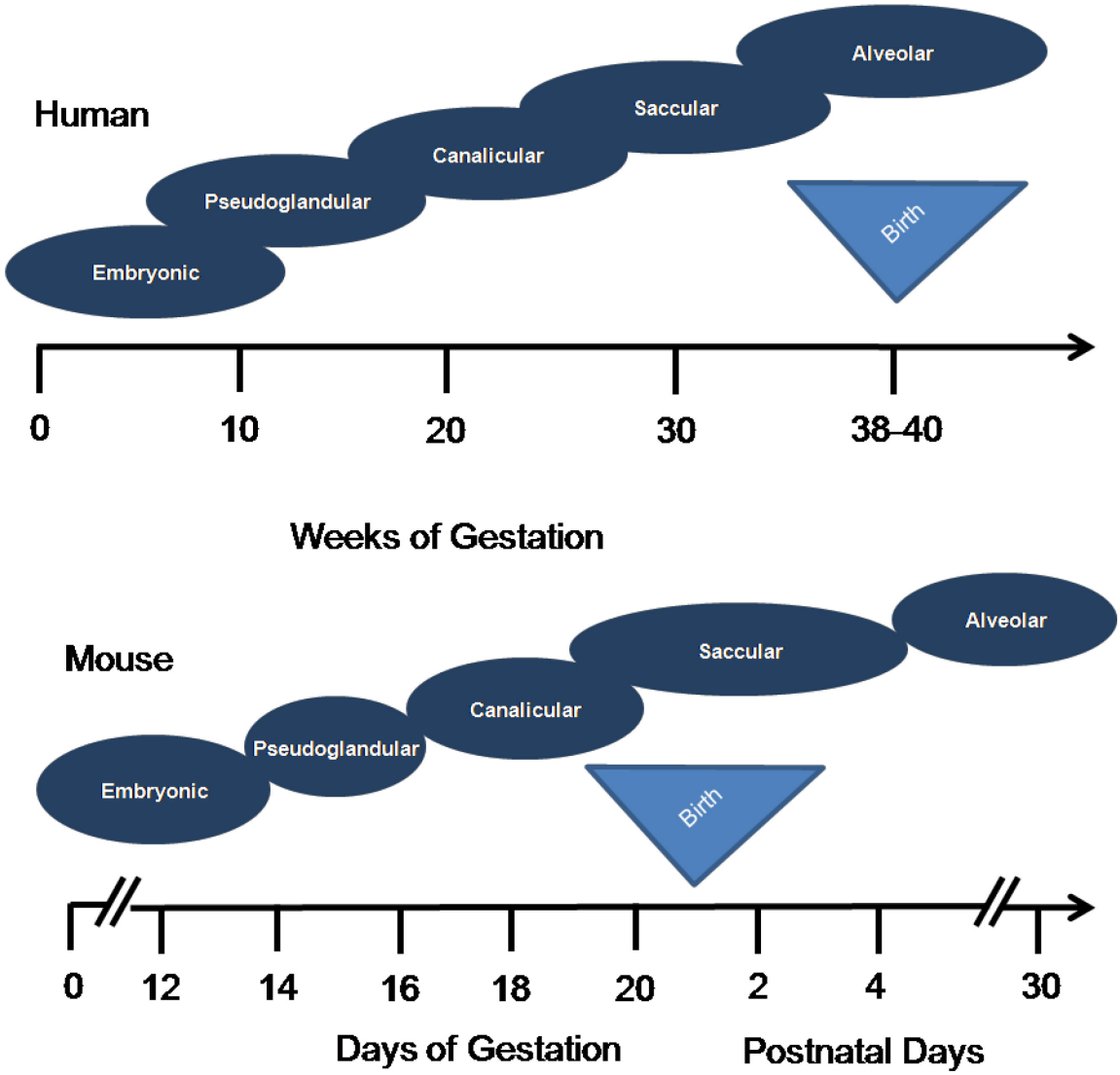

Figure 3 Lung development stages in human and mouse.
Developmental correspondence between human and mouse lung, adapted from (49, 77).

The different stages of prenatal lung development are named and defined by structural changes that take place during this period. The embryonic stage of lung development (1-7 weeks human, 1-14 days in mouse) is when most of the organs are formed, and in human, the lung becomes more evident around the fourth week, when five saccular structures that will later form the five lobes can be observed (23). Early lung development requires epithelial-mesenchymal interactions. When the endodermal epithelium forms the gut, it produces the diverticula, which, after interactions with the subtending mesenchyme, will form the thyroid, liver, pancreas, and lung. It has been already shown 80 years ago in birds and shortly after that in mammals, that the mesenchyme is crucial for lung branching morphogenesis (90, 97).

At week 5-17 (14-16 days in the mouse) the lung enters the pseudoglanular stage, when subdivision of the lung into segments and lobules occurs. In this stage, the formation of the premature gas exchange regions occurs, with alveolar type I and type II cells, that are now differentiated, constituting the epithelial component of the alveoli (48, 93, 112, 113). Type I cells, covering most of the peripheral lung surface (roughly 95%), are very thin cells that connect with pulmonary capillaries and serve as the site of gas exchange (115). The canalicular stage starts at 16-26 weeks in human (16-20 days in the mouse), when many canals are formed in the developing lung parenchyma. The differentiation of type I and type II cells takes place during this time, and pulmonary fibroblasts that interact with the epithelium drive the differentiation of the type II cells (62, 96). The importance of type II cells is underlined by an ability to synthesize, store, release, and recycle the pulmonary surfactant lipoprotein (51, 117) that allows the low surface tension at the air-liquid interface. The physiological importance of pulmonary surfactant's surface tension-lowering properties is shown by the lethality of neonatal respiratory distress syndrome, which is caused by a lack of surfactant in premature human newborns (7).

The saccular or terminal sac stage is defined by widening and lengthening of air spaces called saccules and takes place from week 24 until birth. From the terminal sacs, the alveolar ducts and later the alveoli will arise (23).

The postnatal period is when 85% of alveoli are formed in human lungs (16). In mice, this process happens entirely postnatally, since neonatal mice are in the saccular stage at the time of birth (16). Parenchyma, composed of a double layer of capillaries, forms the primary septa between the sacculi. Small elevations of the saccular wall divide the luminal area. Alveoli are now formed, and the inter-alveolar walls are the secondary septa, with two characteristic regions, the base and the tip of the septum where elastin deposition occurs (108). Alveolarization is closely linked to the deposition of elastin in

the saccular walls meanwhile connective tissue is the central part of the septum. Lung septation is not well understood but there is evidence for several factors that orchestrate lung development. Hepatocyte growth factor (HGF) (79), fibroblast growth factor (FGF) (27, 78, 80), vascular endothelial growth factor (VEGF) (13) and platelet derived growth factor (PDGF) (5, 15) play a role in lung development. Fibroblasts are key players during alveolar septation, since they are the source of ECM and fibroblast malfunction could lead to several diseases that impact lung structure (105).

Microvascular maturation is the final stage of lung development, and occurs over the first 2-3 years in humans, and from postnatal day (P)14 until P30 in mice (19). The double-layered capillary network transforms into the single-layer network, which is the final form found in adult lungs (3, 73).

1.3 Pulmonary fibroblasts

For more than thirty years, fibroblasts have been under continual study in the lung, and their role in pulmonary development, differentiation and diseases has been a constant area of interest for scientists and clinicians (20, 66-68, 85, 87). There have been described three distinguishable fibroblast subsets in lung; platelet derived growth factor receptor-α^+ (PDGFRα^+) fibroblasts, lipofibroblasts and myofibroblasts (81).

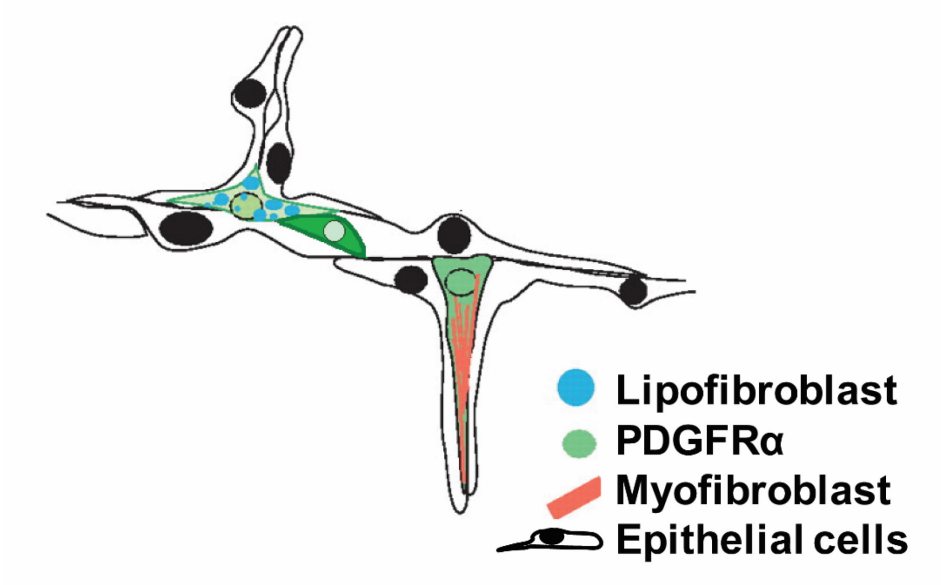

Figure 4 Fibroblast subtypes

Alveolar septum with the three fibroblast subtypes, adapted from (81). All three different fibroblast subtypes express PDGFRα; lipofibroblasts, myofibroblasts and PDGFRα^+ fibroblasts.

1.3.1 PDGFRα$^+$ fibroblasts

PDGFs are a group of dimeric ligands that bind to tyrosine kinase receptors, and after dimerization, they transmit intracellular signals. Four ligands form homo- and hetero-dimers; A, B, C, D and are recognized by two different receptors; PDGFRα and PDGFRβ (5). *In vivo* there is functional evidence for interactions of PDGFAA and PDGFCC via PDGFRα, and PDGFBB via PDGFRβ (38, 100). Activation of the receptors stimulates cell growth, but also causes changes in the form and mobility of cells (6). There are some general expression patterns, such as expression of PDGFB principally in vascular endothelial cells, megakaryocytes, and neurons, and of PDGFA and PDGFC in epithelial cells, muscle, and neuronal progenitors, while PDGFD has been observed in fibroblasts (5). Mesenchymal cells express PDGFRα and PDGFRβ, but PDGFRα is expressed strongly in subtypes of mesenchymal progenitors in lung, skin, and intestine and oligodendrocyte progenitors (5). Meanwhile PDGFRβ is mostly expressed in vascular smooth muscle cells (SMCs) and pericytes (5).

Knock-out studies have revealed that PDGFA is important for the correct differentiation of myofibroblasts and secondary septation (12, 15). The correct interaction between receptor and ligand is essential for the proliferation and the survival of PDGFRα$^+$ cells that will differentiate to alveolar myofibroblasts (15). Disruption of the differentiation signaling at early stages leads to structural disorders of the lung (1, 5, 14, 15). In mice lipid laden PDGFRα$^+$ cells are found at the base of the septum between P4 and P8 and some PDGFRα$^+$ cells expressing α smooth muscle actin (SMA) at the alveolar entrance before deposition of elastic fibers (56). From P12 and on there is a decrease in the size of PDGFRα$^+$ cells population underlined by an increase in apoptosis and a decrease in proliferation of PDGFRα$^+$ cells resulting in thinner alveoli and single layered capillaries that mark the end of alveolarization (64).

1.3.2 Pulmonary Lipofibroblasts

Pulmonary lipofibroblasts represent an interstitial mesenchymal cell population first described in the 1970s by O'Hare (76) and later called interstitial lipid cells (or lipid droplet–laden cells) due to characteristic intracellular lipid droplets (66). Lipofibroblasts are mostly found at the base of the septum. The difference between lipofibroblasts and other interstitial cells containing contractile filaments is the positivity for Thy-1 or CD90 (69). CD90 belongs to a set of markers for mesenchymal stem cells (MSCs) including CD44, CD105, CD73 and CD146 (107). CD90 has been demonstrated to be involved in

lipofibroblast differentiation and to control esterification via peroxisome proliferator-activated receptor-γ (PPAR-γ) (109). *In vitro* studies have revealed two fibroblast groups depending on the CD90 expression. Fibroblasts lacking CD90 have a round, spread phenotype. After stimulation with PPAR-γ agonists, these $CD90^+$ fibroblasts can turn into lipofibroblasts. It was later shown in rats that this is due to transforming growth factor (TGF)-β signaling (119). On the other hand, $CD90^-$ cells with a spindle shape and filopodia did not have this capacity (50, 66, 109) and as shown by Sander et al., these cells differentiate into myofibroblasts (91). The importance of Thy-I has been later shown in *in vivo* studies, where its reduction inhibits normal alveolar development (74).

The abundance of lipofibroblasts has been studied in rodents, and reaches a peak around P7 but declines towards the end of alveolarization (61, 108). Lipofibroblasts contribute to the differentiation of the epithelial cells to type II cells, and provide triglycerides for the production of surfactant, and, therefore, are crucial contributors to early lung development and adult lung repair (66, 88, 101, 102). The mesenchymal-epithelial crosstalk takes place due to type II cells and lipofibroblasts. Type II cells secrete parathyroid hormone-related protein (PTHrP) that is recognized by PTHrP-receptors in lipofibroblasts, which in turn secrete leptin, which is recognized by type II cells (103). This interaction up-regulates the gene product of the Perilipin2 (*Plin2*) gene, adipose differentiation-related protein (ADRP), an amphiphilic protein coating lipid storage droplets. The ADRP is a lipid storage droplet coating protein that allows triglyceride uptake by lipofibroblast and alveolar type II cells (28, 57, 88, 92, 109). Another molecule produced by lipofibroblasts, retinoic acid (RA), which is generated before the maximal level of elastin production during alveolarization, suggesting an important role for these fibroblast subtypes in development (65).

1.3.3 Myofibroblasts

The last fibroblast subtype described here, the myofibroblast, has taken its name due to the expression of contractile filaments such as αSMA thus myofibroblasts are often called αSMA^+ fibroblasts (24, 95). Myofibroblasts are also characterized by the expression of intermediate filaments, such as vimentin, non-muscle myosin (NNM) and smooth muscle myosin heavy chain isoform 1 (SM-MHC or SM1) (40). Myofibroblasts are related to extracellular matrix (ECM) synthesis, for fiber-related tension in the lung (33, 53) and are crucially involved in the secondary septation during development (15). Myofibroblast differentiation and activation can be induced by signaling from inflammatory cells, mechanical stress or TGF-β (25, 39-41). Being the principal cell for ECM production, where the ECM consists largely of

elastin and collagen, myofibroblasts give the elastic properties to the lung and preserve the alveoli during normal respiration. During development, elastin and collagen fibers contribute to primary and secondary septation, by contributing to the elongation of terminal air sacs (18).

Myofibroblasts are most abundant in early life stages and are almost absent in the healthy adult lung (41, 118) but proliferate in interstitial pulmonary fibrosis (IPF), producing excessive amounts of ECM resulting in thicker alveolar walls and subsequently decreased epithelial-endothelial gas exchange and lung compliance (52).

1.4 Diseases that impact the lung structure

The main role of the lung is a proper gas exchange that is facilitated by a large number of alveoli and a thin blood-air barrier. Destruction or blockade of these two structural features leads to currently untreatable diseases such as chronic obstructive pulmonary disease (COPD) in adults (22) and bronchopulmonary dysplasia (BPD) in neonates (58, 94), as well as lung fibrosis (47). These malformations lead to compromised breathing and respiratory failure in affected patients.

Lung fibrosis occurs with alveolar epithelium damage, alveolar inflammatory reactions and a dramatic proliferation of fibroblasts. Therefore, the vessels and capillaries are lost, and the lung structure is damaged. Gas exchange is restricted by increased deposition of connective tissue between the alveoli and the blood vessels, and lung transplantation was the only treatment option available (11) until recently, when pirfenidone application was introduced (9, 11, 42).

An arrest of alveolarization, simplified alveolar structures, and a dysmorphic pulmonary circulation are the hallmarks of BPD, which has a high morbidity and mortality in neonates, and survivors face long-term respiration problems to adulthood (58). No adequate treatment and management options are currently available for the management of BPD patients (76).

The major problem in the treatment of the diseases mentioned above arises from the fact that the mechanisms of alveolar generation and damage are not understood. Revealing the pathways involved in pathological conditions, and enabling lung tissue to regenerate or repair by pinpointing key players in these processes is a desirable strategy for treatment. Lung fibroblasts represent a prominent group of mediators in alveolarization and repair (28).

1.5 Mouse models

To investigate pulmonary diseases, transgenic animals and particularly mice are used as model organisms, since the 1980s (2). The mouse genome is highly similar to the human genome and mice have a short generation time, two features that make mice good experimental animals (98). Genetically modified organisms have genomic modifications such as the introduction of a foreign gene (knock-in) or gene replacement (knock-out). These changes affect the animal phenotype in a manner that allows the investigator to conclude about the properties and function of the locus of interest in the tissue/cell of interest.

In the Cre/loxP recombination system, the enzyme Cre-recombinase originates from the bacteriophage P1 (2) and can excise DNA sections flanked by loxP sequences and reconnect the remaining DNA. The exact orientation and localization of the loxP sites determine whether Cre-recombinase will delete, invert or translocate the gene of interest. Usually mice lines are created separately carrying either Cre or loxP sites and are crossed for experimentation resulting in a Cre/loxP line (72).

Recombination can be additionally controlled in a time- or site-specific manner, where Cre is placed under the control of a cell-type-specific promoter and introduced into the mouse genome. When this mouse line is crossed with another line carrying loxP sites, a conditional knockout is obtained in the particular tissue/cell-type. Even though constitutive Cre expression is a useful tool, there is the chance that the recombination leads to a lethal phenotype if the promoter regulating Cre is already active from the embryonic stages, and this could prevent experimentation at postnatal time-points. Since 2001, a transgenic mouse tool has been available, in which Cre-recombinase is fused with a modified ligand-binding domain of the estrogen receptor (ER). This tool allows temporal-regulation of the recombination, when synthetic tamoxifen binds to ER to induce Cre-recombinase translocation into the nucleus and further DNA recombination. (31, 70).

In this study the Cre/stop loxP system has been used. In the stop loxp system two transgenic lines are crossed; one, carrying the Cre-recombinase gene (either inducible or constitutive) after the cell specific promoter and one carrying a stop codon before a reporter gene. In the offspring of these crossed lines, Cre-recombinase that was expressed in the specific cell type, can excise the stop codon, allowing the reporter gene that follows to be expressed (Figure 5A). In the case of inducible Cre-recombinase lines, this is accomplished in a temporally-controlled manner after tamoxifen administration. A similar system that has been used as well here is the diphtheria toxin fragment A (DTA) activation system (Figure 5B).

In this, the stop codon is found before a DTA gene, thus after the expression of diphtheria toxin, cell specific depletion can be achieved.

For reporter gene activation, a fluorochrome expressing gene is inserted (knock-in) after the gene of interest and cells are labeled with that color allowing visualization of specific cell types (Figure 5C).

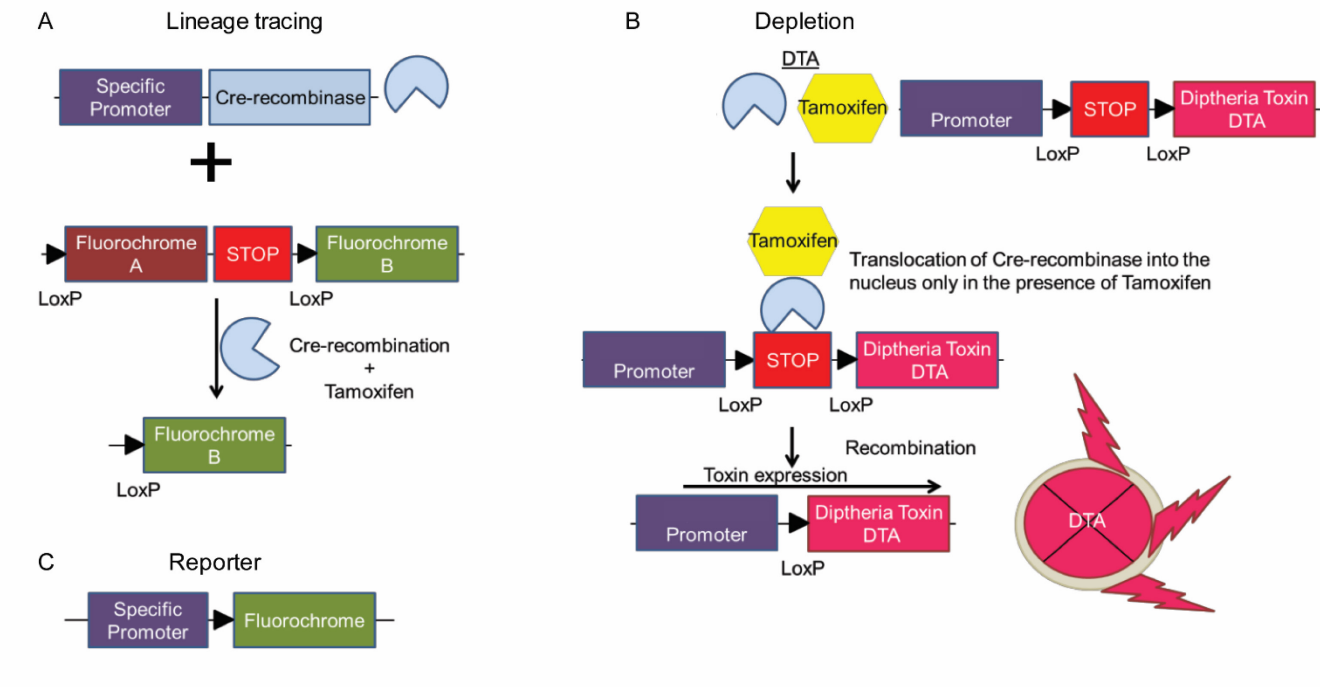

Figure 5 Schematic modeling of the genetic modifications used to label and deplete cell-types.

A. In the stoplox system, a stop codon is located upstream of a fluorochrome. To better control the system there is sometimes another fluorochrome that is constantly expressed in all cell types. When Cre-recombinase is expressed in a specific cell type, it excites the constantly expressed fluorochrome gene and the stop codon, and the other fluorochrome is expressed in the cell type of interest. B. The diphtheria toxin A (DTA) system is similar to the stoplox, but instead of a fluorochrome, DTA is expressed and is depleting the cell type of interest. C. In the simple reporter system, a fluorochrome is expressed under the same promoter of the gene of interest.

1.6 Aims

Induction of alveolarization in the diseased lung represents a desirable new therapeutic approach for structural lung diseases such as COPD, Fibrosis, and BPD. Fibroblast subtypes such as PDGFRα^{+} fibroblasts and lipofibroblasts critically impact on lung development and particularly on the new formation of alveoli, the process of alveolarization. Understanding fibroblast differentiation (lineage specification) and cell type specific function during lung development will provide cellular candidates driving alveolarization and possible target candidates for the development of new therapeutic concepts for pulmonary diseases.

Aims

The present study aimed:

1) To provide new insights into the role of fibroblast subtypes such as PDGFRα^{+} fibroblasts and lipofibroblasts during lung development with special emphasis on alveolarization. Using transgenic mice and knock in mice containing reporter genes (GFP, mCherry) or tools of the CreERT2 loxP system, lineage tracing and cell type specific depletion analysis will provide knowledge of localization, differentiation (lineage specification) and function of fibroblast subtypes during lung development.

2) Against this background, a recently generated mouse Cre-driver line to target lipofibroblasts (the Plin2$^{tm1.1(Cre/ERT2)Mort}$ line) will be characterized and validated if the line represents a valuable tool to target lipofibroblasts.

2 Materials and Methods

2.1 Materials

2.1.1 Devices

100-, 40-µm thick-cell strainers; BD Biosciences, USA

Autoclave; Systec, Germany

BD LSRII flow cytometers with DIVA software, BD Biosciences, USA

BD FACSAriaIII with DIVA Software, BD Biosciences, USA

Cell culture sterile working bench; Thermo Scientific, USA

Centrifuge; Thermo Scientific, USA

Coloring chamber; Roth, Germany

Confocal microscope; Zeiss, Germany

Counting chamber; Marienfeld, Germany

Cytospin™ 4 Cytocentrifuge, Thermo Scientific, USA

Dako Pen Fat Pen; Dako, Denmark

gentleMACS™ Dissociator; MiltenyiBiotec, Germany

InoLab® pH meter; WTW, Germany

Leica automated microtome RM2255; Leica, Germany

Leica tissue embedding center EG1160; Leica, Germany

Leica tissue embedding system EG1150C; Leica, Germany

Leica microscope DM4000B; Leica, Germany

Leica tissue processor ASP200S; Leica, Germany

MicroAmp® FAST 96-well reaction plate; Applied Biosystems, USA

Microcentrifuge tubes: 0.5, 1.5, 2 ml; Eppendorf, Germany

Minispin® centrifuge; Eppendorf, Germany

Multifuge 3 S-R centrifuge; heraeus, Germany

NanoZoomer XR C12000 Digital slide scanner; Hamamatsu, Japan

NanoDrop® ND 1000; PeqLab, Germany

Photometer; Biorad, USA

Pipetboy; Eppendorf, Germany

Pipetmans: P10, P20, P100, P200, P1000; Gilson, France

Pipetman filter tips: 10, 20, 100, 200 and 1000 µl; Greiner Bio-One, Germany

Precellys 24 homogenizer; Peqlab, USA

Precision balance; Denver Instruments, USA

Scales; A&D, USA

Shakers; Heidolph, Germany

StepOnePlus™ Real-Time PCR system; Applied Biosystems, USA

Surgery instruments, F.S.T. Fine Science Tools, Germany

Test tubes: 15, 50 ml; Greiner Bio-One, Germany

Thermocycler; Biometra/Eppendorf, Germany

Vortex mixer; VWR, USA

Microtome LEICA SM 2500; Leica, Germany

2.1.2 Chemicals/Consumables

0.2 ml polypropylene 8-tube strips; GBO, Germany

1.4 mm Precellys ceramic beads kit; Peqlab, USA

1.5 ml and 2 ml reaction tubes; Eppendorf, Germany

2-Propanol; Merck, Germany

15 ml and 50 ml Falcon tubes; Greiner bio-one, Austria

Acetic acid; Roth, Germany

Aceton; Roth, Germany

Bovine serum albumin; PAA Laboratories GmbH, Austria

Collagenase-B; Roche, Switzerland

Goat serum; PAA Laboratories GmbH, Austria

DAPI; Sigma-Aldrich, Germany

Dispase; BD Biosciences, USA

DNase I; SERVA, Germany

dNTP mix; Promega, USA

Dulbecco's Modified Eagle Medium (DMEM); PAA Laboratories GmbH, Austria

EDTA-Solution; Thermo Scientific, USA

Eosin; Sigma-Aldrich, Germany

Eppendorf Mastercycler ep Gradient S thermal cycler; Eppendorf, Germany

Ethanol; Roth, Germany

Ethidium bromide solution 1% (v/v); Roth, Germany

Ethylene diamine tetraacetic acid (EDTA); Roth, Germany

Fuchsin; PanreacQuímica SLU, AppliChem GmbH, USA

FACS-Buffer; Affymetrix ebioscience, USA

Fetal calf serum; PAA Laboratories, Austria

Hematoxylin; Waldeck GmbH & Co. KG, Germany

HEPES; PAA Laboratories, Austria

High capacity reverse transcription Kit; Applied Biosystems, USA

Hydrochloric acid; Sigma-Aldrich, Germany

Isoflurane; CP-Pharma, Germany

Magnesium chloride; Sigma-Aldrich, Germany

Methanol; Fluka, Germany

Methylbutane; Roth, Germany

Microscope slides; Thermo Scientific, USA

Miglyol; Caesar & Loretz GmbH, Germany

Mowiol; Sigma-Aldrich, Germany

Natrim chloride; Roth, Germany

Nuclease-free water; Ambion, USA

Paraformaldehyde; Sigma-Aldrich, Germany

Paraplast, 39601006; Leica, Germany

Penicillin-streptomycin; PAA, Austria

Petri dishes; Greiner bio-one, Austria

Picric acid solution; Sigma-Aldrich, Germany

Platinum® SYBR® Green qPCR SuperMix UDG kit; Invitrogen, USA

Precellys® Lysing Kits; Krackeler Scientific, USA

Proteinase K; Promega, USA

RNeasy Mini Kit; Qiagen, Netherlands

Random hexamers; Applied Biosystems, USA

Resorcin-Fuchsin, Weigert; Waldeck GmbH & Co. KG, Germany

RNase inhibitor; Applied Biosystems, USA

Roti-Histol; Roth, Germany

Saponin; Sigma Aldrich, Germany

SensiMix SYBR No-ROX kit; Bioline, Germany

Sodium chloride; Merck, Germany

Sodium dodecyl sulfate; Roth, Germany

Tamoxifen; Sigma-Aldrich, Germany

Tissue Tek O.C.T. Compound; Sakura, Germany

Triton X-100; Roth, Germany

Tris; Roth, Germany

Trypsin; Sigma-Aldrich, Germany

2.1.3 Buffers & Solutions

Table 1 Buffers and solutions used [1]

1% (w/v) agarose gel	1.5 g agarose, 150 ml TAE-Buffer, 3 µl ethidium bromide 1% (v/v)
10× PBS	potassium hydrogen phosphate, sodium hydrogen phosphate, sodium chloride
10× TAE	0.4 M Tris, 0.01 M EDTA, 0.2 M acetic acid
Cytospin digestion buffer	17.3 ml DMEM, 1.5 ml 10× trypsin, 1 ml Collagenase B, 200 µl DNase I
FACS blocking buffer	FACS buffer, 0.1% (v/v) Triton X-100
FACS staining buffer	FACS buffer, 0.2% (w/v) saponin, 1% (v/v) primary antibody or 0.5% (v/v) secondary antibody
Fe-Hematoxylin	1:1 (v/v) solution A: solution B Weigert hematoxylin
Histobuffer	3% (w/v) BSA/PBS, 0.2% (v/v) Triton X-100
Lysis buffer	50 mM Tris-HCl, 100 mM EDTA, 100 mM NaCl, 1% (v/v) SDS
Resorcin-Fuchsin	10 ml Weigert Resorcin-Fuchsin, 190 ml 1% (v/v) hydrochloric acid in 70% (v/v) ethanol. Total volume 200 ml
$T_{10}E_1$	10 mM Tris, 0.1 mM EDTA
Van Giesson	240 ml Picric acid, 8 ml 2% (w/v) fuchsin, 2 ml 1% (v/v) acetic acid. Total volume 250 ml.

2.1.4 Polymerase chain reaction reagents

Immomix red; Roche, Switzerland

GeneRuler 100 bp DNA Ruler; Thermo Scientific, USA

KAPA Taq DNA polymerase ready mix; Kapa Biosystems, USA

---

[1]BSA: Bovine serum albumin

DMEM: Dulbecco's modified Eagle's medium

EDTA: Ethylenediaminetetraacetic acid

FACS: Fluorescence-activated cell sorting

PBS: Phosphate buffered saline

SDS: Sodium dodecyl sulfate

TAE: Tris-acetate-EDTA

Tris: Tris(hydroxymethyl)aminomethane

Triton X-100: 4-(1,1,3,3-Tetramethylbutyl)phenyl-polyethylene glycol

$T_{10}E_1$: Tris-HCl ten EDTA one

2.2 Experimental animals and animal husbandry

2.2.1 Approval for animal experiments

The animal experiments in this work were carried out under the approval of the Regierungspräsidium Darmstadt (approval number: B2/304). Mice were kept under standard conditions of purified air and water, supplied with food *ad libitum* and exposed equal cycles of 12 h light-darkness prior to experiments.

2.2.2 Transgenic lines

2.2.2.1 Tamoxifen-inducable Cre-mouse lines

PDGFRα^{CreERT2}: This mouse line expresses the Cre-recombinase specifically in cells where the promoter of PDGFRα is active, and is activated upon tamoxifen administration, when is translocated to the nucleus with the ERT2 protein. This mouse line was provided exclusively for this research by Prof. Dr. William Richardson (University College London).

Plin2$^{tm1.1(Cre/ERT2)Mort}$: This knock in mouse line has been generated by Dr. Marten Szibor, Dr, Robert Voswinckel, Isabelle Salwig and Prof. Dr. T. Braun (Max Planck Institute, Bad Nauheim). Into exon 8 of the *Plin2* locus the CreERT2 and a monomeric cherry fluorescent protein (mCherry) have been integrated using homologous recombination. These components were inserted at the end of the endogenous gene and joined by "reading bridges" (T2A segments). Thus, the original gene was not destroyed and remained fully functional even in homozygous mice. The neomycin cassette needed to select the embryonic stem cell clones, was later removed by mating with a flip-deleter mouse strain.

2.2.2.2 Reporter mouse lines

Gt(ROSA)26Sor$^{tm4(ACTB-tdTomato,-EGFP)Luo/J}$ (mTmG): This mouse line expresses a red fluorochome membrane tandemTomato (mtdTomato) in all cell membranes from the Rosa26 gene locus. A stop codon and second reporter gene for green fluorescent protein (GFP) are in line with mtdTomato. Parts of the tomato sequence and the stop codon are flanked by loxP sequences. After Cre-mediated recombination the stop codon is removed, tomato expression will be silenced and GFP will be expressed instead of mtdTomato. Thus after crossing the mTmG reporter line with a Cre-recombinase expressing mouse line, the mT cassette is deleted in the double transgenic offspring in Cre-recombinase expressing tissues, enabling expression of the downstream "membrane-terminated GFP" (mG) cassette. The actin beta (*ACTB*) promoter of this line ensures stronger and prolonged expression of the fluorescent protein (especially in adult cells) compared to the endogenous Gt (Rosa) locus alone. This double-fluorescence system allows visualization of recombined as well as non-recombined cells. It is suitable for internal control in phenotypic analyzes of Cre-recombinase-induced mosaic mutants and offers two possibilities for labeling in cell differentiation studies. By locating the fluorescent protein in the cell membrane, conclusions can be drawn about cell morphology. This mouse line was obtained from the company The Jackson Laboratory (Stock ID: 007576) (71).

B6.129S4-PDGFRα$^{tm1.1(EGFP)Sor/J}$ (PDGFRα^{GFP}): These mice express the h2B-eGFP fusion protein (knock-in) under the endogenous PDGFRα promoter. This allows the precise expression pattern of the gene to be visualized at the respective development time-point. This mouse line was obtained from the company The Jackson Laboratory (Stock ID: 007669) (37).

C57Bl/6-Tg(PDGFRα-Cre)1Clc/J (PDGFRα^{Cre}): This mouse line expresses the Cre-recombinase constitutively only in cells expressing the PDGFRα. These mice were kindly provided by Dr. Botond Roska (Friedrich Miescher Institute for Biomedical Research, Basel) (89).

2.2.2.3 Depletion mouse line

B6.129P2-Gt(ROSA)26Sor$^{tm1(DTA)Lky/J}$ (DTA)**:** This mouse strain contains a floxed-STOP cassette prior to a diphtheria toxin open reading frame. When DTA mice are crossed with a Cre-recombinase line and Cre is active, the floxed-STOP cassette is deleted and the Gt(ROSA)26Sor promoter drives expression of diptheria toxin in the Cre-expressing cells. These DTA mice allow selective ablation in a cell-specific manner. This mouse line was obtained from the company The Jackson Laboratory, USA (STOCK ID: 009669) (110).

2.2.3 Tamoxifen administration

Stock tamoxifen solutions were prepared at a concentration 20 mg/ml (for adult mice in the embryonic experiments), and 16 mg/ml (for postnatal mice) in Miglyol. The injections were performed intraperitoneally at a volume of 50 µl for the mothers (1 mg/animal) and 25 µl (0.2mg/g Tam per animal) for the postnatal mice at one time-point. After injection, the animals were maintained under regular observation.

2.3 PCR

2.3.1 DNA isolation from tail biopsies

In order to determine the genotype of the transgenic mice, the DNA was isolated from a small sample of tail tissue. The biopsies were first lysed over night (o.n.) in 500 µl of lysis buffer with 5 µl of proteinase K at 55 °C. The next day, the lysates were centrifuged for 10 min at 13,000 rpm at 4 °C and the supernatants were transferred into new eppendorfs. Subsequently, the supernatants were mixed with 500 µl isopropanol to precipitate the DNA and centrifuged for 10 min at 13,000 rpm at 4 °C. The supernatants were then discarded and the pellets were washed with 70% (v/v) ethanol. The pellets were then allowed to dry for about 30 min at RT and afterwards dissolved in 50 µl of T10/1 E buffer.

2.3.2 PCR Primers

Table 2 Primer sequences for genotyping PCR

Transgene	Sequence (5′→ 3′)
[1]**Plin2$^{tm1.1(Cre/ERT2)Mort}$**	Adrp_taa_ki_s: AGCGCCTTCGGATCCACCTCT Adrp_taa_wt_as: TGCTCTGGTGACAAGGAGGGGT Adrp_taa_mCh_as: CTCGTGGCCGTTCACGGAGC Adrp_taa_hERLB_s: TGCCCCTCTATGACCTGCTGCT
[2]**mT/ mG**	WT_for: CTCTGCTGCCTCCTGGCTTCT WT_rev: CGAGGCGGATCACAAGCAATA Mut_rev: TCAATGGGCGGGGGTCGTT
[2]**PDGFRα^{GFP}**	WT_for: CCCTTGTGGTCATGCCAAAC WT_rev: GCTTTTGCCTCCATTACACTGG Mut_rev: ACGAAGTTATTAGGTCCCTCGAC
PDGFRα^{CreERT2}	Cre up: CAGGTCTCAGGAGCTATGTCCAATTTACTGACC Cre low: GGTGTTATAACGAATCCCCAGAA
DTA	Mut_for: CGA CCT GCA GGT CCT CG Mut_rev: CTC GAG TTT GTC CAA TTA TGT CAC

[1] For Plin2$^{tm1.1(Cre/ERT2)Mort}$ mice genotyping, a combination of those primers was used for three products; Adrp_taa_ki_s and Adrp_taa_mCh_as for the mCherry gene, Adrp_taa_wt_as and Adrp_taa_hERLB_for the Cre-recombinase gene, and Adrp_taa_ki_s and Adrp_taa_wt_as for the wild type gene

[2] Multiplex PCRs for PDGFRα^{GFP} and mT/ mG lines

2.3.3 Programs

The PCR was carried out for the respective transgene by the following steps:

Plin2$^{tm1.1(Cre/ERT2)Mort}$:

Step	Time
1. Denaturation 95 °C	10 min
2. Denaturation 95 °C	20 s
3. Primer annealing 56 °C	30 s
4. Elongation 72 °C	35 s
5. Final Elongation 72 °C	7 min
6. End 4 °C	

Cycles: Step 2-4, 40 repetitions

Product size: Wild type: 441 base pairs (bp), mutant for Cre: 315 bp; mutant for mCherry: 584 bp; Polymerase: Immomix red

mTmG:

Step	Time
1. Denaturation 95 °C	15 min
2. Denaturation 94 °C	30 s
3. Primer annealing 61 °C	1 min
4. Elongation 72 °C	1 min
5. Final Elongation 72 °C	2 min
6. End 4 °C	

Cycles: Step 2-4, 35 repetitions

Product size: Wild type: 330 bp, mutant: 250 bp; Polymerase: Immomix red

PDGFRα^{GFP}:

Step	Time
1. Denaturation 94 °C	10 min
2. Denaturation 94 °C	30 s
3. Primer annealing 65 °C	1 min
4. Elongation 72 °C	1 min
5. Final Elongation 72 °C	2 min
6. End 4 °C	

Cycles: Step 2-4, 35 repetitions

Product size: Wild type: 451 bp, mutant: 242 bp; Polymerase: Immomix red

PDGFRα^{CreERT2}:

Step	Time
1. Denaturation 94 °C	10 min
2. Denaturation 94 °C	30 s
3. Primer annealing 61 °C	45 s
4. Elongation 72 °C	1 min
5. Final Elongation 72 °C	10 min
6. End 4 °C	

Cycles: Step 2-4, 40 repetitions

Product size: 500 bp; Polymerase: Immomix red

DTA:

Step	Time
1. Denaturation 95 °C	3 min
2. Denaturation 95 °C	15 s
3. Primer annealing 58 °C	15 s
4. Elongation 72 °C	8 s
5. Final Elongation 72 °C	30 s
6. End 4 °C	

Cycles: Step 2-4, 40 repetitions

Product size: 500 bp; Polymerase: Kapa Taq

2.3.4 Electrophoresis

Gel electrophoresis is used for the separation and identification of DNA fragments according to their size and charge. An electric field is applied on a gel matrix to move the negatively charged molecules of nucleic acid. For the matrix 1% (w/v) agarose gels (in 1×TAE buffer) containing 0.002% (v/v) ethidium bromide were created. Since ethidium bromide is intercalated into DNA, PCR products are visible under UV light. For all gels a 100 bp marker was employed.

2.4 Fluorescent-activated cell sorting

Sacrifice of the mice was conducted by decapitation with sharp scissors for mice up to P5, while older animals were killed after receiving an overdose of >5% isoflurane by inhalation, and subsequent exsanguination. The lungs were washed by perfusion though the right heart ventricle with 1×PBS. The lungs were then inflated though the trachea with dispase at 20-cm H_2O hydrostatic pressure, isolated, and placed in a Petri dish covered with 1 ml dispase and incubated for 10 min at RT. The reaction was stopped by the addition of 1 ml FCS and 1 ml DMEM with 2.5% (v/v) HEPES, 1% (v/v) penicillin-streptomycin and 2.1% (v/v) DNase and the lungs were then homogenized by a dissociator. The cell suspension was filtered first though a 100 µm and then though a 40 µm filters before centrifugation at 4 °C at 213 *g* for 10 min. The supernatant was removed and the cell pellets were re-suspended in FACS buffer and permeabilized with 0.2% (w/v) saponin in FACS buffer for 15 min on ice. After centrifugation at 156 *g* for 3 min at 4 °C the cells were re-suspended in 10-µl blocking

solution and 20 µl of the antibody solution afterwards and let for incubation for 20 min at 4 °C in the dark. The antibodies that were used are shown in Table 3.

Cells were washed in 100 µl FACS buffer and centrifuged at 156 *g* for 3 min at 4 °C. The secondary antibodies were then added and incubated for 15 min at 4 °C in the dark. After washing and centrifugation at 156 *g* for 3 min at 4 °C pellets were re-suspended in FACS buffer containing 0.15% (v/v) paraformaldehyde (PFA) in PBS and kept on ice for 15 min. Cells were filtered through a 100 µm filter and centrifuged at 156 *g* for 3 min at 4 °C before being re-suspended in 200 µl FACS buffer for the FACS analysis.

Table 3 Overview of primary and secondary antibodies used[1]

Antibody	Type	Host	Catalog number	Company	Application
ADRP	primary	rabbit	Ab52356	Abcam	IHC, FACS, cytospin
PDGFRα	primary	mouse	Sc-21789	Santa Cruz	IHC
PDGFRα	primary	rat	Ab 90967	Abcam	IHC, cytospin
αSMA	primary	mouse	A 5228	Sigma	IHC, cytospin
αSMA	primary	rabbit	Pa5-19465	Thermo Scientific	IHC, FACS
CD45	primary	rat	553076	BD	IHC
CD44	primary	rabbit	Ab 41478	Abcam	IHC
CD105	primary	rat	Ab81456	Abcam	IHC
CD73	primary	rabbit	13160	Cell Signalling	IHC
CD146	primary	rabbit	04-1147	Millipore	IHC
CD90	primary	rat	Sc-73161	Santa Cruz	IHC
Vimentin	primary	rabbit	Sc- 7558	Santa Cruz	IHC
Collagen I	primary	mouse	C2456	Sigma	IHC
IgG	primary	mouse	10400c	Invitrogen	IHC
IgG	primary	rat	Sc-2026	Santa Cruz	IHC, FACS
IgG	primary	rabbit	2729	Cell Signaling	IHC
CD140α APC	primary	rat	135907	Biolegend	FACS
APC IgG2α	primary	rat	400511	Biolegend	FACS
IgG	primary	rabbit	Pa5-23090	Thermo Scientific	FACS
CD45	primary	rat	103104	Biolegend	FACS
CD326 (EpCAM)	primary	rat	118204	Biolegend	FACS
CD31 (PECAM)	primary	rat	102404	Biolegend	FACS
A555 anti-rabbit IgG	secondary	goat	A21428	Invitrogen	IHC
A555 anti-rat IgG	secondary	goat	A21434	Invitrogen	IHC
A647 anti-mouse IgG	secondary	goat	A21240	Thermo Scientific	IHC
A647 anti-rat IgG	secondary	goat	A21247	Invitrogen	IHC
A647 anti-rabbit IgG	secondary	goat	A21244	Invitrogen	IHC, FACS
A680 anti-mouse IgG	secondary	goat	A21057	Invitrogen	IHC
Brilliant Violet 510	secondary	rat	405233	Biolegend	FACS
APC	secondary	rat	405207	Biolegend	FACS

[1] APC: Allophycocyanin

EpCAM: Epithelial cell adhesion molecule

FACS: Fluorescence-activated cell sorting

IgG: Immunoglobulin G

IHC: Immunohistochemistry

PECAM: Platelet endothelial cell adhesion molecule

2.5 Immunofluorescence

2.5.1 Tissue isolation for immunohistochemistry

Mice were sacrificed as described in Section 2.4. After intratracheal intubation lungs were inflated with 1:1 Tissue Tek 4% (v/v) PFA at 20 cm H_2O hydrostatic pressure. Lungs were kept o.n. in 4% (w/v) PFA at 4°C. Tissues were then fast frozen in a methyl butane bath over dry ice and stored as cryo-blocks at -80 °C. Prior to staining lungs were cut in microtome sections of 10 µm and placed on slides to dry o.n. and stored at -20 °C.

2.5.2 Preparation of mouse lung homogenates for cytospins

Mice were sacrificed as in section 2.4. Lungs were removed and manually homogenized using a scalpel, and then were digested in 3-4 ml cytospin digestion buffer, for a total period of 50 min at 37 °C, with one re-suspension interval after the first 25 min. The enzyme reaction was blocked with FCS and the cells were filtered through a 40 µm mesh. Subsecuently, the cells were re-suspended in 2-3 ml 1×PBS. For the cytospin, an aliquot (2×100 µl) of the cell suspension was spun down on a glass slide by centrifugation for 5 min at 500 rpm at 4 °C, and allowed to dry at RT.

2.5.3 Antibody staining

Tissue sections or cells underwent fixation in a mixture of 1:1 (v/v) methanol/acetone at -20 °C for 20 min. Then the area of interest was circled with a fat pen and was blocked in goat serum for 1 h. The primary antibodies were incubated for 3 h o.n. and the slides were washed in PBS (3×5 min) before incubation with the secondary antibodies for 1 h. After washing in the same manner, nuclei were stained with 4′,6-diamidino-2-phenylindole dihydrochloride (DAPI) for 20 min, the slides were mounted with Mowiol and allowed to dry at RT. The antibodies used are listed in Table 3.

2.5.4 Confocal microscopy imaging

All tissue sections were analyzed using a confocal microscope. For the analysis of cytospins cells of each animal were distributed to three slides. Four optical fields per slide were assessed randomly at the

microscope resulting in twelve optical fields for every mouse for a total of 3-5 animals and data were analyzed with the STEPanizer © stereology tool.

2.6 Histological staining- elastin staining

Mice were sacrificed as in Section 2.4. After intratracheal intubation, lungs were inflated with 4% PFA at 20 cm H_2O hydrostatic pressure. Removed lungs were kept o.n. in 4% PFA at 4 °C. Tissues were then dehydrated with Leica ASP200S tissue processor, and embedded in paraffin blocks with Leica EG1160 and Leica EG1150C. The tissues were then sectioned using Leica RM2255 microtome into 3-µm thick sections and allowed to dry at RT. Deparaffinization of the slides occurred by heating at 59 °C for 60 min. The slides were then placed in Roti-Histol (3×5 min), followed by 5 min steps of embedding in progressively reduced ethanol concentration as follows: 99.6% (v/v), 99.6% (v/v), 96% (v/v), and 70% (v/v) ethanol and let o.n. in Resorsin-Fuchsin solution. The next day, the lung tissues were washed for 15 min in tap water and in for 10 s in dd H_2O, before counter-staining with Weigert hematoxylin. The same washing step was repeated but the tissues were stained with van Gieson solution. Then, the tissues were progressively dehydrated as follows: 2×2 min 96% (v/v) ethanol, 5 min 99.6% (v/v) ethanol, 5 min 2-propanol 99.8% (v/v) ethanol, 3×5 min Roti-Histol and mounted with Pertex. The pictures were generated by nanozoomer at bright field.

2.7 Total RNA isolation and real-time PCR

Total RNA was purified with a Precellys® Lysing Kit according to the manufacturer's instructions. For each sample 100 ng of total RNA was used to synthesize cDNA. Using high capacity cDNA Reverse Transcription KitcDNA, cDNA was synthesized according to the manufacturer's instructions in Eppendorf Mastercycler ep Gradient S thermal cycler. The program for cDNA synthesis was as follows (reaction volume 20 µl):

1: 25 °C for 10 min
2: 37 °C for 120 min
3: 85 °C for 5 min
4: 4 °C hold

Real-time PCR was performed using 2 µl of cDNA and a SensiMix SYBR No-ROX kit according to the manufacturer's instructions. The primers used for the amplifications are listed in Table 4. All the primer pairs were separated by at least one intron to exclude genomic DNA contamination and checked for primer efficiency.

Real-time PCR took place in Bio-Rad C1000 thermal cycler with CFX96 system with the following protocol (reaction volume 15 µl):

1: 95 °C 6 min

2: 95 °C 10 s

3: 59 °C 10 s

4: 72 °C 15 s

Plate Read

5: GO TO 2; 44 more times

6: 95 °C for 10 s

7: Melt Curve 65 °C to 95 °C: Increment 0.5 °C for 3 s

Plate Read

Table 4 Primer sequences for qPCR

Locus	Sequence (5′→ 3′)
GFP[1]	Forward: GAAGCCAACGCCTGCAAAATC Reverse: CCAACGGGTATGAGCTATTCC
Cre	Forward: GACATGTTCAGGGACAGGCA Reverse: GTTGTTCAGCTTGCACCAGG
mCherry	Forward: AAGGGCGAGATCAAGCAGAG Reverse: CCTCGTTGTGGGAGGTGATG
ADRP[2]	Forward: CGACGACACC GATGAGTCCCAC Reverse: TCAGGTTGCGGGCGATAGCC
GAPDH[3]	Forward: TCACCACCATGGAGAAGGC Reverse: GCTAAGCAGTTGGTGGTGCA

[1] GFP: Green fluorescent protein

[2] ADRP: Adipose differentiation related protein

[3] GAPDH: Glyceraldehyde-3-phosphate dehydrogenase

3 Results

3.1 Characterization of PDGFRα^{+} fibroblasts during lung development

3.1.1 Localization of PDGFRα expressing cells during early lung development

The starting point of this study was to analyze the localization of PDGFRα^{+} cells in early lung development using transgenic PDGFRα^{GFP} reporter mice. Lung sections from embryos were stained with antibodies against ADRP, as a marker for lipofibroblasts and against αSMA as a marker for myofibroblasts (Figure 6 B, C, E, F, isotype controls in Figure 34). Nuclei were stained using DAPI. Expression of bright GFP was observed at E14.5 in interstitial cells around the large bronchi and was co-localized with, αSMA in cells in close proximity to the epithelial tubes of the bronchi (Figure 6 A-C). The expression of ADRP was detected in some cells of the more distal mesenchyme (Figure 6 B, C). The distal mesenchyme also contained cells with dim GFP expression which lo-localized with ADRP in some cells (Figure 6 A-C). Later, at E16.5, the canaliculi were formed and the GFP signal still co-localized with αSMA in peribronchial cells (figure 6 E, F). The signal of ADRP was detected in more cells of the distal mesnchyme at E16.5 compared to E14.5 (Figure 6 B, C, E, F). These findings demonstrated co-localization of PDGFRα with αSMA in peribronchial myofibroblasts at E14.5 and E16.5, and co-localization with ADRP in some lipofibroblasts of the distal mesenchyme at E14.5 and E16.5.

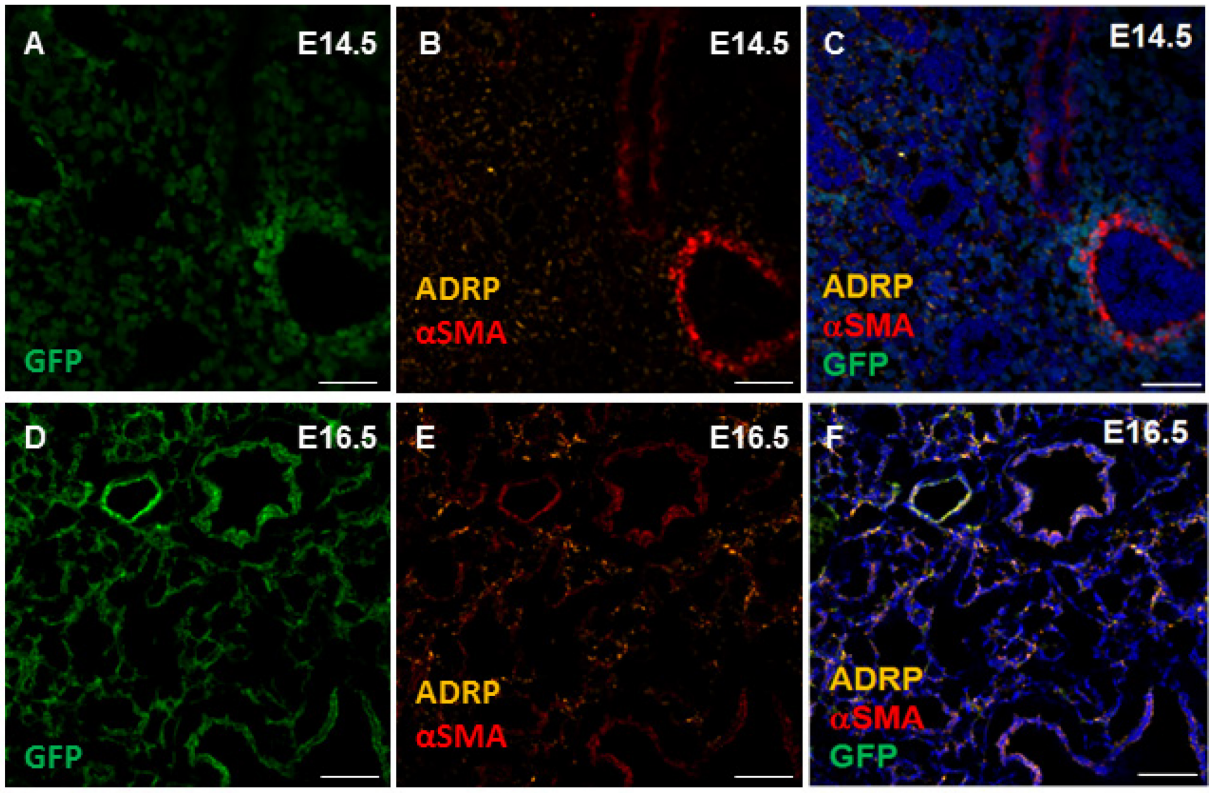

Figure 6 Localization of platelet-derived growth factor receptor α expression at two time-points during embryonic mouse lung development.

(A-F) Lung tissue from PDGFRα^{GFP} mice was stained for adipose differentiation related protein (ADRP) (orange) and α-smooth muscle actin (αSMA) (red), followed by a 4', 6-diamidino-2-phenylindole dihydrochloride nuclear stain (blue). Green fluorescent protein (GFP) (green). (A-C) At embryonic day (E)14.5 bright platelet-derived growth factor receptor α (PDGFRα) expression was restricted to large bronchi which already expressed αSMA, dim expression of PDGFRα was detected in the distal mesenchyme, few cells of the distal mesenchyme expressed ADRP. (D-F) At E16.5 PDGFRα expression was still detected in αSMA-expressing peribronchial cells, more cells of the distal mesenchyme expressed ADRP. Scale bar = 50 μm.

3.1.2 Expression of mesenchymal stem cell markers in PDGFRα$^+$ cells during pre- and postnatal lung development

Since PDGFRα$^+$ cells have been demonstrated to serve as progenitor cells, the expression of markers typical for MSCs was analyzed using PDGFRα^{GFP} mice. Lung tissue from the embryonic stages E14.5, E16.5 and E18.5 and the postnatal stages P3 and P5 was stained for MSC markers CD44 and CD105 with DAPI as nuclear counter stain. At E14.5 and E16.5 CD44 and CD105were not expressed in PDGFRα$^+$ cells (Figure 7 A, B, isotype controls in Figure 34 and in Figure 35). Later in the canalicular

stage at E18.5 some PDGFRα^{+} cells expressed CD44 and CD105 (Figure 7 C). As growth continued, some PDGFRα^{+} cells revealed CD105 expression at P3 but the CD44 signal was not detected in PDGFRα^{+} cells. In early stages of alveolarization, PDGFRα^{+} cells exhibited expression of CD44 within the primary septa at P5, and some tip cells of the secondary crests expressed CD105 (Figure 7 D, E).

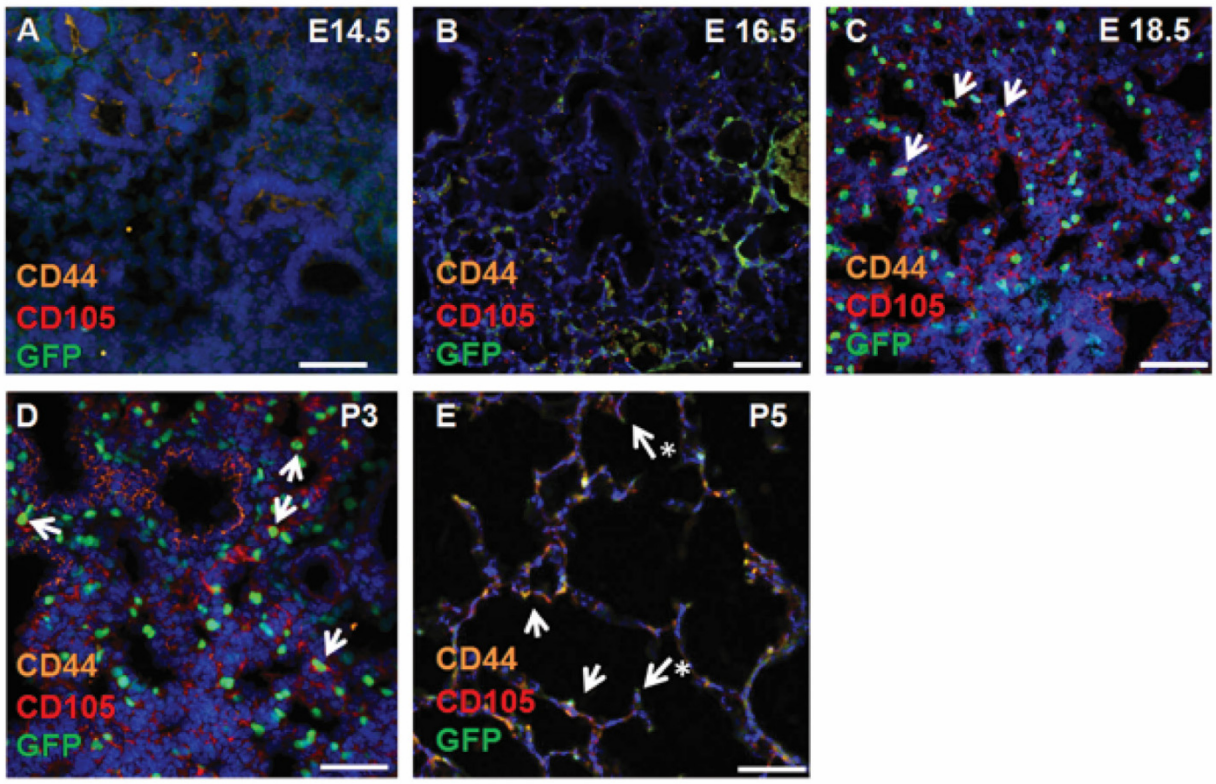

Figure 7 At certain time-points during lung development platelet-derived growth factor receptor α^{+} cells expressed the mesenchymal stem cell markers CD44 and CD105.

(A-E) Lung tissue of prenatal and postnatal PDGFRα^{GFP} mice was stained for the mesenchymal stem cell markers CD44 (orange) and CD105 (red), followed by a 4', 6-diamidino-2-phenylindole dihydrochloride nuclear stain (blue). Green fluorescent protein (GFP) (green). (A-B) At embryonic day (E)14.5 and E16.5 the PDGFRα signal did not co-localize with CD44 and CD105. (C) At E18.5 some platelet-derived growth factor receptor α^{+} (PDGFRα^{+}) cells exhibited CD44 and CD105 expression (arrows). (D) At postnatal day (P)3 some PDGFRα^{+} cells revealed CD105 expression (arrows) but did not exhibit a signal for CD44. (E) At P5 PDGFRα^{+} cells within the primary septa revealed expression of CD44 (arrows). Some tip cells of the secondary crests revealed CD105 expression (arrows with asterisk). Scale bar = 50 μm.

Expression of the MSC marker CD73 was analyzed at the pre- and postnatal stages E14.5, E16.5, E18.5, P3 and P5 in PDGFR^{GFP} mice (Figure 8, isotype controls in Figure 34 and in Figure 35). At E14.5, E16.5 and E18.5 co-localization of PDGFRα and CD73 was not detected (Figure 8 A-C). Conversely, postnatally, PDGFRα^{+} cells were also CD73^{+} at P3 (Figure 8 D). At P5 PDGFRα^{+} cells at

the base of the primary septum and at the tip of the secondary crests expressed CD73 (Figure 8 E). In adult lung tissue the CD73 signal was restricted to some scattered PDGFRα-expressing cells (Figure 8 F).

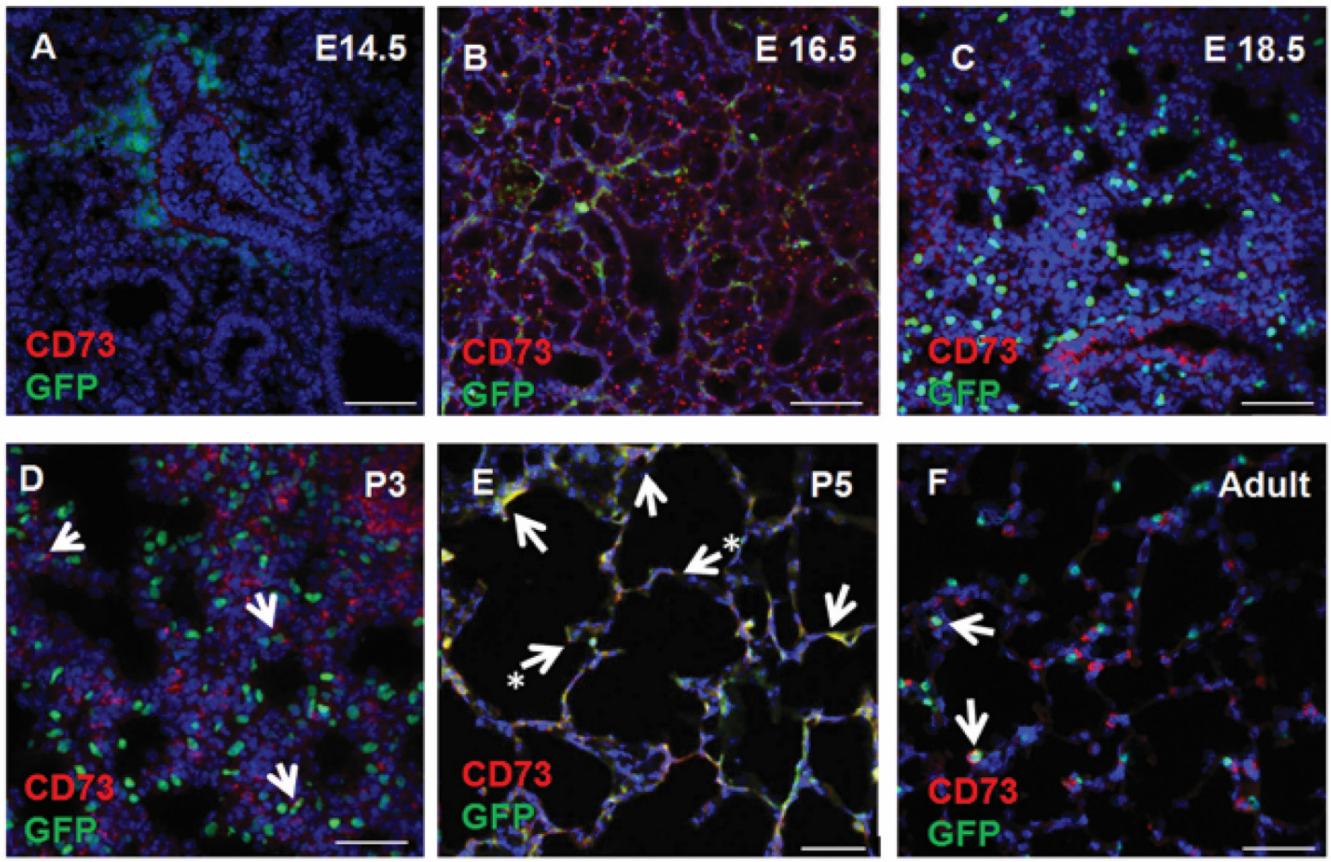

Figure 8 The mesenchymal stem cell marker CD73 was expressed at platelet-derived growth factor receptor α^+ cells at distinct time-points during lung development.

(A-F) Lung tissue of PDGFRα^{GFP} mice was stained for CD73 (red), followed by a 4', 6-diamidino-2-phenylindole dihydrochloride nuclear stain (blue). Green fluorescent protein (GFP) (green). (A-C) At embryonic day (E)14.5, E16.5 and E18.5 the platelet-derived growth factor receptor α PDGFRα signal did not co-localize with CD73. (D) At postnatal day (P)3 some PDGFRα^+ cells exhibited expression of CD73 (arrows). (E) At P5, CD73 expression was detected in PDGFRα^+ cells at the base of the primary septum (arrows) and at the tip of the secondary crests (arrows with asterisk). (F) In the adult lung CD73 expression is restricted to scattered PDGFRα^+ cells (arrows). Scale bar = 50 μm.

The expression of a further MSC marker CD146 was analyzed in PDGFRα^{GFP} mice at pre- and postnatal time-points of the lung development (Figure 9, isotype controls in Figure 34 and Figure 35). At E14.5, E16.5 and E18.5 PDGFRα and CD146did not co-localize (Figure 9 A, B, C). At P3, co-localization of PDGFRα and CD146 was evident in some mesenchymal cells but peribronchial

PDGFRα^{+} cells did not express CD146 (Figure 9 D). Later in development, at P5, PDGFRα^{+} cells in the primary septum and in the tip of the secondary septum expressed CD146 (Figure 9 E). In adult lungs distinct GFP^{+} cells expressed CD146 Figure 9 F).

Expression of the lipofibroblast marker ADRP and the MSC marker CD90 were analyzed in pre- and post-natal lungs of PDGFRα^{GFP} mice (Figure 10, isotype controls in Figure 34 and Figure 35). In early stages during embryonic development (E14.5) PDGFRα^{+} cells were located in peribronchial regions and did not express CD90 nor ADRP (Figure 10 A). In the distal mesenchyme cells did not express PDGFRα and were ADRP^{+}, some of which expressed CD90 (Figure 10 A). At E16.5 there were no PDGFRα^{+} cells that appeared CD90^{+} and ADRP^{+} (Figure 10 B). At E18.5 most of ADRP^{+} cells were also stained for CD90 and some of PDGFRα^{+} cells were also CD90^{+} and ADRP^{+} (Figure 10 C). When lungs were stained at P3 there were PDGFRα^{+} cells also positive for ADRP but not for CD90 (Figure 10 D). Cells positive only for CD90 were abundant in primary septa (Figure 10 D). At P5 cells of the primary septa exhibited co-localization of PDGFRα, ADRP and CD90 (Figure 10 E). Co-expression of CD90 and ADRP appeared at the base of the secondary crests, tip cells expressed PDGFRα and CD90 but not ADRP (Figure 10 E). In adult lung some PDGFRα^{+} cells expressed ADRP and CD90 while other PDGFRα^{+} cells expressed ADRP alone (Figure 10 F). Some cells only expressing CD90 were present in the alveolar walls (Figure 10 F).

To investigate the myogenic character of PDGFRα-expressing cells with regard to CD90 expression, pre- and postnatal lungs of PDGFRα^{GFP} mice were analyzed for αSMA and CD90 expression (Figure 11, isotype controls in Figure 34 and in Figure 35). At prenatal stages there were no triple-positive cells, for PDGFRα, αSMA and CD90 (Figure 11 A, B, C). At E14.5 and E16.5 peribronchial PDGFRα^{+} cells expressed αSMA (figure 11 A, B). Some mesenchymal cells located in the alveolar ducts at E18.5 where double-positive for PDGFRα and αSMA (Figure 11 C) At P3, PDGFRα^{+} cells did not express CD90 but there were some mesenchymal CD90^{+} cells (Figure 11 D). In some cells of the primary septa at P5, PDGFRα and CD90 co-expression was observed, in contrast, cells positive for αSMA and CD90 did not express PDGFRα (Figure 11 E). Expression of αSMA, PDGFRα and CD90 but not ADRP and CD90 was exhibited at the tip cells of secondary crests (Figure 11 E). Only double-positive cells either for PDGFRα and CD90 or for PDGFRα and αSMA were observed in adult lung (Figure 11 F).

In summary PDGFRα^{+} cells exhibited a spatiotemporal expression of MSC markers, lipofibroblast and myofibroblast markers in pre- and postnatal stages. During alveolarization PDGFRα^{+} cells in the

primary septum and at the base of the secondary septum mainly expressed ADRP and tip cells expressed PDGFRα and CD90 but not ADRP. In contrast, PDGFRα^{+} cells in the tip of the secondary crests expressed αSMA. The expression of MSC markers was evident in PDGFRα^{+} cells of the primary and secondary septum.

3.1.3 Quantification of fibroblast subtypes during alveolarization

To investigate the contribution of PDGFRα^{+} cell to the process of alveolarization, lungs of PDGFRα^{Cre}mTmG mice were analyzed at the peak of secondary septation (P7) (Figure 12, isotype controls in Figure 35). Constitutive active Cre expression led to permanent labeling of PDGFRα-expressing cells and their progeny due to constant GFP expression. GFP expression was observed within the primary septa and co-localized with ADRP in cells at the base of secondary septa (Figure 12 A). Co-localization of GFP and αSMA was evident in cells of the primary septa and in cells at the tip of the secondary septa (Figure 12 B). The quantification of the relative numbers of fibroblast subtypes at P7 from total lung cell suspension using cytospins revealed the abundance of the different fibroblast populations such as myofibroblasts (detected as αSMA^{+}), lipofibroblasts (detected as ADRP^{+}) and PDGFRα^{+} cells (detected as GFP^{+}): 7.9±0.6%, ADRP^{+} cells: 5.4±0.2%, αSMA^{+} cells: 4.9±0.4%, Figure 12 C). Furthermore quantification of cells positive for dual marker expression revealed that 3.3±0.6% of all ADRP^{+} cells also expressed GFP and 2.0±0.1% of all αSMA^{+} cells expressed GFP (GFP^{+} and ADRP^{+} cells: 3.3±0.6%, and GFP^{+} and αSMA+ cells: 2.0±0.1%, Figure 12 C).

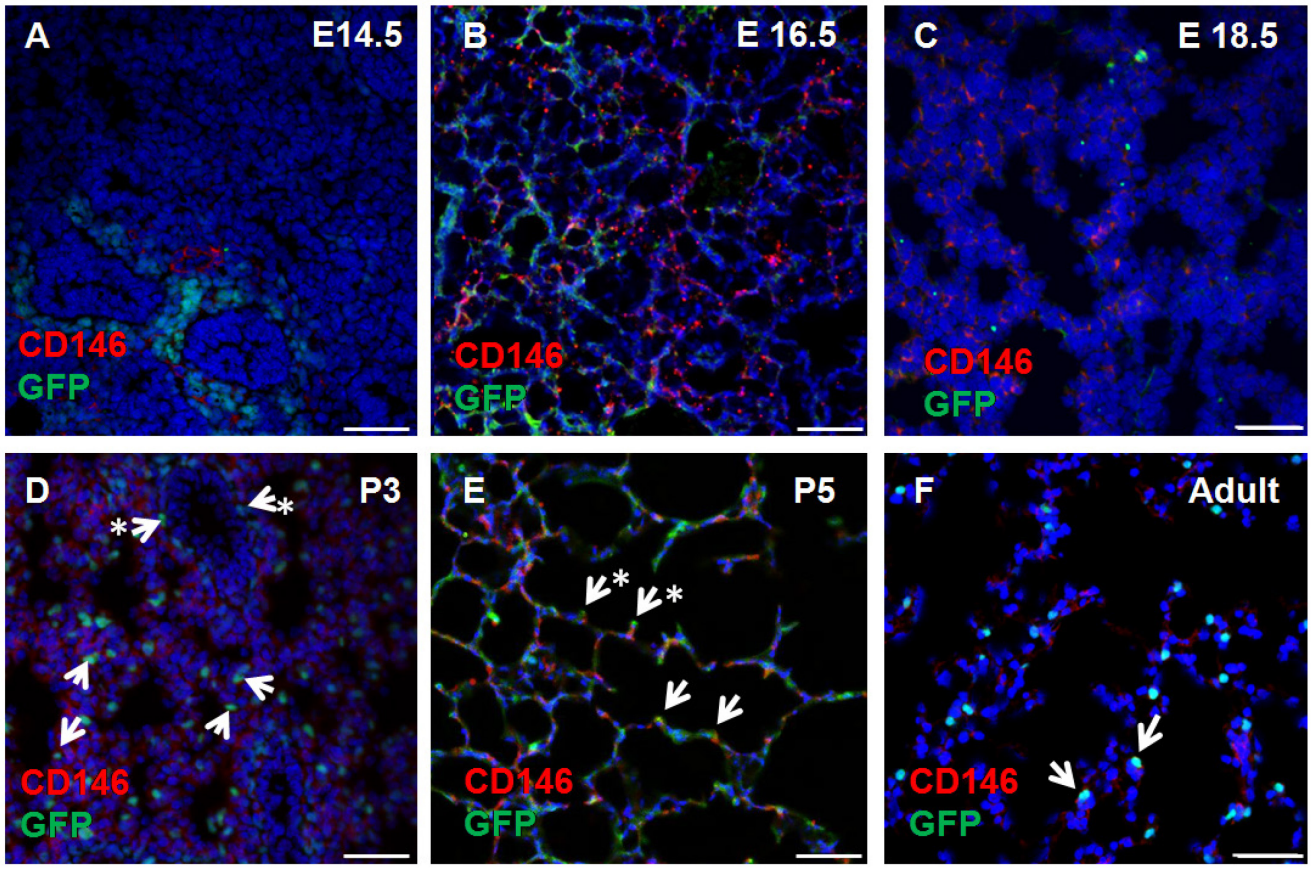

Figure 9 The mesenchymal stem cell marker CD146 was expressed at platelet-derived growth factor receptor α^{+} cells at distinct time-points during lung development.

(A-F) Lung tissue of PDGFRα^{GFP} mice was stained for CD146 (red), followed by a 4', 6-diamidino-2-phenylindole dihydrochloride nuclear stain (blue). Green fluorescent protein (GFP) (green). (A-C) At embryonic days (E)14.5, E16.5 and E18.5 the platelet-derived growth factor receptor α (PDGFRα) signal did not co-localize with CD146. (D) Co-localization of PDGFRα and CD146 (arrows) appeared in some mesenchymal cells at postnatal day (P)3. Peribronchial PDGFRα^{+} cells did not express CD146 (arrows with asterisk) at P3. (E) At P5 PDGFRα^{+} cells of the primary septum (arrows) and at the tip of the secondary crests (arrows with asterisk) exhibit CD146 expression. (F) Some PDGFRα^{+} cells of the adult lung demonstrate CD146 expression (arrows). Scale bar = 50 μm.

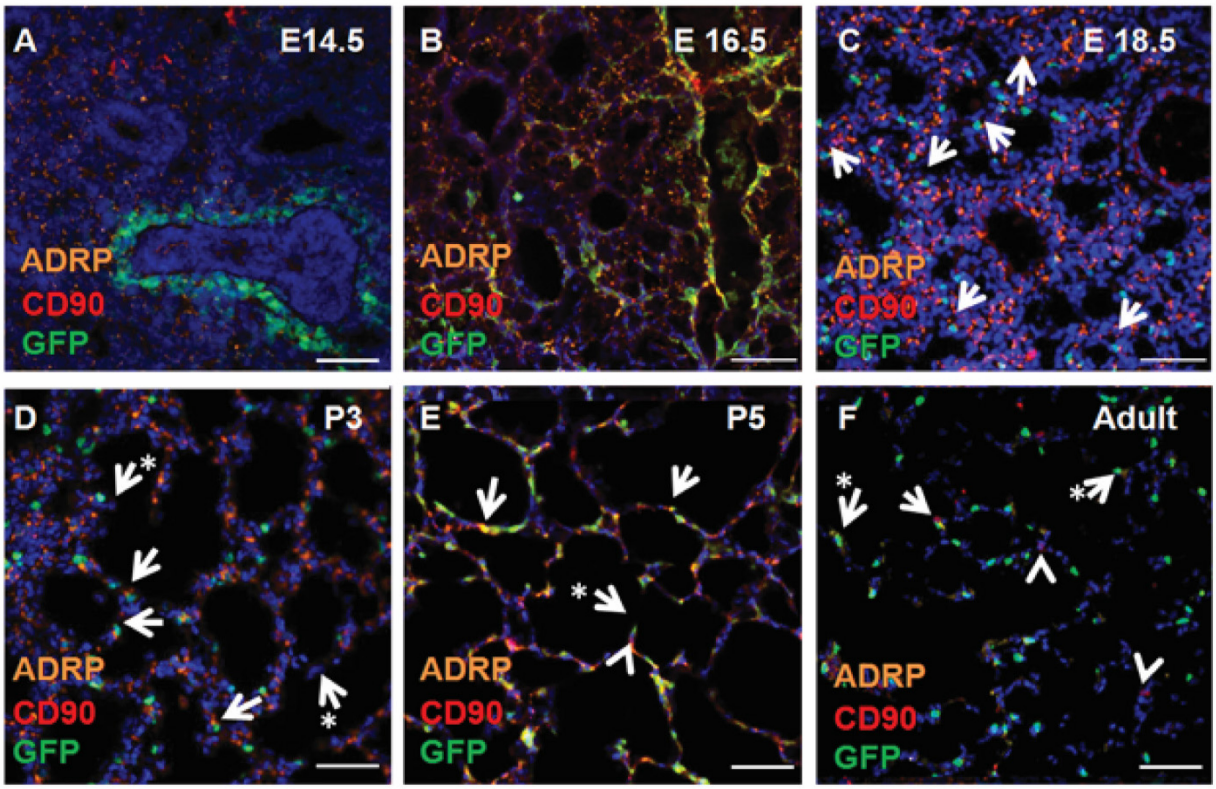

Figure 10 Co-expression of the mesenchymal stem cell marker CD90 and adipose differentiation related protein exhibited by platelet-derived growth factor receptor α^+ cells at particular time-points although this was not the case in tip cells of the secondary crests.

(A-F) Lung tissue of PDGFRα^{GFP} mice was stained for CD90 (red) and adipose related protein (ADRP) (orange), followed by a 4', 6-diamidino-2-phenylindole dihydrochloride nuclear stain (blue). Green fluorescent protein (GFP) (green). (A) At embryonic day (E)14.5 the platelet derived growth factor receptor α (PDGFRα) signal (green) in peribronchial cells did not co-localize with the signals for CD90 and ADRP. Most of the distal mesenchymal cells expressed ADRP. Some ADRP$^+$ cells expressed CD90 without PDGFRα expression. (B) At E16.5 PDGFRα^+ cells did not express CD90 and ADRP. (C) The expression of ADRP and CD90 mostly overlapped at E18.5. Some of the PDGFRα^+ cells revealed co-expression of ADRP and CD90 (arrows). (D) At postnatal day (P)3 some PDGFRα^+ cells co-expressed ADRP without CD90 expression (arrows). Solely CD90$^+$ cells were present in the primary septa (arrows with asterisk). (E) At P5 triple-positive cells for PDGFRα, ADRP and CD90 appeared in the primary septa (arrows). Tip cells of the secondary crests did express CD90 and PDGFRα but not ADRP (arrow with asterisk). Co-expression of CD90 and ADRP appeared at the base of the secondary crests (arrowhead). (F) In the adult lung, some PDGFRα^+ cells expressed ADRP and CD90 (arrows) while other cells expressed ADRP alone (arrows with asterisk). Solely CD90-expressing cells are present in the alveolar walls (arrowheads). Scale bar = 50 μm.

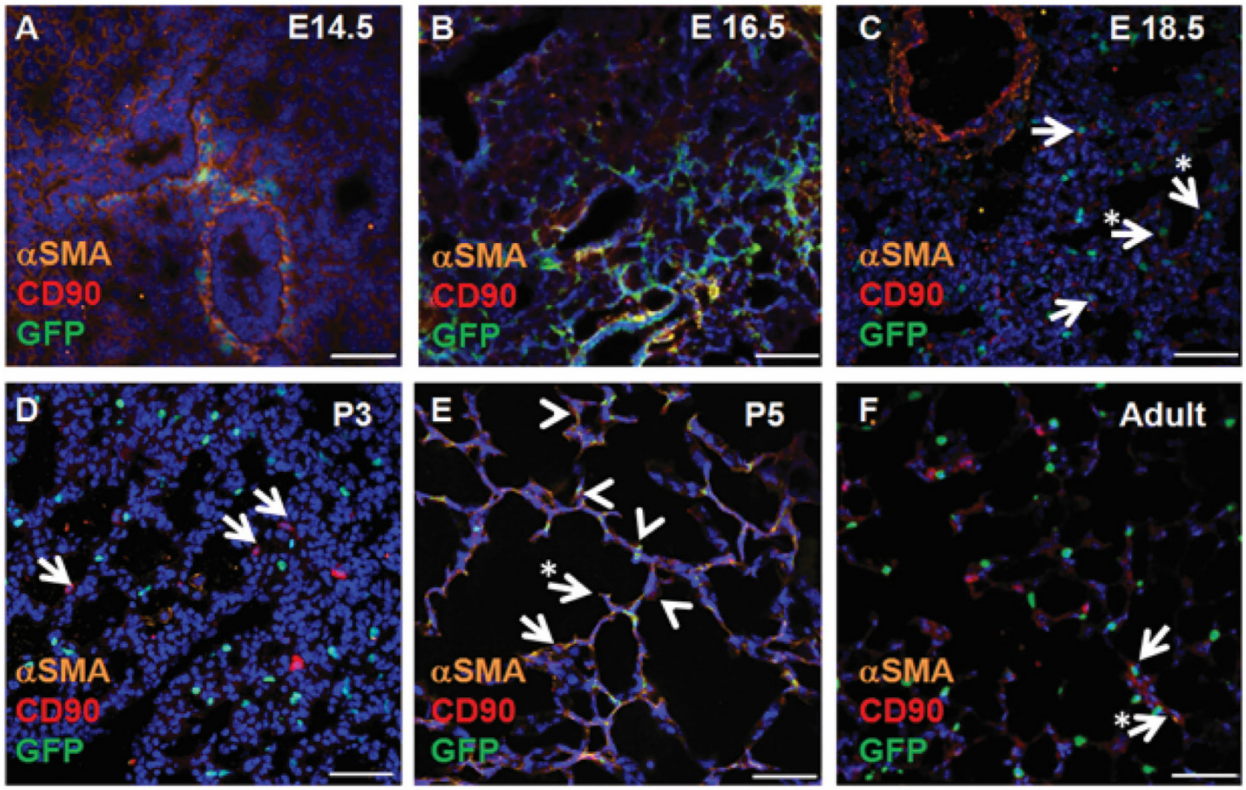

Figure 11 Co-expression of the mesenchymal stem cell marker CD90 and α-smooth muscle actin exhibited by platelet derived growth factor receptor α^+ cells at particular time-points although this was not the case in tip cells of the secondary crests.

(A-F) Lung tissue of PDGFRα^{GFP} mice was stained for CD90 (red) and α-smooth muscle actin (αSMA) (orange), followed by a 4', 6-diamidino-2-phenylindole dihydrochloride nuclear stain (blue). Green fluorescent protein (GFP) (green). (A) At embryonic day (E)14.5 platelet derived growth factor receptor α^+ (PDGFRα^+) cells of the peribronchial region co-expressed αSMA and lack CD90 expression. (B) At E16.5 PDGFRα^+ cells did not express CD90 but peribronchial PDGFRα^+ cells did express αSMA. (C) Some PDGFRα^+ cells reveal expression of αSMA and CD90 in the mesenchyme between the alveolar ducts (arrows) at E18.5. Around the alveolar ducts, some PDGFRα^+ cells expressed αSMA (arrows with asterisk). (D) At postnatal day (P)3 PDGFRα^+ cells did not express CD90. Single cells within the mesenchyme expressed only CD90 (arrows). (E) At P5, PDGFRα^+ cells within the primary septa express CD90 (arrowheads). In some cells within the primary septum (arrows) which did not express PDGFRα (PDGFRα^-), CD90 co-localized with αSMA. Tip cells of the secondary crests expressed αSMA and PDGFRα and CD90 (arrows with asterisk). (F) In the adult lung, some PDGFRα^+ cells expressed CD90 (arrows). Co-expression of αSMA and CD90 appeared also to be present in some PDGFRα^- cells (arrows with asterisk). Scale bar = 50 μm.

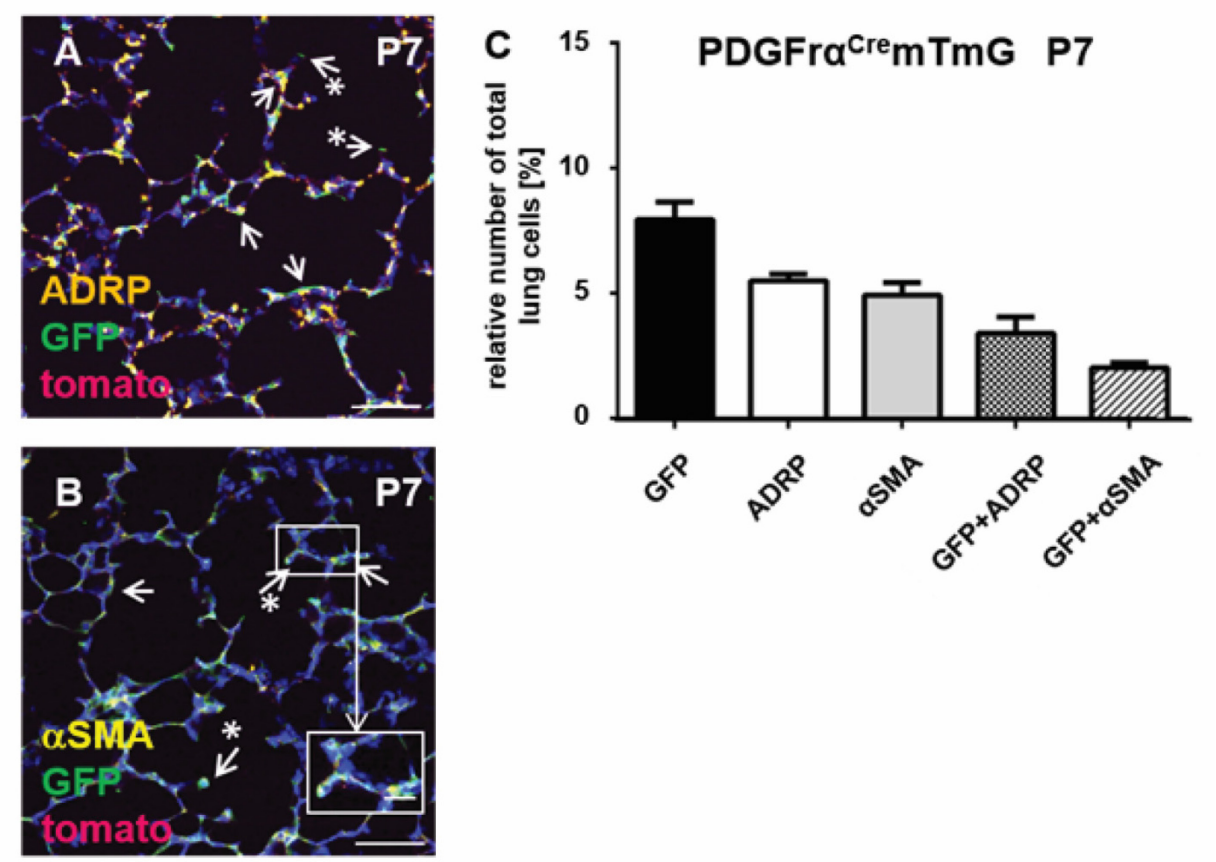

Figure 12 Localization and quantification of platelet-derived growth factor receptor α^+ cells and fibroblast subtypes at the peak of secondary septation at postnatal day 7, using constitutively active PDGFRα^{Cre}mTmG mice.

Cells which underwent Cre-recombination expressed green fluorescent protein (GFP) (green), non-recombined cells kept the tomato signal (red). A 4', 6-diamidino-2-phenylindole nuclear stain (blue) was used for all the tissues. (A) Platelet-derived growth factor receptor α^+ (PDGFRα^+) cells (green) were located in the primary septa (arrows) and expressed adipose differentiation related protein (ADRP orange) in cells at the base of the secondary septum. Cells at the tip of the secondary crests expressed GFP but not ADRP (arrows with asterisk). (B) In the primary septa (arrows) and at the tip cells of the secondary crests (arrows with asterisk and insert) PDGFRα^+ cells (green) expressed α-smooth muscle actin (αSMA, yellow). Scale bar = 50 µm, scale bar of the insert = 20 µm. (C) Relative numbers of fibroblast subtypes from total lung cell suspension (n=6). Bar graphs show mean values ± SEM.

3.1.4 Lineage tracing of early postnatal PDGFRα expressing cells

Using lineage tracing the mode of differentiation of early postnatal PDGFRα-expressing cells was analyzed. Inducible PDGFRα^{CreERT2}mTmG were injected with tamoxifen at P1 to induce *in vivo* Cre-recombination resulting in permanent labeling (due to GFP expression) of PDGFRα-expressing cells at P1 and all progeny (Figure 13, isotype controls in Figure 36). The time-points P7 and P9 were chosen for analysis to cover the peak of secondary septation (P7, Figure 13 A, B, C) and one time-point after the peak (P9, Figure 13 D, E, F). Early postnatal (at P1) PDGFRα^{+} gave rise to ADRP-expressing cells in the primary septa at P7 and to cells at the tip of the secondary septa which did not express ADRP (Figure 13 A). Lineage labeled cells at the tip of the secondary crests expressed αSMA (Figure 13 B). Furthermore, PDGFRα^{+} cells at P1 gave rise so αSMA^{+} cells at P7 in the primary septa (Figure 13 B). Quantification of lineage labeled cells (PDGFRα^{+} cells at P1) using cytospins at the peak of secondary septation (P7) revealed that 5.6±0.5% of all lung cells expressed the lineage label GFP, 9.2±0.5% expressed ADRP and 4.8±0.7% expressed αSMA (Figure 13 C). Quantification of cells expressing GFP and contributing to the lipofibroblast or myofibroblast populations revealed that 4.1±1.0% of all lung cells expressed ADRP and GFP, 1.9±0.3% of all lung cells expressed αSMA and GFP (Figure 13 C). Analysis of lineage traced cells (PDGFRα^{+} cells at P1) after the peak of secondary septation at P9 revealed that cells at the tip of the secondary crests expressed GFP but not ADRP (Figure 13 D). Cells at the base of the secondary septa and in the primary septa expressed GFP and ADRP (Figure 13D). Expression of αSMA was detected in GFP^{+} cells in the primary septa and in GFP^{+} cells at the tip of the secondary septa (Figure 13 E). Quantification of the relative numbers of lineage labeled cells and different fibroblast subtypes was performed using cytospins at P9 (Figure 13 F). After the peak of secondary septation at P9 the lineage label GFP was expressed in 6.2±0.7% of all lung cells, ADRP-expressing cells represented 4.0±0.4% of all lung cell cells, αSMA was expressed in 3.2±0.4% of all lung cells (Figure 13 F). To reveal the contribution of early postnatal PDGFRα^{+} cells (positive at P1) to late alveolar lipofibroblast and myofibroblast populations, double-positive cells were quantified. The GFP^{+} cell population which also expressed ADRP represented 3.2±0.5% of all lung cells, the GFP^{+} cell population which also expressed αSMA represented 2.8±0.6% of all lung cells (Figure 13 F).

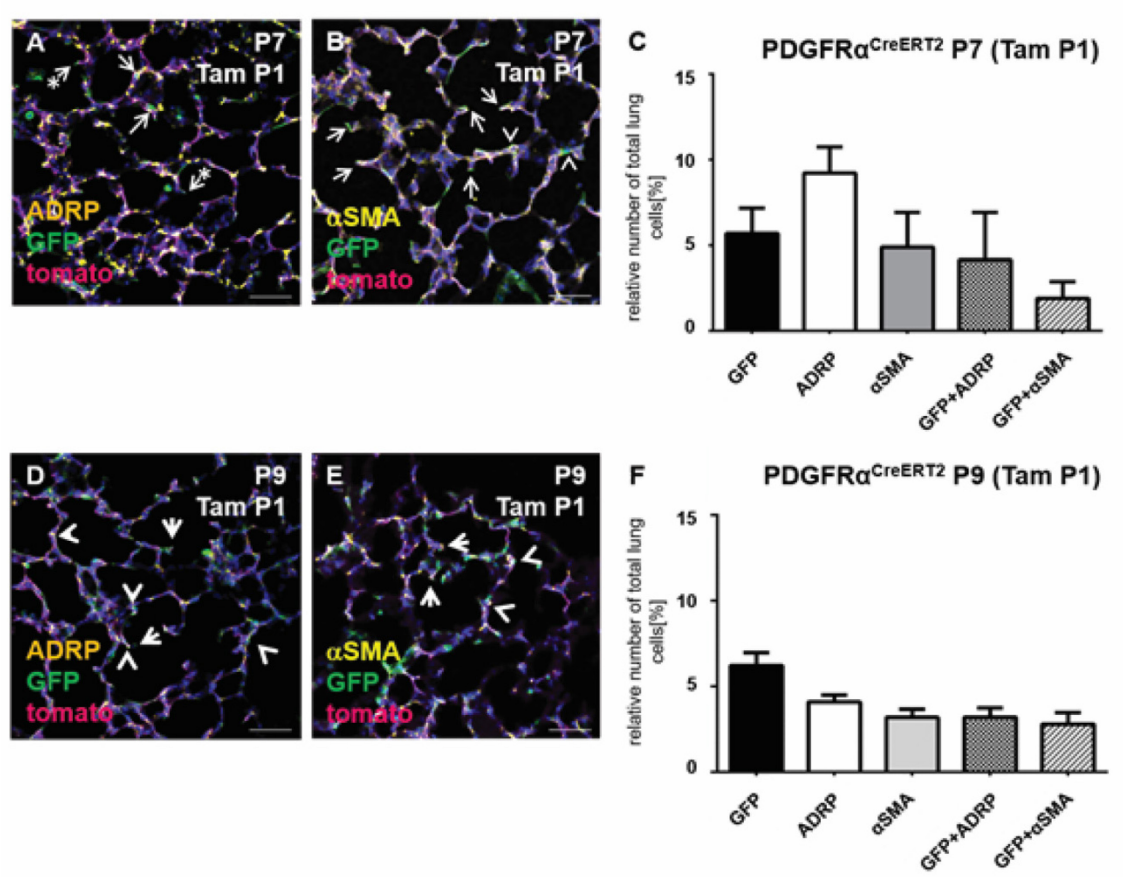

Figure 13 Lineage tracing of early postnatal platelet-derived growth factor receptor α^+ cells at the peak of alveolarization and after the peak of secondary septation using PDGFR$\alpha^{CreERT2}$mTmG mice.

Using tamoxifen (Tam) injection in PDGFR$\alpha^{CreERT2}$mTmG mice at postnatal day (P)1, platelet-derived growth factor receptor α^+ (PDGFRα^+) cells were permanently labeled due to constant expression of green fluorescent protein (GFP) (green). Non recombined cells kept the tomato signal (red). A 4', 6-diamidino-2-phenylindole nuclear stain (blue) was used for all the tissues. (A) At P7, PDGFRα expression (here GFP expression, green) co-localized with adipose differentiation related protein (ADRP) (orange) in the primary septa (arrows). Tip cells of the secondary crests expressed PDGFRα but not ADRP (arrow with asterisk). (B) At P7, PDGFRα co-localized with α-smooth muscle actin (αSMA) (yellow) in the tip cells of the secondary crests (arrows) and within the primary septa (arrowheads). Scale bar = 50 µm. (C) Bar graphs show mean values ± SEM of the relative numbers of lineage labeled cells (GFP$^+$) and of different fibroblast subtypes at P7 (n=7). (D) At P9 tip cells of the secondary crests (arrows) expressed GFP (green) but not ADRP (orange). The GFP signal co-localized with ADRP in cells of the primary septa and at the base of some secondary crests (arrowheads). (E) At P9 αSMA (yellow) co-localized with GFP (green) in tip cells of the secondary crests (arrows) and in cells of the primary septa (arrowheads). Scale bar = 50 µm. (F) Bar graphs show mean values ± SEM of the relative numbers of lineage labeled cells (GFP$^+$) and of different fibroblast subtypes at P9 (n=6).

3.2 Depletion of PDGFRα-expressing cells during early alveolarization

To analyze the functional impact of PDGFRα-expressing cells in alveolarization, PDGFRα-expressing cells were depleted using tamoxifen injection at P3 or P1 in PDGFR$\alpha^{CreERT2}$DTA mice. Cre-mediated

recombination led to constant expression of diphtheria toxin in PDGFRα-expressing cells. Lungs were analyzed using after the completion of secondary septation at P14 to quantify the amount of lineage cell depletion and the provoked impact on lung structure (Figure 14 and Figure 15). Single transgenic mice (DTA, PDGFRα^{CreERT2}) as well as double transgenic mice (PDGFRαCre^{ERT2}DTA) were analyzed using FACS for the relative numbers of PDGFRα^{+}cells in total lung cell suspension (Figure 14 A, B, C). Representative FACS zebra-plot analysis demonstrated a clear distribution of PDGFRα^{+} and PDGFRα^{-} cells compared to IgG control staining (Figure 14 A, B, C). The population of PDGFRα^{+} cells at P14 was reduced from 2.6±0.22% in control (non-depleted) PDGFRα^{CreERT2} mice, to 1.48±0.36% in PDGFRα^{CreERT2}DTA mice (n=3) after tamoxifen injection at P3 (Figure 14 D). This represents a reduction of 43.07% of PDGFRα^{+} cells. Histochemical staining of lung sections for elastin fibers was used to visualize lung structure (Figure 14 E and D). At first view, strong changes in lung structure were not observed in PDGFRα^{+}cell depleted (PDGFRα^{CreERT2}DTA mice, Figure 14 F) versus control lungs (PDGFRα^{CreERT2}, Figure 14 E). Airspaces and alveolar wall thickness appeared not to be different. However, secondary septum formation with elastin deposition at the tip cell was less evident in PDGFRα^{+}cell depleted (Figure 14 F) versus control lungs (Figure 14 E) Since the previous findings suggested a mild impact on lung structure was observed when PDGFRα^{+} cells were depleted at P3, an earlier time-point (P1) was chosen to deplete PDGFRα^{+} cells (Figure 15). Control pubs demonstrated a normal growth and maturation, PDGFRα^{+} cell depleted mice appeared weak and less active. Therefore all mice were analyzed at P5 (Figure 15) Representative FACS zebra-plot analysis demonstrated a clear distribution of PDGFRα^{+} and PDGFRα^{-} cells compared to IgG control staining (Figure 15 A,B,C). Again, the evidence for the depletion of PDGFRα^{+} cells was clearly demonstrated. The population of PDGFRα^{+} cells was reduced from 5.47±0.48% to 2.03±0.2% of all lung cells when measured at P5 in PDGFRα^{CreERT2}DTA mice comparing to PDGFRα^{CreERT2} mice (Figure 15 D). This represents a reduction of 62.89% of PDGFRα^{+} cells. This time, histochemical staining of lung sections for elastin fibers revealed a change in lung structure in PDGFRα^{+} cell depleted (PDGFRα^{CreERT2}DTA mice, Figure 15 F) versus control lungs (PDGFRα^{CreERT2} mice, Figure 15 E). Lungs from three PDGFRα^{+} cell depleted mice demonstrated a moderate emphysema-like phenotype with thinner alveolar septal walls, broader alveolar airspaces and again secondary septa with elastin deposition at the tip cells were less evident compared to control lungs (Figure 15 E, F). Elastin fibers were abundant in PDGFRα^{+} cell depleted lungs and control lungs, however, the distribution of elastin fibers was changed in PDGFRα^{+} cell depleted lungs

since secondary septa were less abundant (Figure 15 E, F) Taken together depletion of PDGFRα^+ cells during early postnatal days affected the process of alveolarization. Depletion at P3 caused a mild lung phenotype with lungs demonstrating less prominent secondary septa at P14 (Figure 14 E, F). Depletion at P1 caused an emphysema-like lung phenotype which seemed to affect the activity of postnatal pups (Figure 14 E, F).

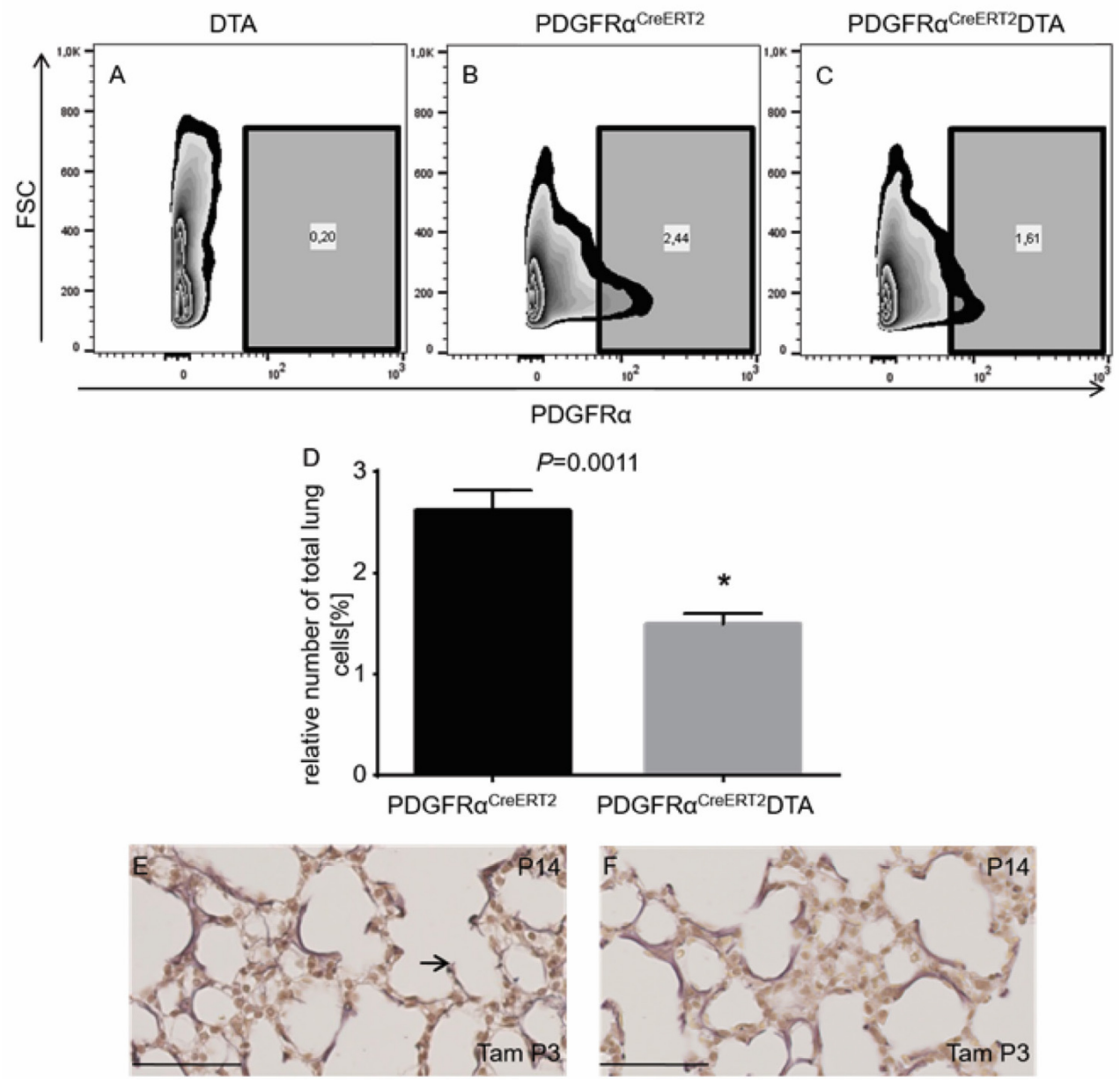

Figure 14 Depletion of platelet-derived growth factor receptor α⁺ cells at postnatal day 3 using PDGFRα^{CreERT2}DTA mice.

Using tamoxifen (Tam) injection, platelet-derived growth factor receptor α⁺ (PDGFRα⁺) cells were depleted by diphtheria toxin A (DTA) expression at postnatal day (P)3 lungs were analyzed at P14. (A-C) Representative fluorescence-activated cell sorting (FACS) plot analysis for PDGFRα⁺ and PDGFRα cells. FCS: forward scatter. (D) Quantification of PDGFRα⁺ cells showed evidence of depletion of PDGFRα⁺ cell by 43.07% in PDGFRα^{CreERT2}DTA mice comparing to PDGFRα^{CreERT2} mice (n=3). Bar graphs show mean values ± SEM of PDGFRα⁺ cells in PDGFRα^{CreERT2}DTA mice. Statistical significance between the groups of PDGFRα^{CreERT2}DTA and PDGFRα^{CreERT2} mice was estimated using the unpaired Student's t test (n=3 per group). (E-F) Histochemical stainings for elastin fibers of tissue sections of PDGFRα^{CreERT2} (E) and PDGFRα^{CreERT2}DTA (F) mice at P14 demonstrated a mild lung phenotype upon depletion of PDGFRα⁺cells at P3. Secondary septa with elastin deposition at the tip (arrow in E) were less evident in PDGFRα^{CreERT2}DTA mice (F) comparing to PDGFRα^{CreERT2}mice (E). Scale bar = 100 μm.

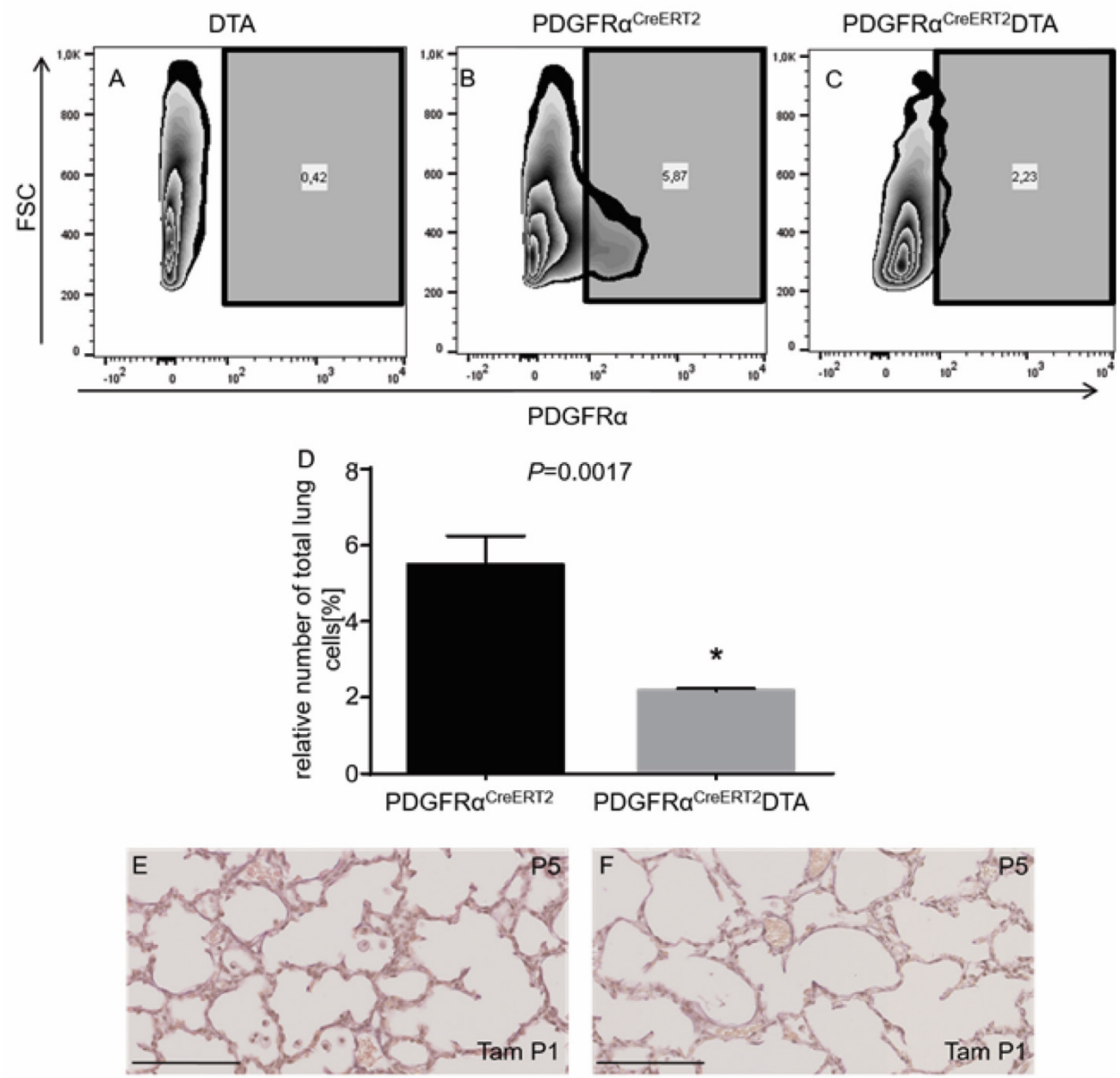

Figure 15 Depletion of platelet-derived growth factor receptor α^+ cells at postnatal day 1 using PDGFR$\alpha^{CreERT2}$DTA mice.

Using tamoxifen (Tam) platelet-derived growth factor receptor α^+ (PDGFRα^+) cells were depleted by diphtheria toxin A (DTA) expression at postnatal day (P)1, lugs were analyzed at P5. (A-C) Representative fluorescence-activated cell sorting (FACS) plot analysis for PDGFRα^+ and PDGFRα^- cells. FCS: forward scatter. (D) Quantification of PDGFRα^+ cells showed evidence of depletion of PDGFRα^+ cell by 62.89% in PDGFR$\alpha^{CreERT2}$DTA mice comparing to PDGFR$\alpha^{CreERT2}$ mice (n=3). Bar graphs show mean values ± SEM of PDGFRα^+ cells in PDGFR$\alpha^{CreERT2}$DTA mice. Statistical significance between the groups of PDGFR$\alpha^{CreERT2}$DTA and PDGFR$\alpha^{CreERT2}$ mice was estimated using the unpaired Student's t test (n=3 per group). (E-F) Histochemical stainings for elastin fibers of tissue sections of PDGFR$\alpha^{CreERT2}$ (E) and PDGFR$\alpha^{CreERT2}$DTA (F) mice at P5 demonstrated an emphysema-like lung phenotype (F) upon depletion of PDGFRα^+cells at P1. Secondary septa with elastin deposition at the tip were less evident in PDGFR$\alpha^{CreERT2}$DTA mice (F) comparing to PDGFR$\alpha^{CreERT2}$mice (E). Scale bar = 100 μm.

3.3 Validation and characterization of a newly generated inducible Cre mouse line to target lipofibroblasts

3.3.1 Validation of mRNA expression of CreERT2, mCherry and Cre-recombination driven GFP

Since the role of lipofibroblasts in alveolarization is not well understood, a new Cre-driver mouse line to target lipofibroblasts (the Plin2$^{tm1.1(Cre/ERT2)Mort}$ mouse) has been generated recently (2.2.2.1). Series of characterization experiments were performed using the Plin2$^{tm1.1(Cre/ERT2)Mort}$ mouse line. To evaluate the specificity of the knock in system, mRNA expression levels of four genes of interest were measured by qPCR (Figure 16). The different genes were ADRP as marker for lipofibroblasts, mCherry and Cre-recombinase that were parts of the transgenic insert after the ADRP promoter in Plin2$^{tm1.1(Cre/ERT2)Mort}$ mice and GFP as evidence of the recombination upon tamoxifen administration in Plin2$^{tm1.1(Cre/ERT2)Mort}$mTmG mice. All mice were analyzed at P14. Only Plin2$^{tm1.1(Cre/ERT2)Mort}$mTmG mice were injected at P1 using tamoxifen. All mice demonstrated expression of ADRP. The transgenes Cre-recombinase and mCherry were amplified in Plin2$^{tm1.1(Cre/ERT2)Mort}$mTmG and Plin2$^{tm1.1(Cre/ERT2)Mort}$ mice and not in wild type nor mTmG mice. Expression of GFP was restricted in Plin2$^{tm1.1(Cre/ERT2)Mort}$mTmG mice. To calculate ΔCt values the amplification of glyceraldehyde 3-phosphate dehydrogenase (GADPH) gene was measure at for every sample and Ct values higher than 30 cycles were not taken into consideration.

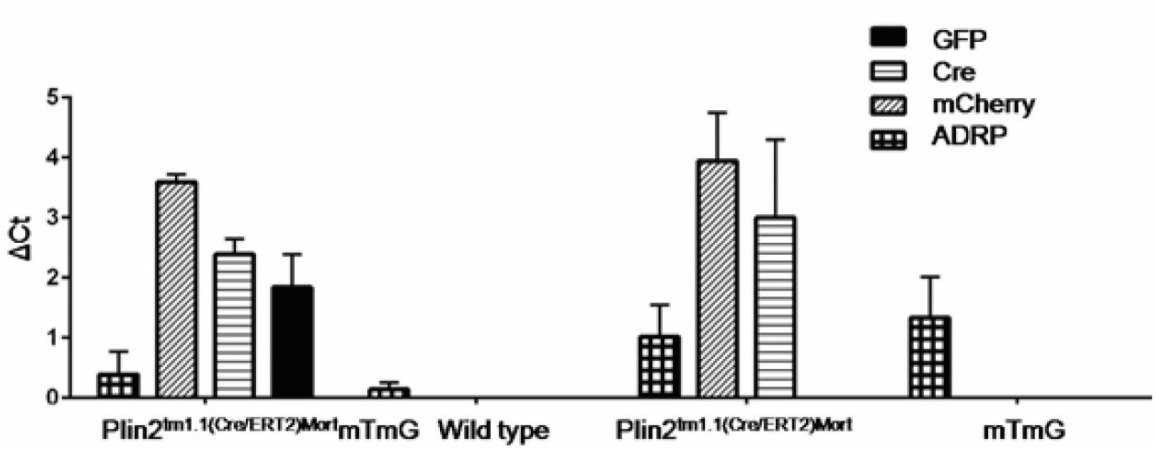

Figure 16 Specific expression of transgenes after tamoxifen injection.

After tamoxifen administration at postnatal day (P)10 mice from four different mouse lines were analyzed on P14. The transgenes Cre-recombinase (Cre) and mCherry were amplified in Plin2$^{tm1.1(Cre/ERT2)Mort}$mTmG and Plin2$^{tm1.1(Cre/ERT2)Mort}$ mice and not in wild type or mTmG. The endogenous locus for the adipose differentiation related protein (ADRP) was amplified in all the mice, meanwhile green fluorescent protein (GFP) expression was observed only in Plin2$^{tm1.1(Cre/ERT2)Mort}$mTmG mice. The estimation of ΔCt was performed using glyceraldehyde 3-phosphate dehydrogenase as a reference gene. Bar graphs show mean values ± SEM (n=3-5 per group). Ct values exceeding 30 were not considered in the analysis.

3.3.2 Validation of inducible activation of Cre-recombination driven GFP reporter gene expression

The confirmation of inducible Cre-recombinase activity was demonstrated analyzing Plin2$^{tm1.1(Cre/ERT2)Mort}$mTmG and mTmG mice 24 h and 48 h after tamoxifen injection (Figure 17). Cells from the total lung homogenate were labeled for the non-mesenchymal populations using PECAM, CD45 and EpCAM as exclusion markers. The relative numbers of GFP$^+$ cells were quantified by FACS. Expression of GFP was demonstrated in the mesenchymal and the non-mesenchymal populations already at 24 h after tamoxifen injection (Figure 17 C, E). The relative number of GFP$^+$ cells increased from ≈1.5% 24 h after injection of tamoxifen to ≈6% 48 h after tamoxifen injection (Figure 17 E) and in the mesenchymal population of GFP$^+$ cells from ≈2% to ≈6% accordingly (Figure 17 F). There was no GFP expression in control mTmG mice, neither 24 h nor 48 h after treatment.

To demonstrate specific activation of Cre-recombination upon tamoxifen injection, Plin2$^{tm1.1(Cre/ERT2)Mort}$mTmG mice were analyzed at P14 with (Figure 18 A-C) and without (Figure 18 D-F) tamoxifen injection at P1 tamoxifen. There was evidence of Cre-mediated recombination (represented by GFP expression) in interstitial cells from Plin2$^{tm1.1(Cre/ERT2)Mort}$mTmG

mouse lungs upon tamoxifen injection (Figure 18A and C) and not without tamoxifen injection (Figure 18 D, F). Non recombined cells kept the tomato signal (Figure 18 B, C, E, F).

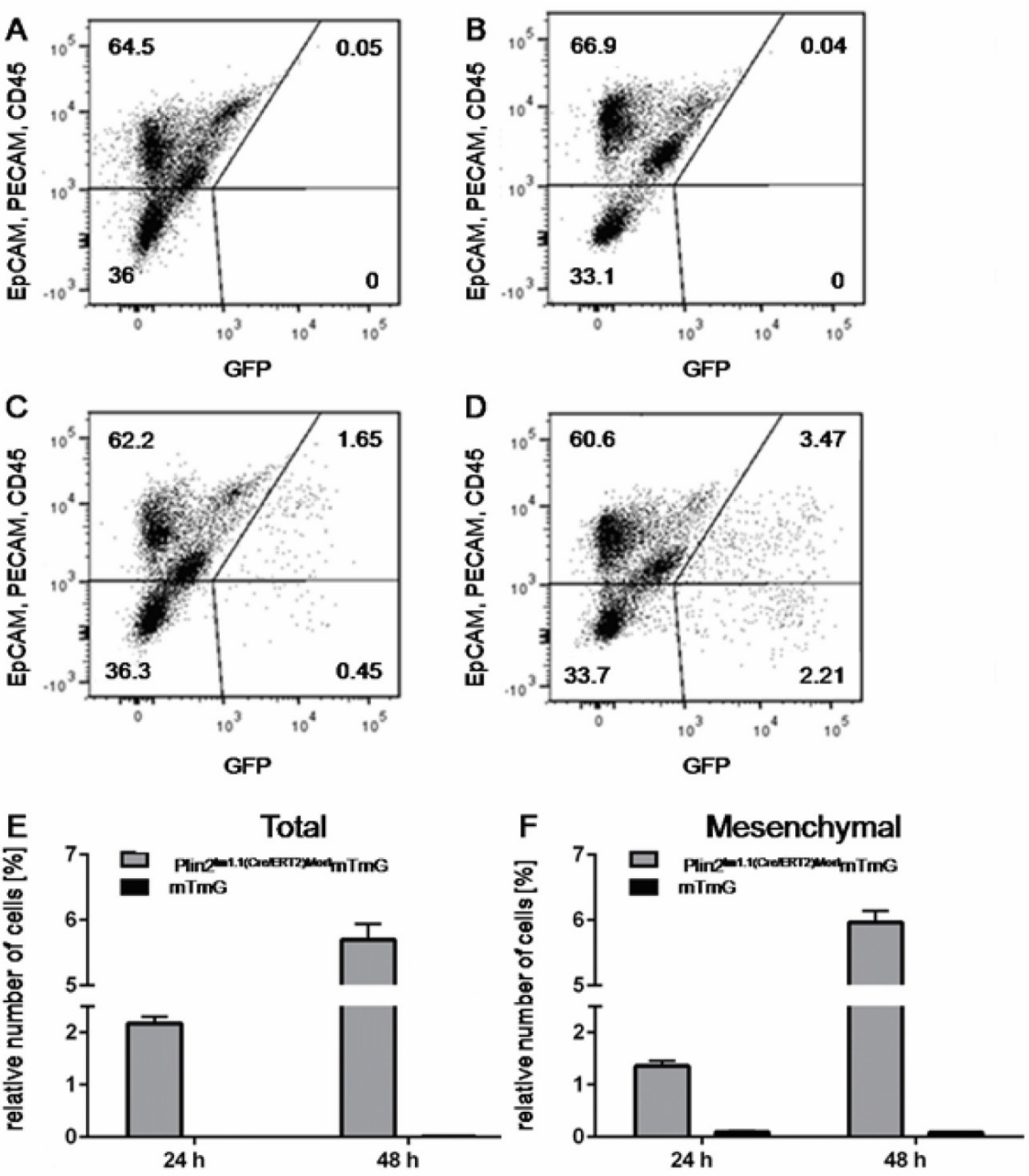

Figure 17 Relative number of green fluorescent protein-expressing cells due to Cre-mediated recombination 24 h and 48 h after tamoxifen injection.

After 24 h and 48 h from tamoxifen injection at postnatal day (P)10, Plin2$^{tm1.1(Cre/ERT2)Mort}$mTmG and mTmG mice were analyzed and the number of green fluorescent protein^{+} (GFP^{+}) cells was quantified by fluorescence-activated cell sorting (FACS). (A-D) Representative dot plot images from total lung cell suspension of mTmG mice (A, B) and Plin2$^{tm1.1(Cre/ERT2)Mort}$mTmG mice (C, D) 24 h (A,C) and 48 h (B,D) after tamoxifen injection. (E, F) Relative numbers of GFP^{+} cells from total lung homogenate (E) or from the mesenchymal cell population (F) 24 h and 48 h after tamoxifen injection in Plin2$^{tm1.1(Cre/ERT2)Mort}$mTmG (grey) and mTmG (black) mice (n=3 per group). Bar graphs show mean values ± SEM.

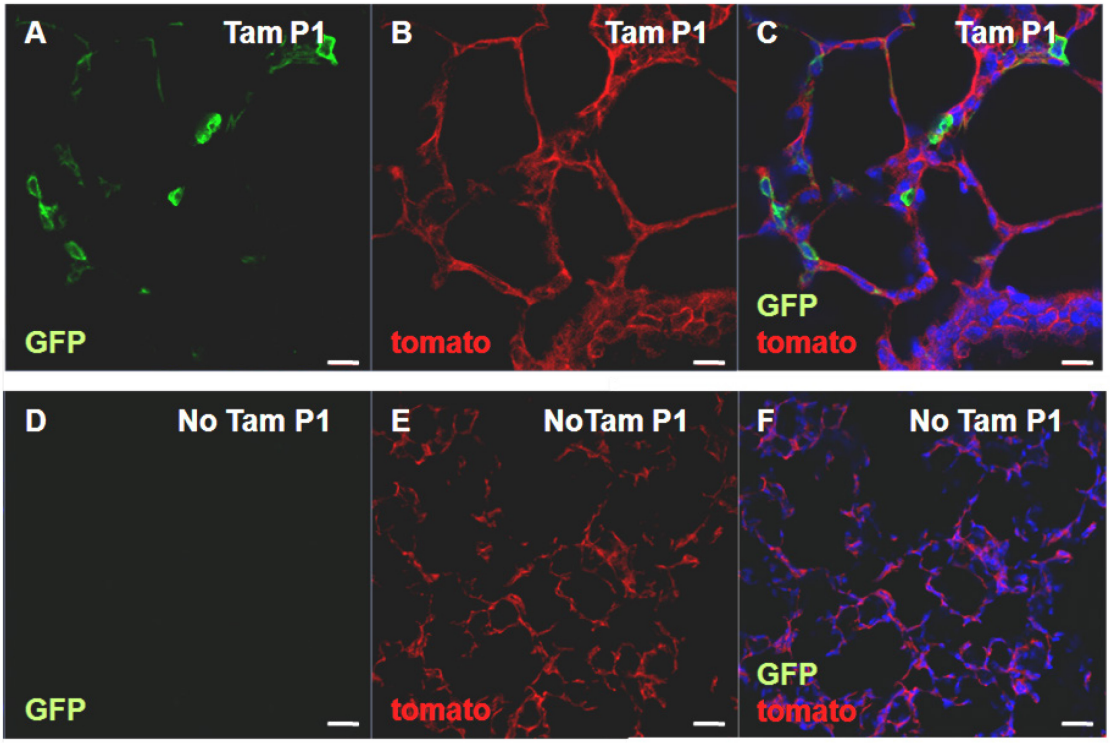

Figure 18 Expression of green fluorescent protein with and without tamoxifen injection at postnatal day 1 in Plin2$^{tm1.1(Cre/ERT2)Mort}$mTmG mice at postnatal day 14.

Cells expressing the *Plin2* gene at P1, permanently expressed the reporter gene green fluorescent protein (GFP) due to Cre-mediated recombination. A 4', 6-diamidino-2-phenylindole nuclear stain (blue) was used for all the tissues. (A-C) Plin2$^{tm1.1(Cre/ERT2)Mort}$mTmG mice received tamoxifen (Tam) injection at P1, analysis was performed at P14. The lineage label GFP (green) was expressed in interstitial cells (A, C) non recombined cells kept the tomato signal (red, B, C). Plin2$^{tm1.1(Cre/ERT2)Mort}$mTmG mice without Tam injection did not express GFP (D-F). Scale bar = 50 µm.

3.3.3 Characterization of lineage traced cells

Since a specific labeling of ADRP-expressing cells at P14 was demonstrated after Tam injection at P1 using the previously newly generated Plin2$^{tm1.1(Cre/ERT2)Mort}$ line, it was questioned whether the targeted cells represent lipofibroblasts. Therefore, GFP$^+$ cells were analyzed for the expression of fibroblast makers such as ADRP, αSMA and PDGFRα (Figure 19, isotype controls in Figure 37). Cells of the ADRP lineage of P1 (GFP$^+$ cells) were distributed in the interstitial alveolar and peribronchial regions of the lung at P14 (Figure 19 A, C, E). Most of the ADRP-expressing cells were lineage traced and expressed the lineage label GFP (Figure 19 A, B). Single GFP$^+$ and ADRP$^-$ cells were also demonstrated (Figure 19 A, B). Peribronchial spindle shaped GFP$^+$ cells were located in close proximity to

αSMA-expressing cells (Figure 19 C, D) Some alveolar GFP^+ cells expressed PDGFRα, peribronchial GFP^+ cells were in close proximity to peribronchial $PDGFR\alpha^+$ cells (Figure 19 E, F). To further investigate the fibroblast nature of GFP^+ cells, immunostaining against collagen I and vimentin was performed (Figure 20 A, B, E, F, isotype controls in Figure 37). Both markers were expressed in GFP^+ cells, however, cells expressing vimentin or collagen I without expressing GFP were also demonstrated (Figure 20 A, B, E, F). Since ADRP expression previously has been reported in macrophages, it was questioned, if GFP^+ cells in the lung express a leucocyte marker such as CD45. Some GFP^+ cells expressed CD45, $CD45^+$ GFP^- cells were located in close proximity to GFP^+ cells (Figure 20 C, D).

3.3.4 Expression of the lineage label in further organs

Expression of ADRP is also found in other organs such as the heart, the liver and the spleen. To confirm the labeling and abundance of this cell population, postnatal tissues from heart, liver and spleen were stained for ADRP at P14 from $Plin2^{tm1.1(Cre/ERT2)Mort}$mTmG mice that had received tamoxifen at P1 (Figure 21, isotype controls in Figure 37). There was evidence of lineage traced GFP^+ cells in the heart, the liver and the spleen (Figure 21 A-F). Some GFP^+ cells in all three organs expressed ADRP (Figure 20 A-F).

3.3.5 Quantification of lineage labeled cells and fibrobast subtypes in the postnatal lung

Proceeding with the quantification of lineage traced ADRP-expressing cells of P1 (day of tamoxifen injection), FACS analysis for from total lung homogenate of $Plin2^{tm1.1(Cre/ERT2)Mort}$mTmG mice and mTmG mice at P14 was performed (Figure 22). Representative FACS histograms demonstrated a clear GFP^+ cell population in $Plin2^{tm1.1(Cre/ERT2)Mort}$mTmG mice (Figure 22 B) which was lacking in mTmG control mice (Figure 22 A). The lineage label GFP was expressed in 9.5±0.54% of total lung cells in $Plin2^{tm1.1(Cre/ERT2)Mort}$mTmG mice, n=3 (Figure 22 C). To reveal the amount of fibroblast subtypes such as lipofibroblasts and myofibroblasts which were targeted after lineage tracing, antibody staining against ADRP, PDGFRα and αSMA was performed (Figure 22 C). All $ADRP^+$ cells represented 9±0.47% from total lung cells, $PDGFR\alpha^+$ cells 6%±0.51% and αSMA^+ cells 3±0.08% (Figure 22 C). Double-positive cells which also expressed the lineage label GFP represented 7±0.42% $ADRP^+$ and GFP^+, 4±0.06%,

GFP$^+$ and PDGFRα$^+$ and 1.5±0.05% GFP$^+$ and αSMA$^+$ from total lung cells (Figure 22 C). The data demonstrated that ≈78% of all ADRP$^+$ cells expressed the lineage label GFP and ≈74% of all GFP$^+$ cells expressed ADRP. Representative FACS dot plats demonstrated a clear separation of lineage traced cells and fibroblast subtypes expressing ADRP, PDGFRα or αSMA (Figure 22 D-F).

3.3.6 Validation of the *Plin2* promoter-driven knock in reporter gene mCherry expression

To investigate the expression of the reporter mCherry gene, driven by the *Plin2* promoter, it was important to prove that the recently generated mouse strain could label lipofibroblasts as validated by ADRP antibody staining. Lung tissue sections from Plin2$^{tm1.1(Cre/ERT2)Mort}$ mice were analyzed at P14 after immunostaining against fibroblast markers. Cells positive for mCherry (mCherry$^+$ cells) were located in the alveolar walls and peribronchially (Figure 23 A-F, isotype controls in Figure 38). Most of mCherry$^+$ cells expressed ADRP (Figure 23 A, B). A few mCherry$^+$ cells of the alveolar regions expressed αSMA (Figure 23 C, D). Most of the mCherry-expressing cells expressed PDGFRα (Figure 23 E, F). To address the mesenchymal and fibroblast feature of mCherry$^+$ cells, immunostaining against collagen I and vimentin was performed in lung tissue sections from Plin2$^{tm1.1(Cre/ERT2)Mort}$ mice at P14. Since ADRP expression previously has been reported in macrophages immunostaining against CD45 was accomplished (Figure 24 A-F). All mCherry$^+$ cells expressed collagen I, however, collagen I$^+$ but mCherry$^-$ cells were also observed (Figure 24 A, B, isotype controls in Figure 38). Vimentin was expressed in all mCherry$^+$ cells, mCherry$^-$ but vimentin$^+$ cells were also detected (Figure 24 E, F) The leucocyte marker CD45 was expressed in some mCherry$^+$ cells, mCherry$^-$ but CD45$^+$ cells were located in close proximity to mCherry$^+$ cells (Figure 24 C,D). The expression of mCherry in the heart, the liver and the spleen was analyzed together with the expression of ADRP using immunostaining against ADRP (Figure 25, isotype controls in Figure 358). In the heart mCherry was expressed in a notably amount of cells, some mCherry$^+$ cells expressed ADRP (Figure 25 A, B) In the liver, all cells expressed ADRP, some mCherry$^+$ cells expressed ADRP (Figure 25 C, D) Few cells of the spleen expressed mCherry, the minority of mCherry$^+$ cells expressed ADRP (Figure 25 E, F).

Taken together, the *Plin2* promoter-driven reporter gene mCherry was robustly expressed in pulmonary cells which were of mesenchymal and fibroblast nature, few mCherry$^+$ cells demonstrated

immune cell character. All Cherry^{+} cells demonstrated lipofibroblast features, some expressed PDGFRα, few mCherry^{+} cells appeared to be of myofibroblast nature. Furthermore, mCherry was also expressed in the heart, liver and spleen.

3.3.7 Quantification of the knock in reporter gene mCherry-expressing cells in the lung

Relative numbers of pulmonary cells expressing the *Plin2* promoter-driven reporter gene mCherry and cells of different fibroblast populations were obtained using FACS measurement of total lung cells of Plin2$^{tm1.1(Cre/ERT2)Mort}$ mice after immunostaining against ADRP, PDGFRα and αSMA at P14 (Figure 26) representative histograms demonstrated a clear population of mCherry-expressing cells which was lacking in wild type mice (Figure 26 A,B) The distribution of analyzed cell type at P14 was 11.84±1.17% mCherry^{+} cells, 12.02±0.96% ADRP^{+} cells, 6.13±0.35% PDGFRα^{+} cells and 0.61±0.08% αSMA^{+} cells (Figure 26 C). Double-positive cells, expressing mCherry and a further fibroblast marker were 10.73±0.38% mCherry^{+} and ADRP^{+} cells, 4.17±0.25% mCherry^{+} and PDGFRα^{+} cells and 0.22±0.01% mCherry^{+} and αSMA^{+} cells (Figure 26C). Notably ≈89% of all ADRP^{+} cells expressed mCherry and ≈91% of all mCherry^{+} cells expressed ADRP.

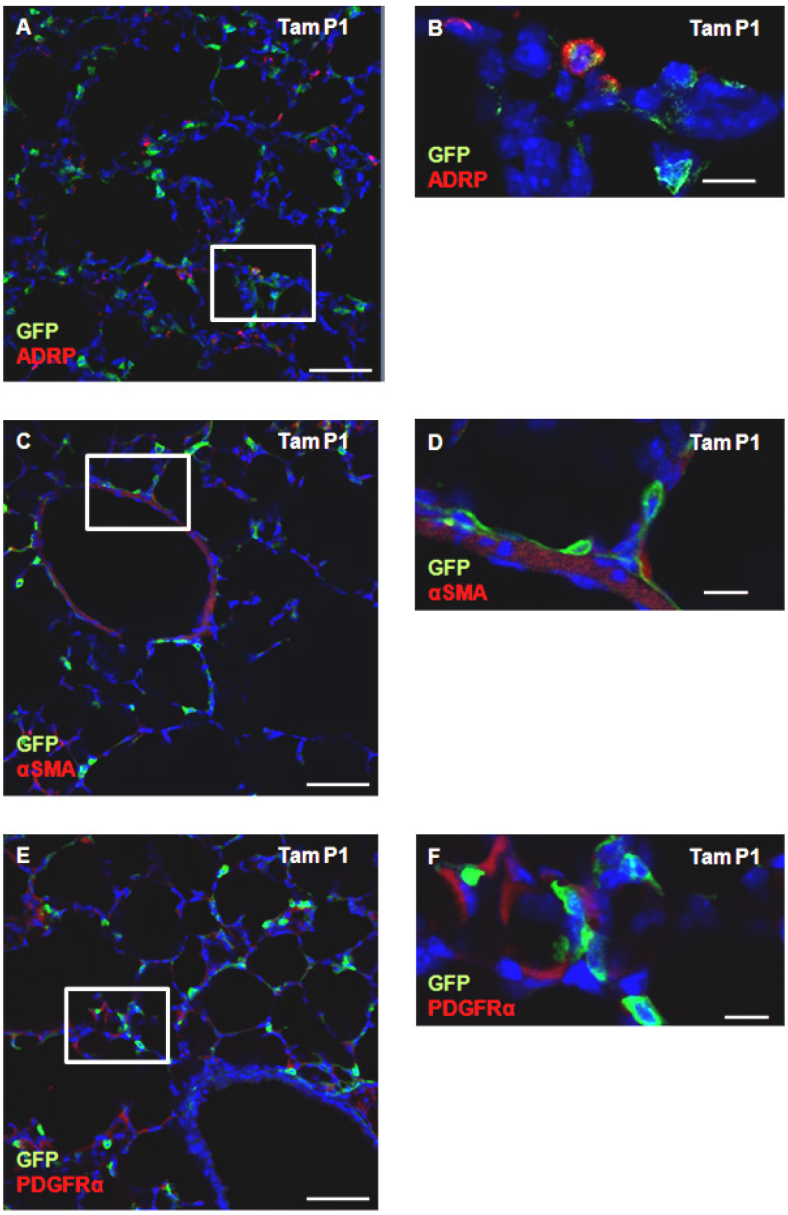

Figure 19 Expression of fibroblast markers and green fluorescent protein in lungs of Plin2$^{tm1.1(Cre/ERT2)Mort}$mTmG mice at postnatal day 14, adipose differentiation related protein-expressing cells were labeled at postnatal day 1.

Lineage traced cells and their progeny expressing green fluorescent protein (GFP) (green) after Cre-mediated recombination at postnatal day (P)1 in all adipose differentiation related protein (ADRP)-expressing cells were stained at P14 against the fibroblast subtypes markers ADRP (red), α-smooth muscle actin (αSMA) (red), platelet-derived growth factor receptor (PDGFR) α (red), followed by a 4', 6-diamidino-2-phenylindole nuclear stain (blue). (A-F) Cells expressing GFP were abundant in the interstitial regions of the alveoli, some GFP$^+$ cells were located in the peribronchial regions. Most of the ADRP$^+$ cells expressed the lineage label GFP, GFP$^+$ but ADRP$^-$ cells were also demonstrated (A, B). Peribronchial GFP$^+$ cells were located in close proximity to αSMA-expressing cells (C, D). Some alveolar GFP$^+$ cells expressed PDGFRα, peribronchial GFP$^+$ cells were located in close proximity to peribronchial PDGFRα$^+$ cells (E, F). Tam = tamoxifen. (A, C, E) Scale bar = 50 µm. (B, D, F represent inserts of A, C, E). Scale bar = 20 µm.

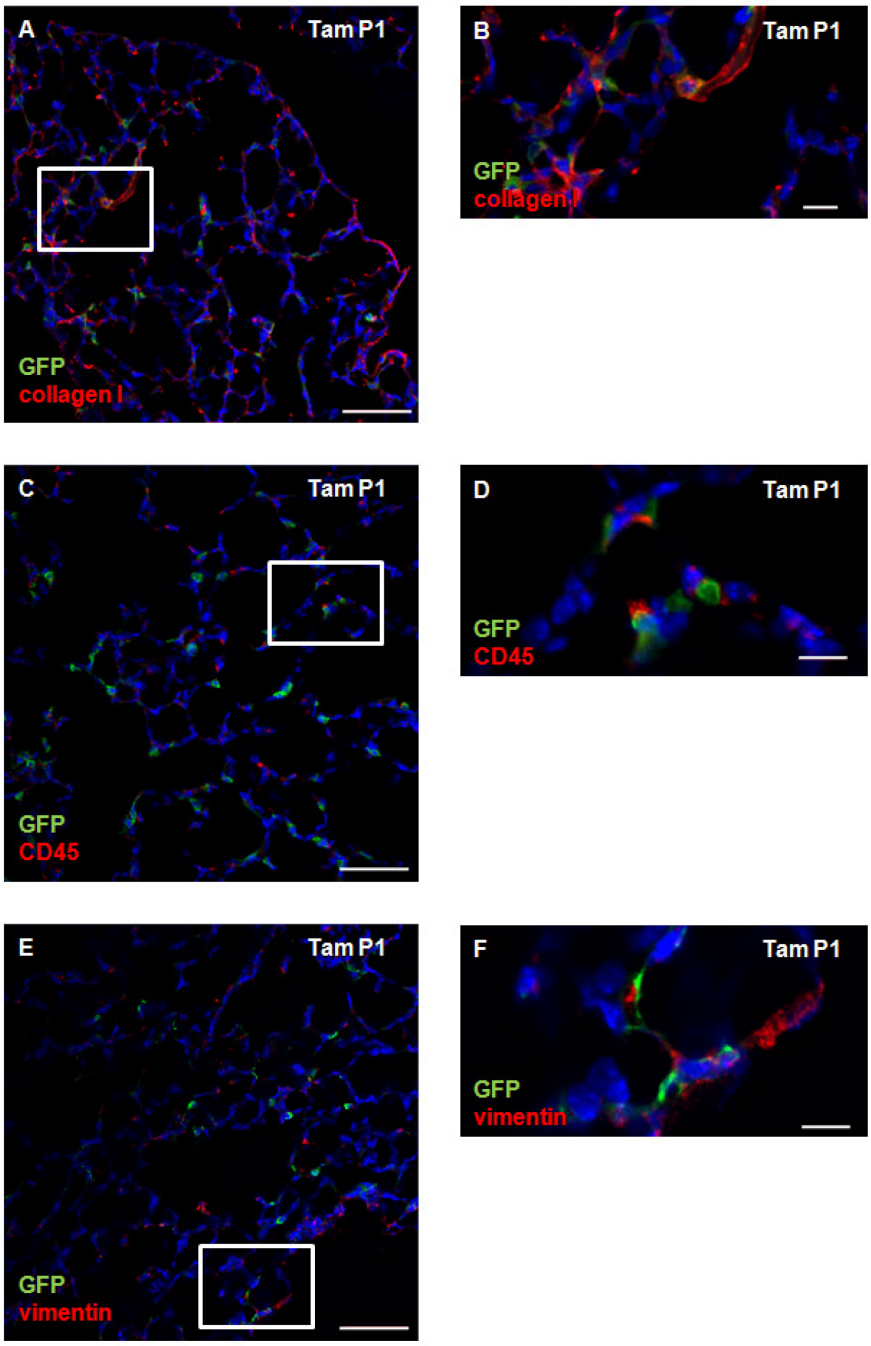

Figure 20 Expression at postnatal day 14 of the lineage label green fluorescent protein and markers for connective tissue, leucocytes and mesenchymal markers in lungs of Plin2$^{tm1.1(Cre/ERT2)Mort}$mTmG mice, adipose differentiation related protein-expressing cells were labeled at postnatal day 1.

(A, B) Cells expressing green fluorescent protein (GFP) (green) expressed collagen I (red), collagen I^{+} but GFP^{-} cells were also demonstrated. (C, D) The leucocyte marker CD45 (red) was expressed in alveolar GFP^{+} CD45^{+} but GFP^{-} cells were located in close proximity to GFP^{+} cells. (E, F) The fibroblast marker vimentin was expressed in GFP^{+} cells, vimentin^{+} but GFP^{-} cells were also demonstrated. A 4', 6-diamidino-2-phenylindole nuclear stain (blue) was used at all tissue sections. Tam = tamoxifen. (A, C, E) Scale bar = 50 µm. (B, D, F represent inserts of A, C, E). Scale bar = 20 µm.

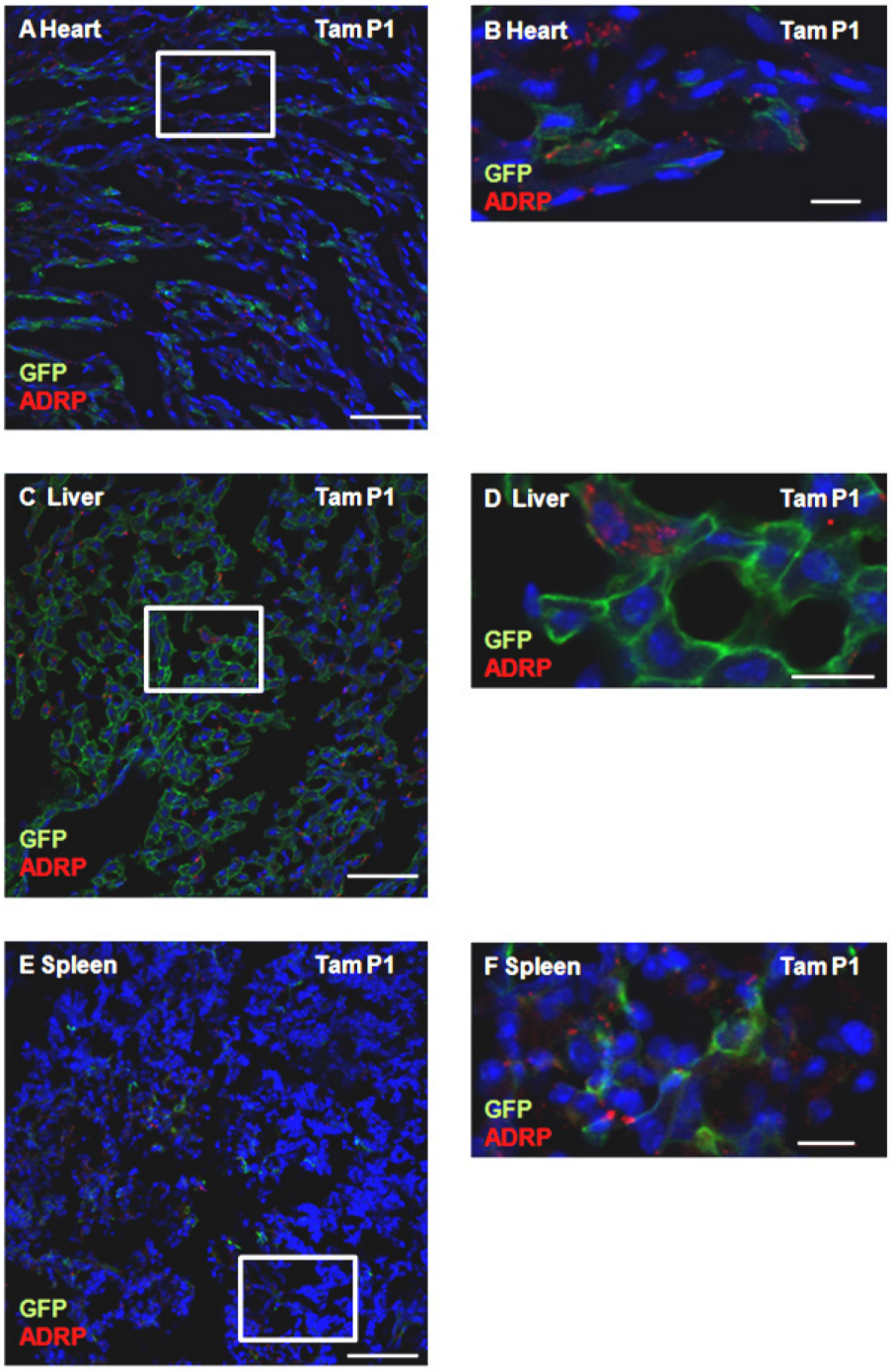

Figure 21 Expression of green fluorescent protein in the heart, the liver and the spleen of Plin2$^{tm1.1(Cre/ERT2)Mort}$mTmG mice at postnatal day 14, adipose differentiation related protein-expressing cells were labeled at postnatal day 1.

(A-F) Immunostaining against adipose differentiation related protein (ADRP) (red), lineage label green fluorescent protein (GFP) (green). A 4', 6-diamidino-2-phenylindole nuclear stain (blue). In the heart, GFP$^+$ cells were demonstrated, some GFP$^+$ cells expressed ADRP (A, B). In the liver, most of the cells expressed GFP, and some GFP$^+$ cells expressed ADRP (C, D). In the spleen few cells expressed GFP, and some GFP$^+$ cells expressed ADRP (E, F). Tam = tamoxifen. (A, C, E) Scale bar = 50 μm. (B, D, F represent inserts of A, C, E). Scale bar = 20 μm.

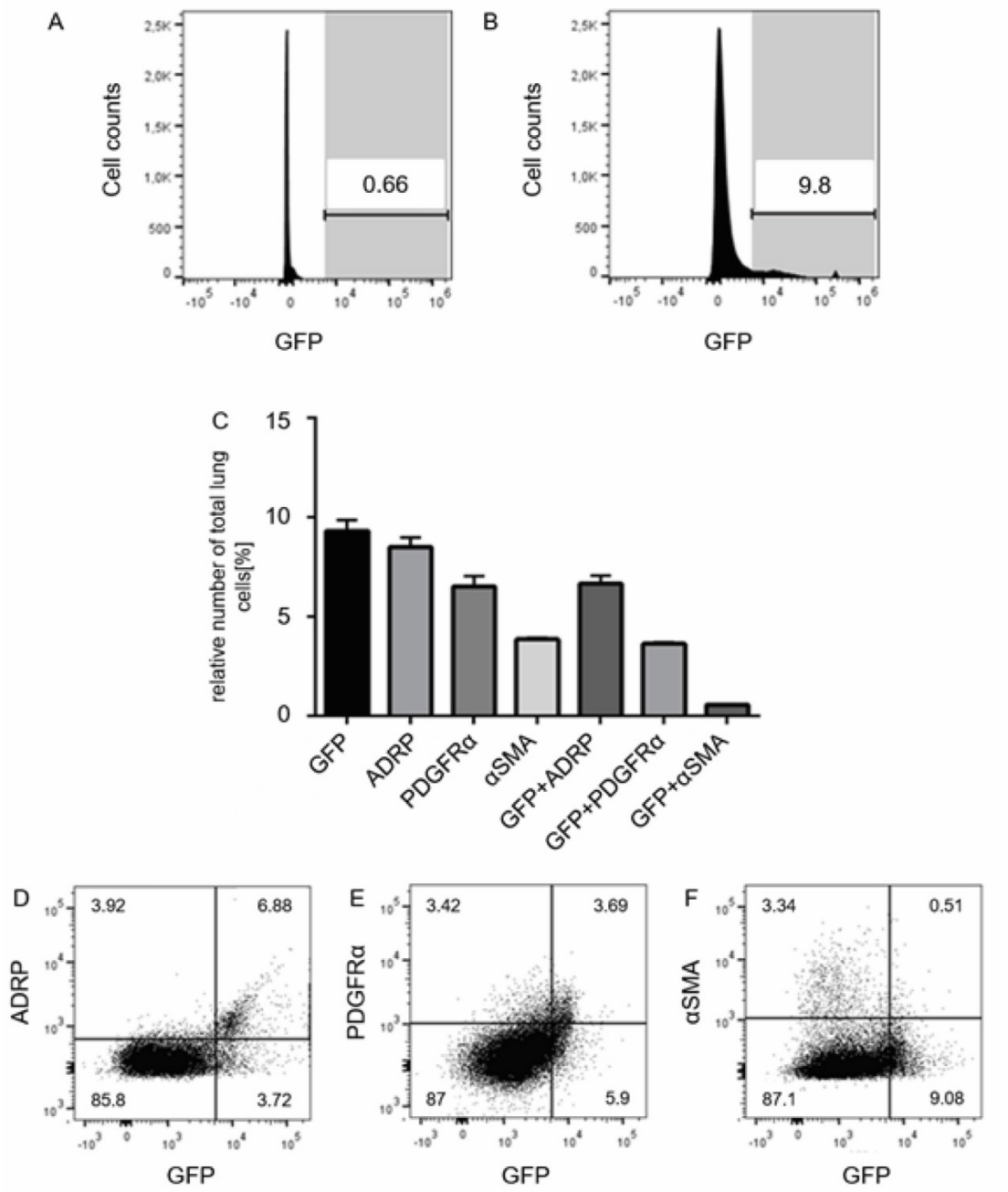

Figure 22 Quantification of lineage labeled cells at postnatal day 1 analyzing Plin2$^{tm1.1(Cre/ERT2)Mort}$mTmG mice at postnatal day 14.

Tamoxifen was injected at postnatal day (P)1, Plin2$^{tm1.1(Cre/ERT2)Mort}$mTmG mice were analyzed at P14. (A-B) Representative fluorescence-activated cell sorting (FACS) histograms demonstrating the percentage of green fluorescent protein^{+} (GFP^{+}) cells from total cells of lung homogenate in mTmG (A) and Plin2$^{tm1.1(Cre/ERT2)Mort}$mTmG (B) mice. (C) Bar graphs show mean values ± SEM of the relative numbers of GFP^{+} cells, of different fibroblast subtypes and of fibroblast subtypes expressing the lineage label GFP, in Plin2$^{tm1.1(Cre/ERT2)Mort}$mTmG mice at P14 (n=3). (D-F) Representative dot plots of the different fibroblast subtypes in relation to GFP^{+} cells.

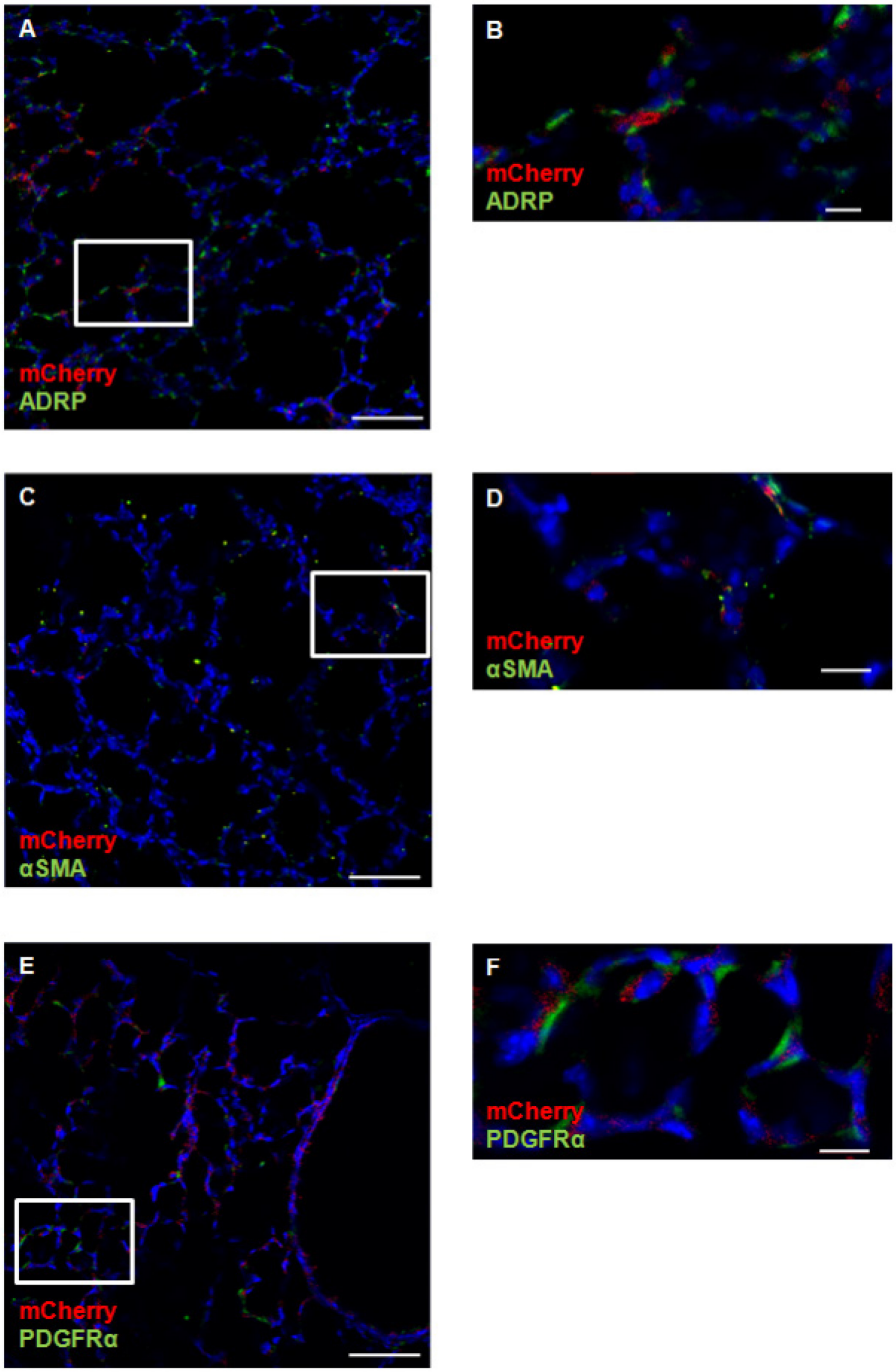

Figure 23 Expression of fibroblast markers and the *Plin2* promoter-driven knock in reporter gene mCherry in lungs of Plin2$^{tm1.1(Cre/ERT2)Mort}$ mice at postnatal day 14.

The reporter gene mCherry (red) and the fibroblast subtypes markers adipose related protein (ADRP) (green), α smooth muscle actin (αSMA, green), platelet-derived growth factor receptor (PDGFR)α (green) were expressed in lungs of Plin2$^{tm1.1(Cre/ERT2)Mort}$ mice at P14.. (A-F) Abundance of mCherry^{+} cells was observed in alveolar walls and peribronchially. Most of the mCherry^{+} cells expressed ADRP (A, B). Few mCherry^{+} cells in the alveolar walls expressed αSMA (C, D). Most of the mCherry^{+} cells expressed PDGFRα (E, F). A 4', 6-diamidino-2-phenylindole nuclear stain (blue) was used at all tissue sections. (A, C, E). Scale bar = 50 µm. (B, D, F inserts of A, C, E respectively). Scale bar = 20 µm.

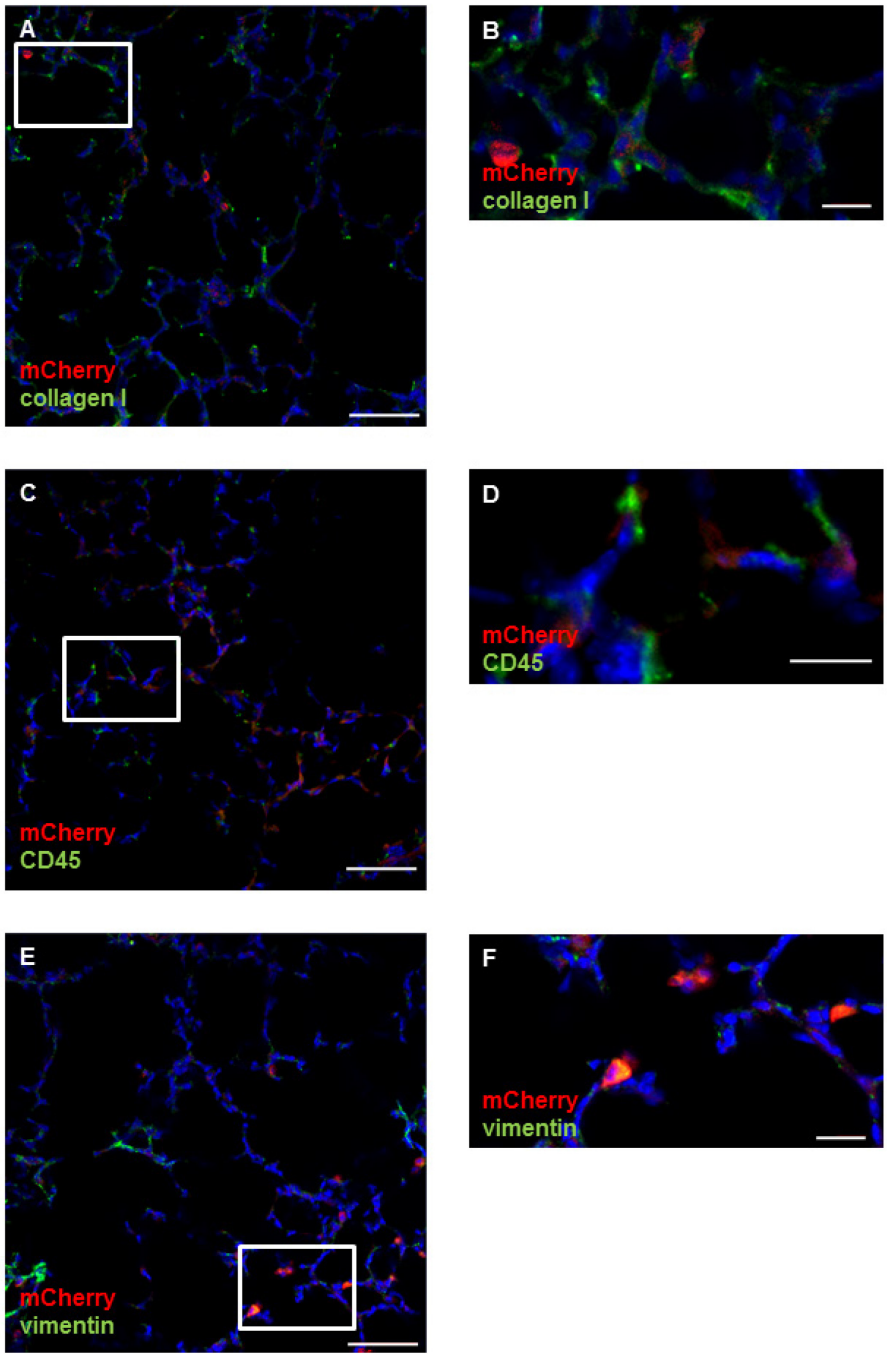

Figure 24 Expression of the *Plin2* promoter-driven reporter gene mCherry, collagen I, CD45 and vimentin in lungs of Plin2$^{tm1.1(Cre/ERT2)Mort}$ mice at postnatal day 14.

The reporter gene mCherry (red), collagen I (green), CD45 (green) and vimentin (green) were expressed in lungs of Plin2$^{tm1.1(Cre/ERT2)Mort}$ mice at P14. (A-B) All cells expressing mCherry expressed collagen I, collagen I^{+} and mCherry^{-} cells were also observed. (C, D) The leucocyte marker CD45 was expressed in some mCherry^{+} cells, CD45^{+} and mCherry^{-} cells were located in close proximity to mCherry^{+}cells (E, F) All mCherry^{+} cells expressed vimentin, vimentin^{+} but mCherry^{-} cells were also observed. (F). A 4', 6-diamidino-2-phenylindole nuclear stain (blue) was used at all tissue sections. (A, C, E) Scale bar = 50 µm. (B, D, F inserts of A, C, E respectively). (B, D, F) Scale bar = 20 µm.

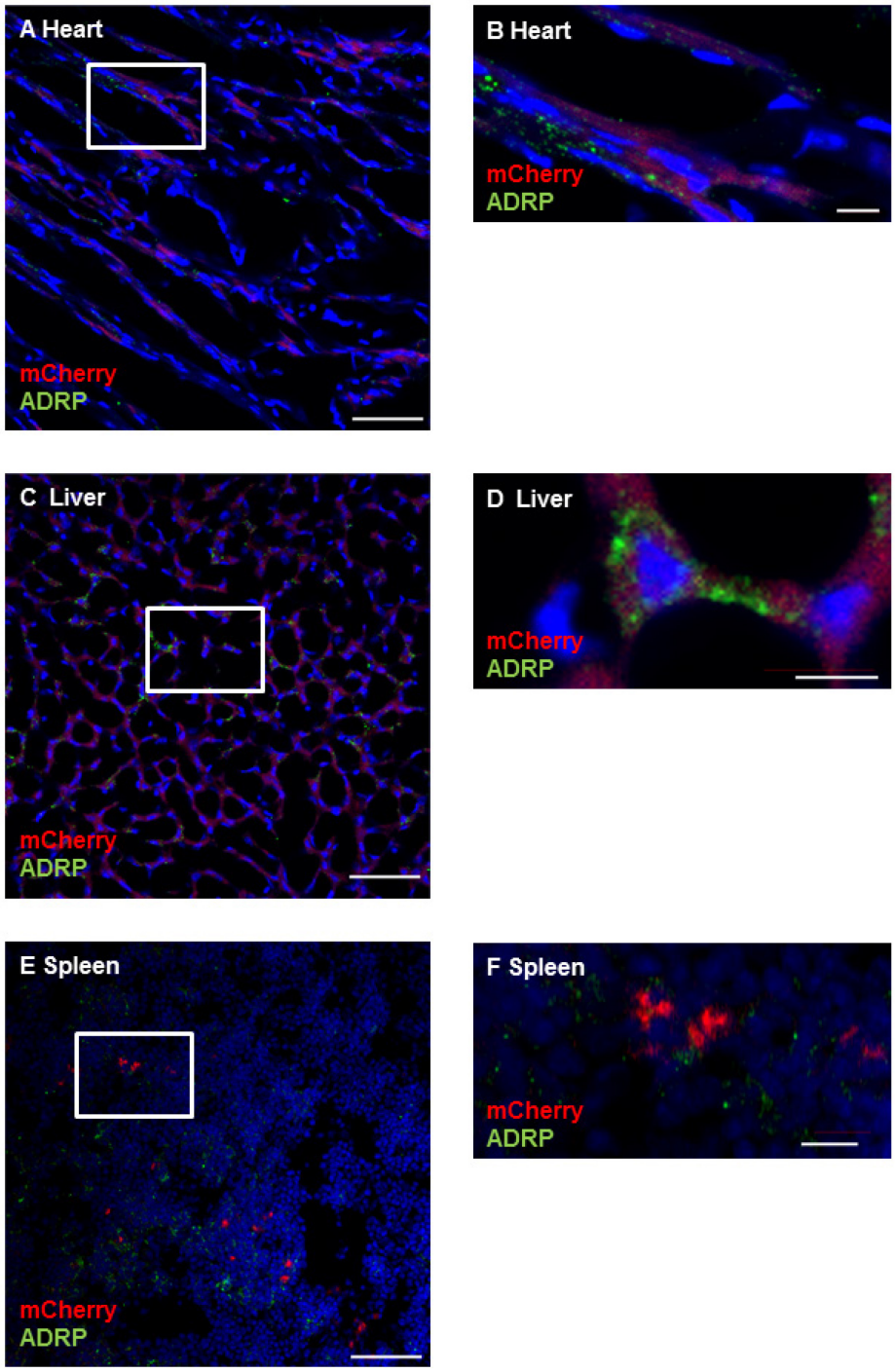

Figure 25 Expression of the *Plin2* promoter-driven reporter gene mCherry, and adipose differentiation related protein in the heart, the liver and the spleen of Plin2$^{tm1.1(Cre/ERT2)Mort}$ mice at postnatal day 14.

(A-F) The reporter gene mCherry (red) and adipose differentiation related protein (ADRP) (green) were expressed in the heart, the liver and the spleen of Plin2$^{tm1.1(Cre/ERT2)Mort}$ mice at P14. A 4', 6-diamidino-2-phenylindole nuclear stain (blue) was used at all tissue sections. (A-B) In the heart some cells expressed mCherry, some mCherry^{+} cells expressed ADRP. (C-D) In the liver most of the cells expressed mCherry, some mCherry^{+} cells expressed ADRP. (E, F) In the spleen few cells expressed mCherry, a minority of mCherry^{+} cells expressed ADRP. (A, C, E) Scale bar = 50 μm. (B, D, F inserts of A, C, E respectively). Scale bar = 20 μm.

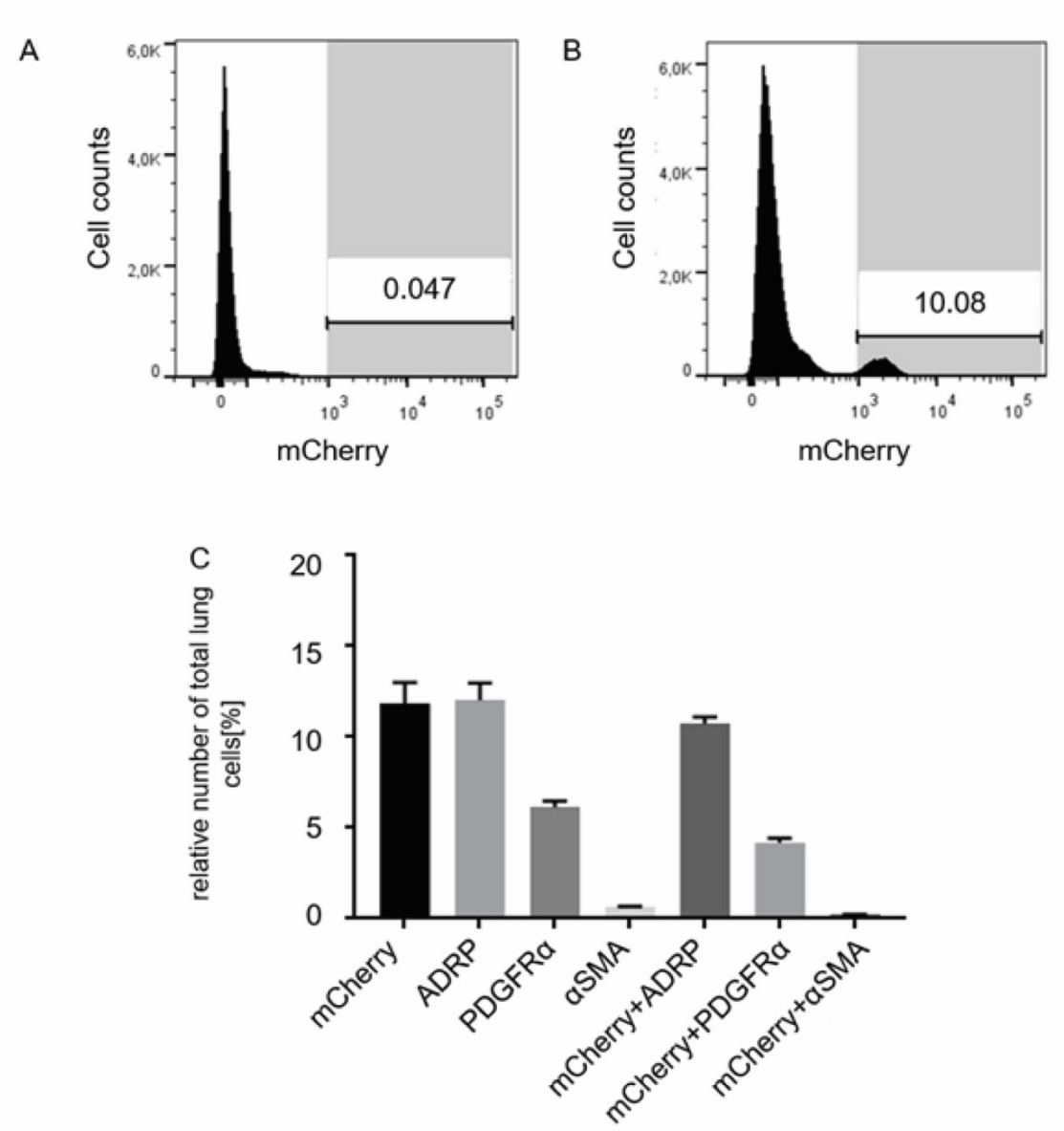

Figure 26 Quantification of *Plin2* promoter-driven reporter gene mCherry-expressing cells and fibroblast subtypes in lungs of Plin2$^{tm1.1(Cre/ERT2)Mort}$ mice at postnatal day 14.

(A-B) Representative histograms of flow cytometry quantification demonstrating the percentage of mCherry^{+} cells, from the total lung homogenate in wild type (A) and Plin2$^{tm1.1(Cre/ERT2)Mort}$ (B) mice, which were analyzed at P14. (C) Bar graphs show mean values ± SEM of the relative numbers of mCherry^{+} cells and of different fibroblast subtypes at P14 in lungs of Plin2$^{tm1.1(Cre/ERT2)Mort}$ mice (n=3). Notably ≈89% of all ADRP-expressing cells expressed mCherry and ≈91% of all mCherry-expressing cells expressed ADRP.

3.4 Lineage tracing and cell depletion of postnatal lipofibroblasts in the lung using Plin2$^{tm1.1(Cre/ERT2)Mort}$mTmG mice

3.4.1 Lineage tracing of lipofibroblasts in the lung using Plin2$^{tm1.1(Cre/ERT2)Mort}$mTmG mice

To analyze the fate and differentiation of lipofibroblasts (ADRP$^+$ cells) which are present during the peak of secondary septation at P7, after the peak of secondary septation, at P10, and at the completion of secondary septation at P14, lineage tracing using Plin2$^{tm1.1(Cre/ERT2)Mort}$mTmG mice was performed (Figure 27-30). At P7, P10 and P14 respectively Plin2$^{tm1.1(Cre/ERT2)Mort}$mTmG mice were injected with tamoxifen to permanently label ADRP-expressing cells (lineage labeled cells, expressing the lineage label GFP). Lungs were immunostained against ADRP, αSMA and PDGFRα respectively and analyzed at P14 (tamoxifen injection at P7 and P10) or at P21 (tamoxifen injection at P14). When tamoxifen was given at P7 and P10 GFP$^+$ cells were abundant in the alveolar walls and peribronchially (tamoxifen injection at P10) at P14 (Figure 27 A-D, isotype controls in Figure 39). Lineage traced cells from P10 (Figure 27 C, D) seemed to be less abundant comparing with lineage traced cells from P7 (Figure 27 A, B). Co-expression of GFP and ADRP was demonstrated in most of the GFP$^-$ labeled cells (Figure 27 A-F). When Plin2$^{tm1.1(Cre/ERT2)Mort}$mTmG mice were injected with tamoxifen at P14 there were still some cells labeled and even though the total ADRP$^+$ population appeared low, some double-positive cells could still be detected (Figure 27 E, F).

To address if cells of the indicated postnatal ADRP cell-lineages contribute to the myofibroblast pool of P14 or P21, αSMA expression was analyzed (Figure 28, isotype controls in Figure 38). At P14 αSMA expression was abundant in alveolar interstitial cells and peribronchial cells (Figure 28 A) After labeling at P7 some double-positive cells for GFP and αSMA could be detected in the alveolar walls but not peribronchially at P14 (Figure 28 A,B). After tamoxifen injection at P10 few cells were double-positive cells for GFP and αSMA (Figure 28 C, D). At P21 αSMA expression was less abundant in alveolar interstitial cells but prominent in peribronchial cells (Figure 28 E, F). Labeling of ADRP$^+$ cells at P14, resulted in few peribronchial double-positive cells for GFP and αSMA at P21 (Figure 28 E, F).

Since we and others previously demonstrated the expression of PDGFRα in lipofibroblasts it was questioned whether PDGFRα was expressed in the indicated postnatal ADRP cell-lineages. To address this question immunostaining against PDGFRα was performed at P14 and P21 (Figure 29, isotype

controls in Figure 38) At P14 and P21 PDGFRα^{+} cells were abundant in the alveolar walls (Figure 29 A-F). When tamoxifen was given at P7 most of the GFP^{+} cells expressed PDGFRα, few PDGFRα^{+} but GFP^{-} cells were observed (Figure 29 A, B). When tamoxifen was given at P10, GFP^{+} cells seemed to be less abundant (comparing with lineage labeled cells from P7) however, most of the GFP^{+} cells expressed PDGFRα at P14 (Figure 29 C, D). At P21 the GFP^{+} cells, were less abundant after lineage tracing at P14 but still most of the GFP^{+} cells expressed PDGFRα (Figure 29 E, F). Since co-expression of ADRP and the leucocyte marker CD45 has been reported previously, the expression of CD45 in the postnatal ADRP cell-lineages of P7, P10 and P14 was analyzed at P14 and P21 respectively (Figure 30 isotype controls in Figure 38). All three postnatal ADRP cell-lineages (from P7, P10 and P14) labeled few round shaped CD45^{+} cells which were located in the alveolar walls at P14 and P21 (Figure 30 A-F). The majority of GFP^{+} cells did not express CD45, round shaped and elongated CD45^{+} but GFP^{-} cells were also observed in the alveolar walls at P14 and P21 (Figure 30). Lineage tracing of postnatal ADRP-expressing cells at P7, P10 and P14, revealed expression of ADRP and PDGFRα in most of the GFP^{+} cells at P14 and P21 respectively. The expression of αSMA was observed in a minority of GFP^{+} cells in the alveolar regions (when cells were labeled at P7 and P10 respectively) and restricted to peribronchial GFP^{+} cells at P21 of the ADRP cell-lineage of P14.

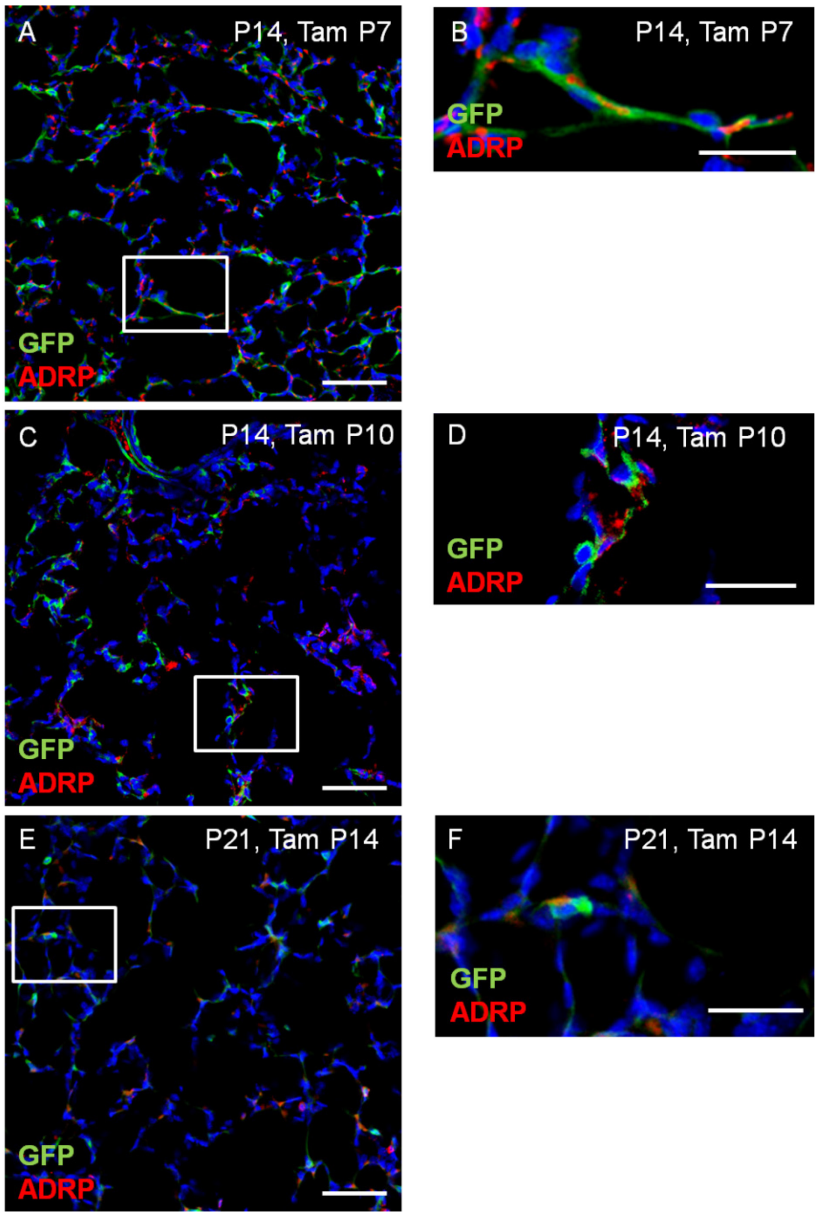

Figure 27 Lineage tracing of postnatal adipose differentiation related protein-expressing cells. Expression of green fluorescent protein and adipose differentiation related protein in lungs of Plin2$^{tm1.1(Cre/ERT2)Mort}$mTmG mice at postnatal day 14 and 21, adipose differentiation related protein-expressing cells were labeled at postnatal day 7, 10 and 14.

Lineage traced adipose differentiation related protein (ADRP)-expressing cells from postnatal day (P)7, P10 and P14 expressed the lineage label green fluorescent protein (GFP) (green) at P14 and P21, immunostaining against ADRP labeled lipofibroblasts (red) at P14 and P21. (A, B) At P14 cells expressing the lineage label GFP which was induced at P7 were abundant in the alveolar walls, some GFP$^+$ cells expressed ADRP. (C, D) At P14 cells expressing the lineage label GFP which was induced at P10 were abundant in the alveolar walls and peribronchial regions, some GFP$^+$ cells expressed ADRP. (E, F) At P21 cells expressing the lineage label GFP which was induced at P14 seemed to be less prominent but present in the alveolar walls, few GFP$^+$ cells expressed ADRP. Cells expressing ADRP also appeared to be less abundant. A 4', 6-diamidino-2-phenylindole nuclear stain (blue) was used at all tissue sections. Tam = tamoxifen. (A, C, E) Scale bar = 50 µm. (B, D, F inserts of A, C, E respectively) Scale bar = 20 µm.

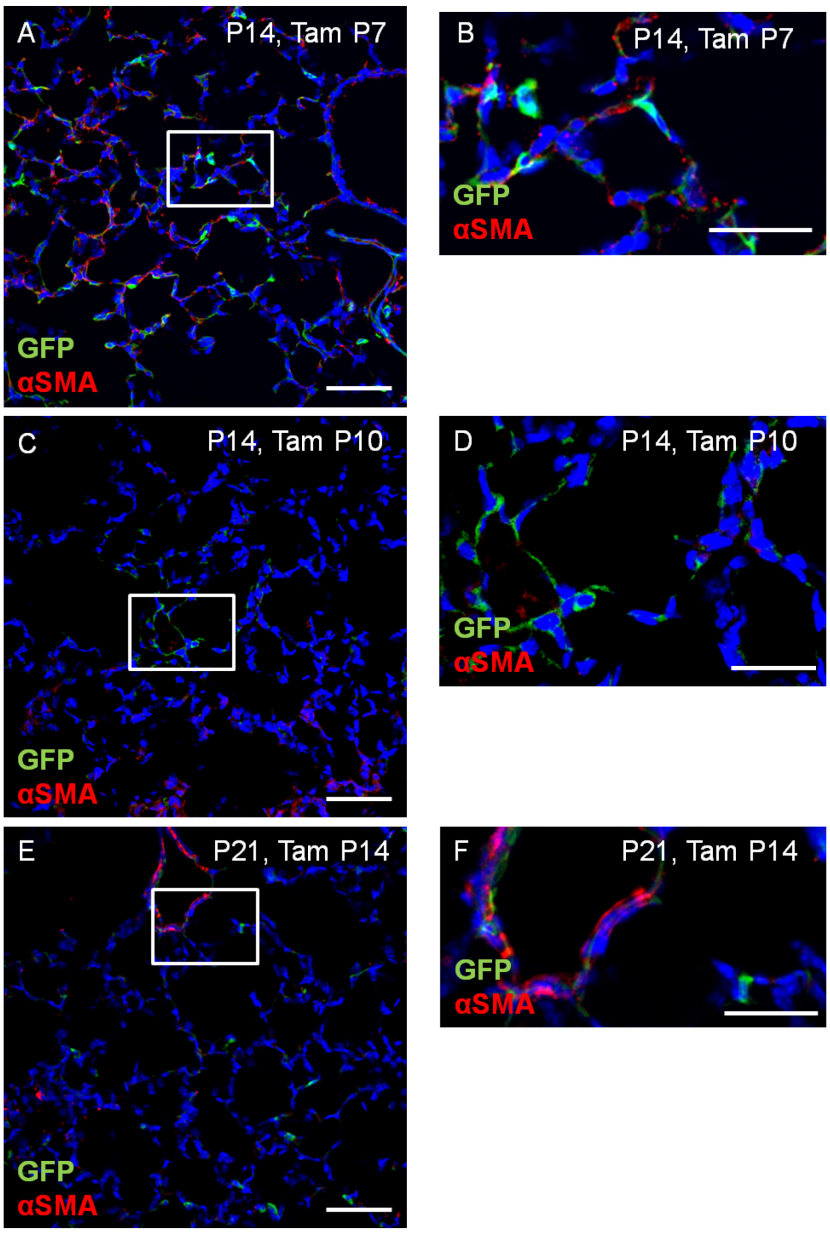

Figure 28 Lineage tracing of adipose differentiation related protein-expressing cells and α smooth muscle actin expression. Expression of green fluorescent protein and α smooth muscle actin in lungs of Plin2$^{tm1.1(Cre/ERT2)Mort}$mTmG mice at postnatal day 14 and 21, adipose differentiation related protein-expressing cells were labeled at postnatal day 7, 10 and 14.

Lineage traced postnatal adipose differentiation related protein (ADRP)-expressing cells from postnatal day (P)7, P10 and P14 expressed the lineage label green fluorescent protein (GFP) (green) at P14 and P21, immunostaining against α smooth muscle actin (αSMA)- labeled myofibroblasts (red) at P14 and P21. (A, B) At P14 cells expressing the lineage label GFP which was induced at P7 were abundant in the alveolar walls, few GFP$^+$ cells expressed αSMA. (C, D) At P14 GFP$^+$ cells which were labeled at P10 were abundant in the alveolar walls, few GFP$^+$ cells expressed αSMA. (E, F) At P21 GFP$^+$ cells which were induced at P14 seemed to be less prominent but present in the alveolar walls, few GFP$^+$ cells expressed αSMA. Cells expressing αSMA also appeared to be less abundant. A 4', 6-diamidino-2-phenylindole nuclear stain (blue) was used at all tissue sections. Tam = tamoxifen. (A, C, E) Scale bar = 50 μm. (B, D, F inserts of A, C, E respectively) Scale bar = 20 μm.

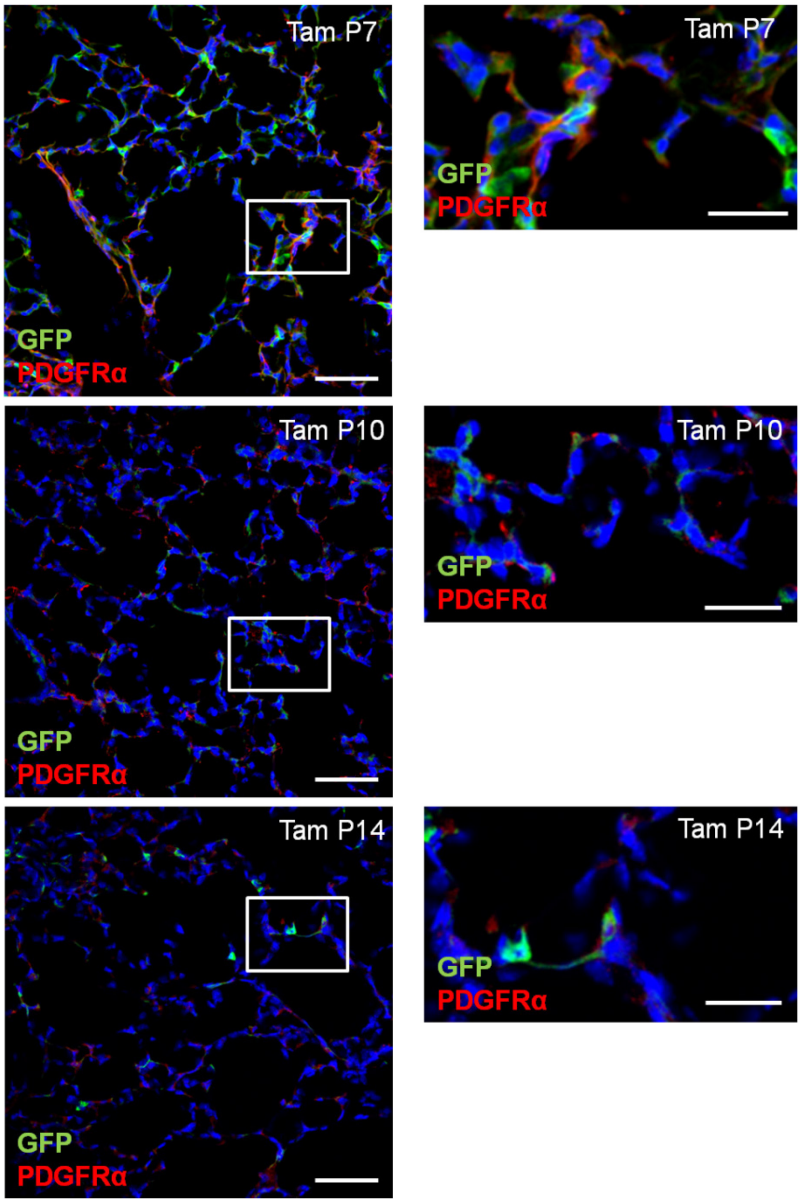

Figure 29 Lineage tracing of postnatal adipose differentiation related protein-expressing cells and platelet-derived growth factor receptor α expression. Expression of green fluorescent protein and platelet-derived growth factor receptor α in lungs of Plin2$^{tm1.1(Cre/ERT2)Mortm}$TmG mice at postnatal day 14 and 21, adipose differentiation related protein-expressing cells were labeled at postnatal day 7, 10 and 14.

Lineage traced adipose differentiation related protein (ADRP)-expressing cells from P7, P10 and P14 expressed the lineage label green fluorescent protein (GFP) (green) at postnatal day (P)14 and P21, immunostaining against platelet-derived growth factor receptor α (PDGFRα) (red) was performed at P14 and P21. (A, B) At P14 GFP$^+$ cells which were labeled at P7 were abundant in the alveolar walls, most of the GFP$^+$ cells expressed PDGFRα. (C,D) At P14 GFP$^+$ cells which were labeled at P10 were abundant in the alveolar walls, most of the GFP + cells expressed PDGFRα. (E,F) At P21 GFP$^+$ cells which were induced at P14 seemed to be less prominent but present in the alveolar walls, most of the GFP$^+$ cells expressed PDGFRα. Cells expressing PDGFRα appeared to be more abundant comparing with GFP$^+$ cells. A 4', 6-diamidino-2-phenylindole nuclear stain (blue) was used at all tissue sections. Tam = tamoxifen. (A, C, E) Scale bar = 50 μm. (B, D, F inserts of A, C, E respectively) Scale bar = 20 μm.

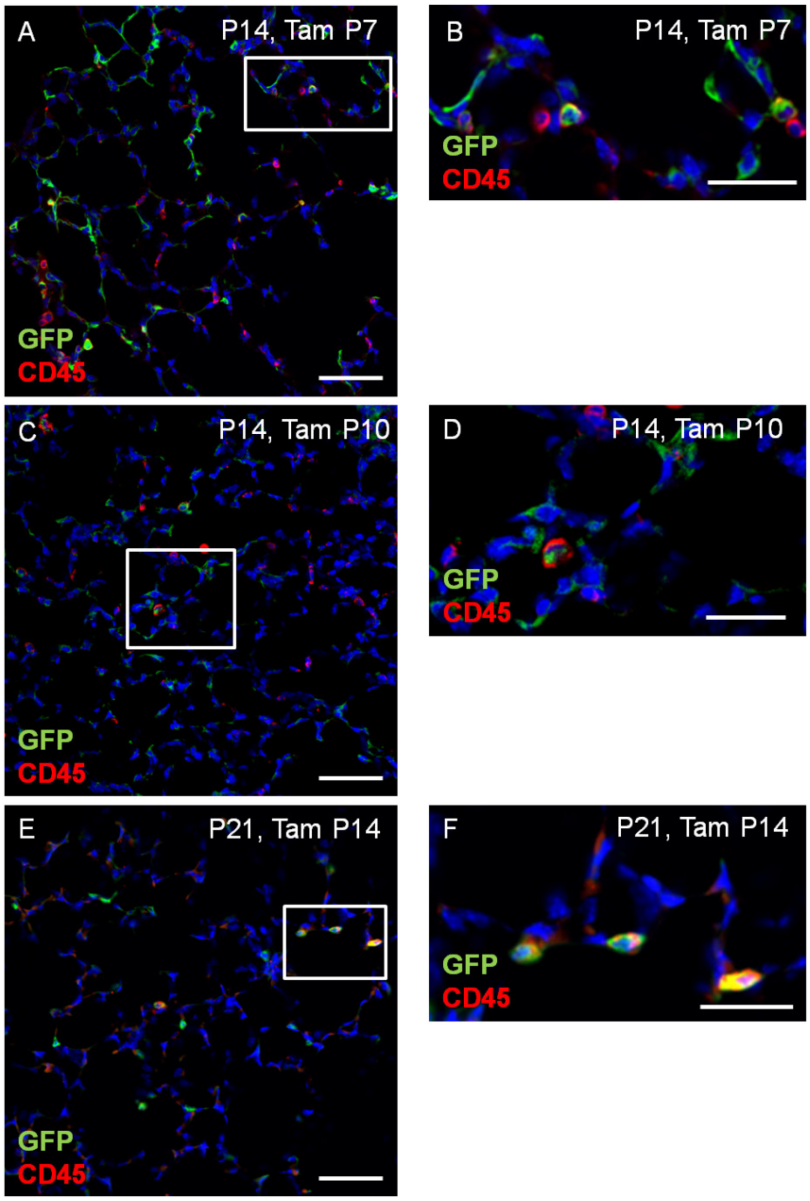

Figure 30 Lineage tracing of postnatal adipose differentiation related protein-expressing cells and CD45 expression. Expression of green fluorescent protein and CD45 in lungs of Plin2$^{tm1.1(Cre/ERT2)Mort}$mTmG mice at postnatal day 14 and 21, adipose differentiation related protein-expressing cells were labeled at postnatal day 7, 10 and 14.

Lineage traced adipose differentiation related protein (ADRP)-expressing cells from postnatal day (P)7, P10 and P14 expressed the lineage label green fluorescent protein (GFP) (green) at P14 and P21, immunostaining against CD45 was performed at P14 and P21. (A, B) At P14 GFP$^+$ cells which were labeled at P7 were abundant in the alveolar walls, few GFP$^+$ cells expressed CD45 and exhibited a round cell shape. (C, D) At P14 GFP$^+$ cells which were labeled at P10 were located in the alveolar walls, few GFP$^+$ cells expressed CD45 and exhibited a round cell shape. (E, F) At P21 GFP$^+$ cells which were induced at P14 seemed to be less prominent but present in the alveolar walls, few GFP$^+$ cells expressed CD45. Cells expressing CD45 without expressing GFP appeared to be more abundant comparing with GFP$^+$ cells. A 4', 6-diamidino-2-phenylindole nuclear stain (blue) was used at all tissue sections. Tam = tamoxifen. (A, C, E) Scale bar = 50 µm. (B, D, F inserts of A, C, E respectively) Scale bar = 20 µm.

3.4.2 Depletion of lipofibroblasts using Plin2$^{tm1.1(Cre/ERT2)Mort}$DTA mice

Specific depletion of early postnatal ADRP^{+} cells using diphtheria toxin revealed the importance of lipofibroblast function for proper alveolarization and provided important aspects of putative functions of lipofibroblasts during alveolar septum formation. Using the DTA approach, ≈50% of all lipofibroblasts (here mCherry^{+} cells) were depleted when Plin2$^{tm1.1(Cre/ERT2)Mort}$DTA mice received tamoxifen at P1 and lungs were analyzed at using FACS at P8 (Figure 31). Representative FACS plot analysis demonstrated a clear mCherry^{+} population in Plin2$^{tm1.1(Cre/ERT2)Mort}$ Mice which was lacking in DTA mice and reduced in Plin2$^{tm1.1(Cre/ERT2)Mort}$DTA (Figure 31 A, B, C). The mCherry^{+} cell population was reduced from 4.58±0.93% in Plin2$^{tm1.1(Cre/ERT2)Mort}$ to 2.268±0.66% in Plin2$^{tm1.1(Cre/ERT2)Mort}$DTA mice, n=3 (Figure 31 D).

The amount of cell depletion was also estimated later at P14 after tamoxifen injection at P1 (Figure 32) Representative FACS plot analysis demonstrated a clear mCherry^{+} population in Plin2$^{tm1.1(Cre/ERT2)Mort}$ Mice which was lacking in DTA mice and reduced in Plin2$^{tm1.1(Cre/ERT2)Mort}$DTA (Figure 32 A, B, C). The mCherry^{+} cell population was reduced from 10.57±1.4% in Plin2$^{tm1.1(Cre/ERT2)Mort}$ to 4.38±0.09% in Plin2$^{tm1.1(Cre/ERT2)Mort}$DTA mice, representing a reduction by ≈59% (Figure 32 D). Histochemical staining against Elastin fibers and nuclei revealed a strong impact on lung structure at P14 upon depletion of the ADRP cell-lineage of P1 (Figure 32 E, F). A strong disruption of alveolarization let to condensed tissue areas and emphysema-like enlargements of the premature air-sacs (Figure 32 F). Control lungs of Plin2$^{tm1.1(Cre/ERT2)Mort}$ mice demonstrated a normal lung structure (Figure 32 E).

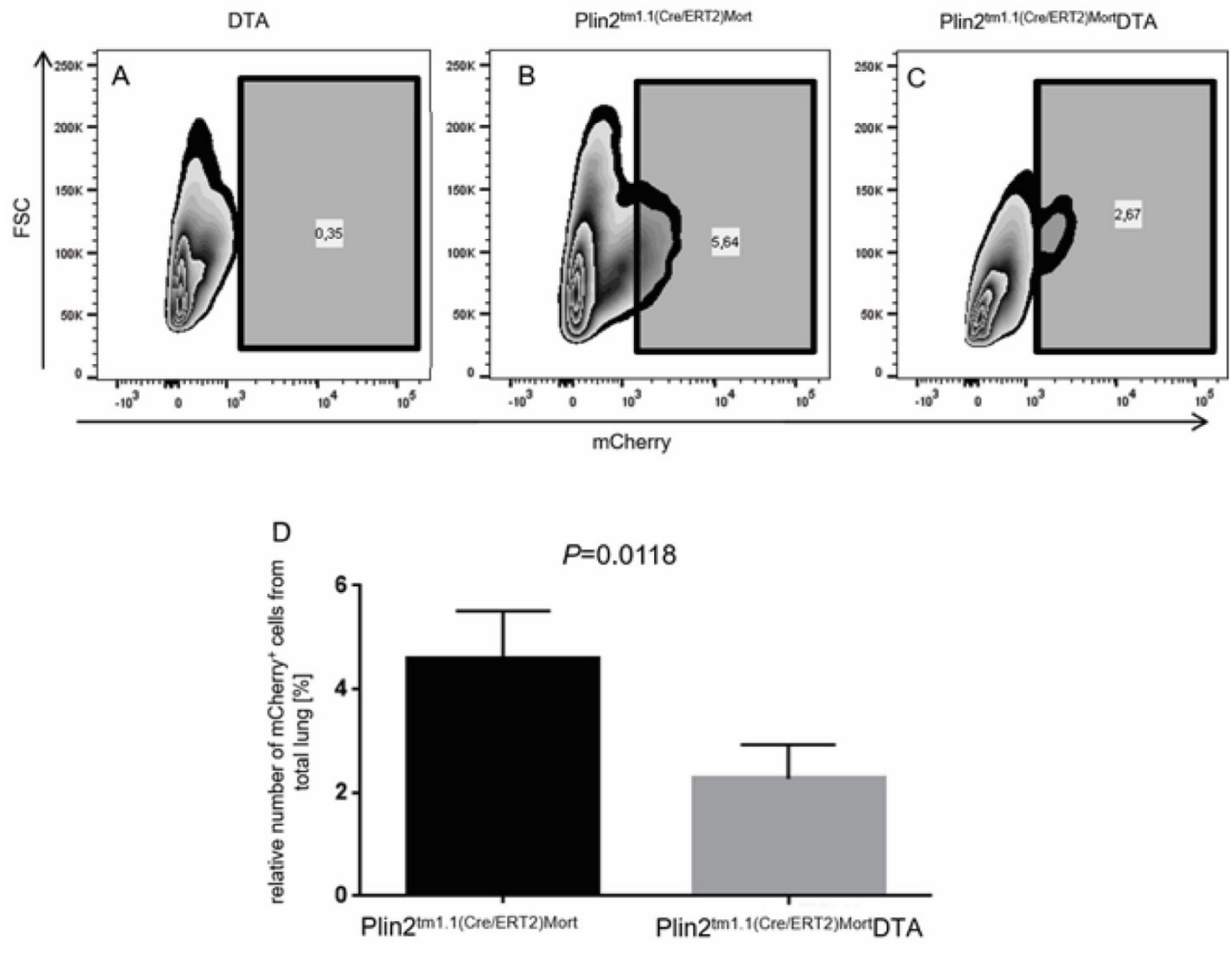

Figure 31 Depletion of adipose differentiation related protein^{+} cells at postnatal day 1 using Plin2$^{tm1.1(Cre/ERT2)Mort}$DTA mice.

Using tamoxifen (Tam) injection, adipose differentiation related protein^{+} (ADRP^{+}) cells were depleted at postnatal day (P)1, Plin2$^{tm1.1(Cre/ERT2)Mort}$DTA mice were analyzed at P8 for the relative number of Cherry^{+} cells to total lung cells using fluorescence-activated cell sorting (FACS). (A-C) Representative FACS plot analysis demonstrate a mCherry^{+} population in Plin2$^{tm1.1(Cre/ERT2)Mort}$ mice (B) which was reduced in DTA mice (A) and reduced in Plin2$^{tm1.1(Cre/ERT2)Mort}$DTA mice (C). FSC: forward scatter. (D) Quantification of the relative number of mCherry^{+} cells from total lung cells at P8 showed clear depletion of mCherry^{+} cells by ≈50% in Plin2$^{tm1.1(Cre/ERT2)Mort}$DTA mice comparing to Plin2$^{tm1.1(Cre/ERT2)Mort}$ mice after Tam injection at P1. Bar graphs show mean values ± SEM. Statistical significance was estimated using the unpaired Student's t test (n=3 per group).

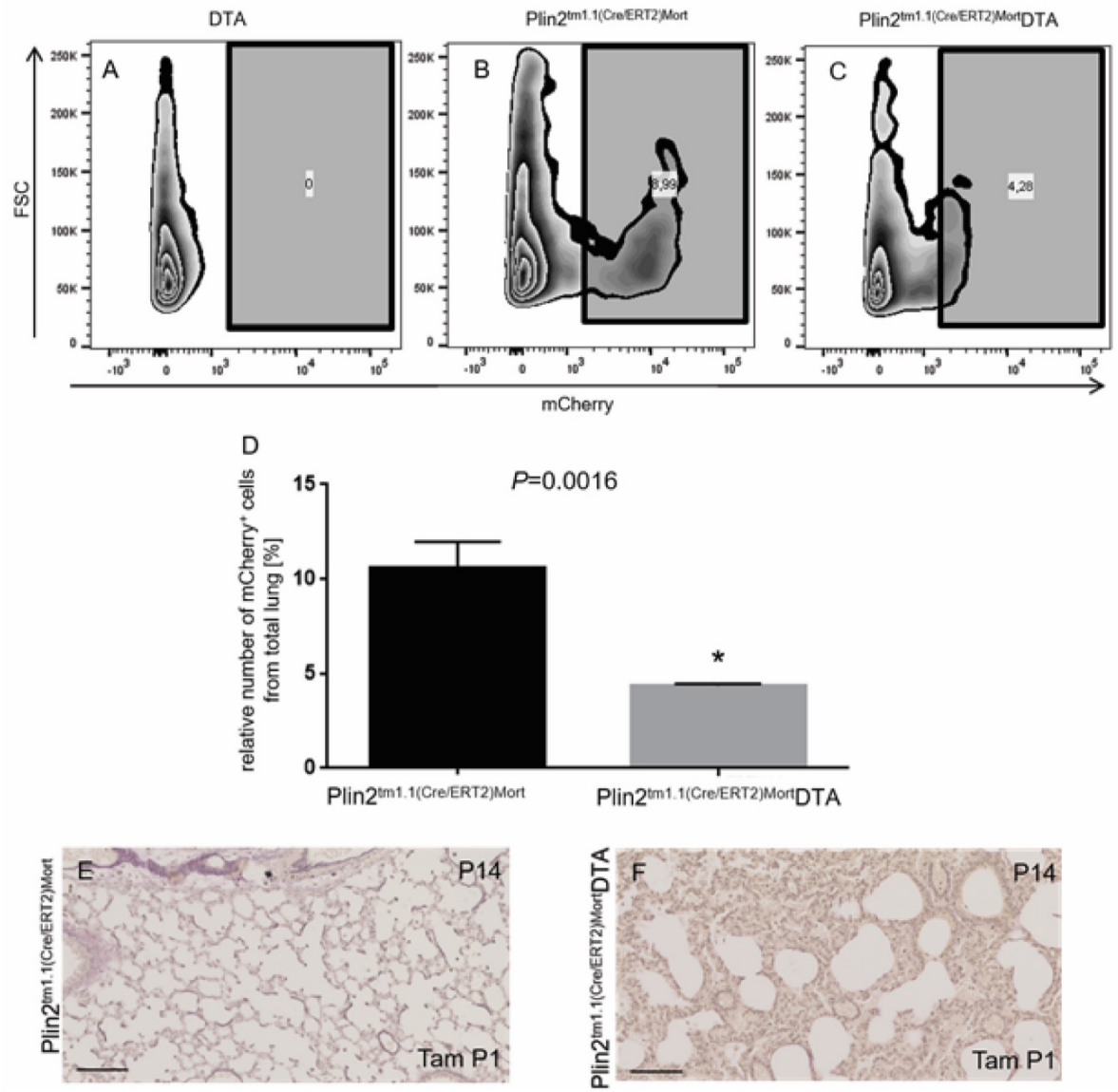

Figure 32 Depletion of adipose differentiation related protein^{+} cells at postnatal day 1 using Plin2$^{tm1.1(Cre/ERT2)Mort}$DTA mice.

Using tamoxifen (Tam) injection, adipose differentiation related protein^{+} (ADRP^{+}) cells were depleted at postnatal day (P)1, Plin2$^{tm1.1(Cre/ERT2)Mort}$DTA mice were analyzed at P14 for the relative number of Cherry^{+} cells to total lung cells using fluorescence-activated cell sorting (FACS). (A-C) Representative FACS plot analysis demonstrate a mCherry^{+} population in Plin2$^{tm1.1(Cre/ERT2)Mort}$ mice (C) which was missing in DTA mice (A) and reduced in Plin2$^{tm1.1(Cre/ERT2)Mort}$DTA mice (B). (D) Quantification of the relative number of mCherry^{+} cells from total lung cells at P14 showed clear depletion of mCherry^{+} cells by ≈59% in Plin2$^{tm1.1(Cre/ERT2)Mort}$DTA mice comparing with Plin2$^{tm1.1(Cre/ERT2)Mort}$ mice after Tam injection at P1. Bar graphs show mean values ± SEM. Statistical significance was estimated using the unpaired Student's t test (n=3 per group). (E-F) Representative images demonstrating histochemical staining against elastin fibers from lungs of Plin2$^{tm1.1(Cre/ERT2)Mort}$ mice (E) and Plin2$^{tm1.1(Cre/ERT2)Mort}$DTA mice (F) at P14, Scale bar 100 µm. Depletion of mCherry^{+} cells led to severe disruption of alveolarization resulting in an abnormal lung structure with condensed tissue areas and emphysema like enlargements of the immature airsacs (F) Lungs of Plin2$^{tm1.1(Cre/ERT2)Mort}$ mice demonstrated a normal lung structure with secondary septa and proper elastin deposition at the tips of the secondary septa (E).

4 Discussion

Insights into the localization, differentiation and function of fibroblast subtypes during alveolar septum formation can reveal cellular and molecular target candidates for the development of new therapeutic strategies for structural diseases of the lung such as COPD or fibrosis in adults, and BPD in preterm neonates. Understanding the process of alveolarization to gain the potential to induce alveolarization in the diseased lung (neo-alveolarization) represents a desirable approach to regenerative medicine. The aim of the present study was to characterize the populations of PDGFRα^{+} fibroblasts in terms of localization and plasticity during lung development and to develop an *in vivo* tool to target lipofibroblasts in the lung.

4.1 Characterization of PDGFRα^{+} fibroblasts

The PDGFRα^{+} cell population was studied during the pseudoglandular, canalicular, saccular and the alveolar stages of lung development until adulthood in mice. The importance of PDGFRα^{+} cells has been previously highlighted as a fibroblast population that is critically involved in the process of septum formation, plausibly by influencing myofibroblast differentiation and elastin production (14, 15, 56). More specifically, using the PDGFRα^{GFP} knock-in mice it was demonstrated that PDGFRα^{+} fibroblasts accumulate at the alveolar entry ring during the process of secondary septation during the period P4-P12 (64). A spatiotemporal variation of PDGFRα^{+} cells was also observed. One group of PDGFRα^{+} cells expressed αSMA and elastin at the alveolar entry ring, and another exhibited lipofibroblast features at the alveolar base during secondary septation (P2-P8) (64). What was observed in this study matched the pattern demonstrated in the current work, since it was demonstrated that αSMA^{+} PDGFRα^{+} cells are located at the tips of the secondary crests and ADRP^{+} PDGFRα^{+} cells in the primary septa and at the base of the secondary crests at P5. Furthermore, there was evidence for PDGFRα^{+} cells located around the developing airways, the epithelial tubes of the pseudoglandular phase, and later in the canalicular stage, there was a decrease in the peribronchial abundance and increased appearance of PDGFRα^{+} cells in the more distal walls of the developing air sacs. Regarding secondary septation, these data demonstrate that PDGFRα^{+} cells appeared in the primary septa and in the tip cells of the secondary crests. These findings were in line with previous studies demonstrating that PDGFRα expression and myofibroblast appearance during the peak of secondary septation coincided (16, 29, 34, 64, 68). Those

shifts in localization throughout development might be caused by cytokinesis and chemotaxis, as also suggested by McGowan and co-workers (67). The idea that PDGFRα$^+$ fibroblasts operate as progenitor cells has been questioned, therefore the present study aimed to analyze the expression of markers characterizing MSCs such as CD44, CD105, CD73, CD146 and CD90 (107) in PDGFRα$^+$ cells during lung development to confirm the progenitor cell character. Data presented in the current study demonstrated that MSC markers were indeed differentially expressed in PDGFRα$^+$ cells over the course of late lung development. Despite that in the early stages pseudoglandular and canalicular stages, no co-expression of PDGFRα and MSC markers was detected until the saccular stage, when CD44, CD105 and CD90 were expressed in some PDGFRα$^+$ cells. During the alveolar stage at P5, all five markers for MSCs were expressed in PDGFRα$^+$ cells in primary septa. At secondary crest formation, at P5, CD73 and CD90 were expressed in PDGFRα$^+$ cells at the base of the secondary septa when tip cells demonstrated co-expression of CD105, CD73, CD146 and CD90. The differential expression of MSC markers in PDGFRα$^+$ cells suggests a high differentiation capacity and progenitor cell characteristics of PDGFRα$^+$ cells. Among those markers, the impact of CD90 on lipofibroblasts is well established, since the lipogenic phenotype is driven by CD90 involving PPAR-γ (86, 109). These findings support the data presented in the current study since CD90 expression was demonstrated to be mostly evident in ADRP$^+$ cells. Specifically, at P5, CD90 and ADRP were co-localized in line with previous descriptions about lipofibroblasts (17). In contrast, the current study demonstrated CD90 expression in αSMA$^+$ and PDGFRα$^+$ tip cells of the secondary septa. This might reflect a transient fibroblast subtype, still expressing CD90 but in the process of differentiation towards myofibroblast. It is known that loss of CD90 *in vivo* impaired alveolarization and increased fibroblast proliferation, TGF-β signaling, as well as increased collagen and elastin production (74, 111). Fibroblasts negative for CD90 exhibited higher levels of PDGFRα expression and showed increased proliferation in response to PDGF-A, compared to CD90$^+$ fibroblasts (36). Data presented here further support the suggestion that CD90 impacts on the differentiation of PDGFRα$^+$ progenitor cells into lipo- or myo-fibroblasts respectively (75). Using a model of compensatory lung growth after pneumonectomy, the phenomenon that PDGFRα$^+$ cells might serve as progenitor cells for myofibroblasts has also been studied in re-alveolarization, where the PDGFRα$^+$ cell population abundance was briefly increased after the operation (21). In the same study, blockage of FGF signaling and PPARγ activation (by Rosiglitazone) inhibited the differentiation of PDGFRα$^+$ cells into myofibroblasts, and led to alveolar simplification after pneumonectomy (21). This finding again supports the idea that PDGFRα$^+$ cells might serve as progenitor cells for myofibroblasts

and is consistent with the quantitative data generated in the present study on the different fibroblasts subtype populations. The quantitative data presented here exhibit presence of single PDGFRα$^+$ cells, as well as double-positive ADRP$^+$ and PDGFRα$^+$ cells during alveolarization. It was also possible to demonstrate the presence of PDGFRα$^+$ cells in adulthood. Taken together, the data of this study add to the growing body of evidence that PDGFRα$^+$ cells might serve as progenitor cells for myofibroblasts and lipofibroblasts (29, 34, 68).

4.2 Lineage tracing and depletion of PDGFRα$^+$ fibroblasts during alveolarization

Using lineage tracing to prove the differentiation of PDGFRα$^+$ cells during alveolarization it was demonstrated in the current study that early postnatal PDGFRα$^+$ cells at P1 can give rise to both myo- and lipo-fibroblasts during the peak of secondary septation, at P7, and thereafter, until P9. However, previous studies demonstrated that the time-points of determination of both cell types were different. Myofibroblasts appeared to be derived from PDGFRα$^+$ cells before P2, since induction at P2 or P5 did not give rise to double-positive cells for GFP and αSMA (75). In contrast lipofibroblasts were already generated through the induction at P2 but also not at P5 (75). On the other hand, after induction at P1 and the usage of the constitutively-recombining model the PDGFRα$^+$ lineage gave rise to myofibroblasts and lipofibroblasts. Due to the presence of single αSMA$^+$ cells at P7, P9 and P14 which were not traced by the PDGFRα lineage, it can be suggested that αSMA$^+$ but PDGFRα$^-$ cells at this stage may rise from a different progenitor cell-type, and contribute largely to the emergence of peribronchial and perivascular smooth muscle cells. This pool could be derived from the FGF10$^+$ cell-lineage as it has been previously found to give rise to parabronchial and vascular smooth muscle cells (28) and FGF signaling is known to be required for the induction of αSMA in PDGFRα$^+$ myofibroblasts (81). Furthermore the Gli-1 cell-lineage has been demonstrated to give rise to alveolar myofibroblasts (54). Concerning the lipofibroblast pool the current study demonstrated that also not the entire population was traced by the PDGFRα$^+$ cell-lineage. Again it is also probable that there might be further precursors, besides the PDGFRα$^+$ cells, for lipofibroblasts (21). However, due to the partial labeling of lipofibroblasts or myofibroblasts using this model, it is also possible that the precursor characteristic of PDGFRα$^+$ cells was not properly demonstrated, due to incomplete recombination that might have led to labeling of less lipofibroblasts or myofibroblasts. The data presented here demonstrated double-positive cells for GFP and ADRP located in the alveolar regions in the primary

septa and at the base of the secondary crests, proposing their participation in secondary septation. Indeed lipofibroblasts have been reported to play a crucial role in lung development in rodents (46, 61). But lipofibroblasts also have been detected in human lung biopsies (86). A further study questioned the presence of lipofibroblasts in the human lung analyzing different mammalian species including humans using light and electron microscopic stereology (99). Different reasons may underlie these contradictory results (4). In BPD hyperoxia models it has been demonstrated, that a transition from a lipofibroblast, of unknown origin, to a myofibroblast, was prevented by Rosiglitazone treatment (86), supporting the link between these fibroblasts and PDGFRα+ cells. Furthermore, defects in PDGFR signaling have been demonstrated to be involved in the development of human BPD (82).

The current study demonstrated that the early postnatal PDGFRα$^+$ cell-lineage contributed to the myo- and lipofibroblast pool which participates in secondary septation. However, further progenitor cell types might exist. To address the relevance of this targeted early postnatal PDGFRα$^+$ cell pool, cell type specific depletion experiments were performed. The depletion approach presented here highlighted the time-specific differentiation, since induction of depletion at P3 caused different effects on lung structure than earlier induction of depletion at P1. Both approaches disrupted the normal elastin deposition and distribution, most likely leading to a reduction of secondary septation evident from the reduced abundance of secondary septa in PDGFRα$^+$ cell depleted lungs. Early induction of depletion of PDGFRα$^+$ cells (at P1) caused a more severe phenotype compared to later induction at P3. The emphysema- like lung structure was even evident when lungs were analyzed at P5 (before the peak of secondary septation). This might be caused since both cell types, lipofibroblasts and myofibrobalsts were affected by the loss of the distinct PDGFRα$^+$ cell-lineage. The study presented here clearly demonstrated a crucial role of early postnatal PDGFRα$^+$ cells in secondary septation. Future studies are needed to explore the cellular hierarchy of this effect. Future studies will reveal if fibroblast subtypes and ECM production directly cause this effect or if the function of epithelial cell types also might be affected by the loss of PDGFRα$^+$ cells. Recent studies point out a supportive role of PDGFRα$^+$ cells in alveolar type II cells (10). This report revealed that type II cells form alveolospheres when placed into 3D culture (10). Growth and differentiation of these alveolospheres were stimulated in co-cultures with PDGFRα$^+$ fibroblasts (10).

Taken together it has been previously clearly demonstrated the importance of PDGFRα$^+$ mesenchymal cells in septum formation, the generation of αSMA$^+$ myofibroblasts and elastin fibers

(15, 56). Nevertheless, the precursor function of PDGFRα$^+$ cells for myofibroblasts and lipofibrobalsts has not been demonstrated. The present study demonstrated the generation of myofibroblasts and lipofibroblasts from PDGFRα$^+$ cells. Furthermore, it was demonstrated, that this specific cell-lineage is necessary to drive proper septum formation and growth since depletion of the early postnatal PDGFRα$^+$ cells led to a disruption of secondary septation.

A distinct and balanced regulation of the differentiation of PDGFRα$^+$ cells towards the lipogenic or myogenic phenotype seems to be essential for alveolarization. The present study demonstrated both ways of differentiation and characterized the presence of PDGFRα$^+$ cells in a spatiotemporal manner during lung development. Further studies are needed to discover the factors regulating the differentiation of PDGFRα$^+$ cells in alveolarization and regeneration to be exploited for the development of new therapeutic strategies for structural lung diseases of the neonatal and adult lung.

4.3 Validation and characterization of a newly generated inducible Cre mouse line to target lipofibroblasts

Recently, a new Cre-driver mouse line, the Plin2$^{tm1.1(Cre/ERT2)Mort}$ mouse line had been generated to target lipofibroblasts *in vivo*. The present study aimed to validate and characterize this generated Cre driver line before studying lipofibroblasts using this new tool to genetically target and manipulate pulmonary fibroblasts of the ADRP cell-lineage *in vivo*. The mRNA of the integrated mCherry and CreERT2 sequence were robustly and specifically expressed in lungs of Plin2$^{tm1.1(Cre/ERT2)Mort}$ mice. Furthermore the successful inducible activation of Cre was demonstrated 24 h and 48 h after Tamoxifen treatment resulting in a robust expression of the reporter gene GFP of Plin2$^{tm1.1(Cre/ERT2)Mort}$ mTmG mice. One single injection of tamoxifen at P1 led to efficient Cre-mediated recombination, in the lung resulting in the expression of the lineage label GFP after the completion of secondary septation at P14 in pulmonary mesenchymal cells and some leucocytes. The quantification of the lineage-labeled GFP-expressing cells using FACS revealed approximately 5% of GFP-expressing cells from total lung cell suspension and by exclusion labeling with endothelial, epithelial and leukocyte markers, the mesenchymal character of the ADRP cell-lineage was confirmed. After lineage tracing, the numbers of GFP$^+$ cells were lower than those of ADRP$^+$ cells, supporting the specific labeling of the Plin2$^{tm1.1(Cre/ERT2)Mort}$ mouse. Quantification of the mCherry$^+$ cells at P14 using FACS, revealed 10% of mCherry-expressing cells at P14, and confirmed the co-expression of ADRP and to a lesser extent, CD45, in these cells. That, was similar to what was shown in the PDGFRα study about the abundance of ADRP-expressing cells during alveolarization. However, mCherry-expressing cells which were negative for the ADRP signal were also detected.

Lungs were analyzed during postnatal stages, emphasizing alveolarization during the postnatal period of lung development (106). As expected, in tissue staining, the GFP signal co-localized with the signal of the antibody staining against ADRP, but there was a lack of a complete overlap of the ADRP and GFP signal, which might result from the Cre-mediated recombination comparing to the antibody staining. The GFP signal exclusively reflected the cells which expressed ADRP at P1 (day of tamoxifen injection) and all progeny until P14. The ADRP signal, based on antibody staining, demonstrated all ADRP-expressing cells at P14. Cells expressing the lineage label GFP, which were constantly labeled at P1 might have lost ADRP expression due to differentiation at P14. This explains the presence of GFP$^+$ but ADRP$^-$ cells. Furthermore, ADRP-expressing cells from an earlier or later time-point of lung

development might also contribute to the ADRP-expressing lipofibroblast pool at P14, which were not labeled in the present setting. This explains the presence of $ADRP^+$ but GFP^- cells. Finally further lineages such as the FGF10 lineage might also serve as progenitor cells for lipofibroblasts as recently demonstrated (27, 28). The present study identified PDGFRα expression in GFP-expressing cells, which is in line with data on PDGFRα characterization, demonstrating that $PDGFR\alpha^+$ cells can give rise to lipofibroblasts during lung development and regeneration after pneumonectomy (35, 75). Since the generation of αSMA^+ myofibroblasts from PDGFRα-expressing fibroblasts (15, 64, 75) has been further demonstrated in this and other studies, the heterogeneity of pulmonary fibroblasts might explain the co-expression of αSMA and GFP as presented in this ADRP lineage tracing study. Furthermore, the expression of ADRP has been reported in macrophages (32) and explains the expression of CD45 in some of the GFP-expressing cells. This $Plin2^{tm1.1(Cre/ERT2)Mor}$ mouse Cre driver line lineage-labeled a pulmonary mesenchymal fibroblast population which has been assigned as lipofibroblasts and participates in alveolarization (43, 68, 75, 109). Moreover, the expression of the knock-in reporter gene mCherry in the postnatal lung reflected expression patterns of ADRP and also co-localized with further mesenchymal markers and with CD45. The expression of ADRP has been previously reported in adipocytes, muscle tissue, hepatocytes and macrophages (32, 44, 45, 55, 60) leading to the conclusion that the expression of GFP in $CD45^+$ cells of the lung and the expression of GFP in the postnatal heart, liver and spleen, as demonstrated in the present study, can be regarded as specific lineage label. The lipofibroblast character of labeled cells in the heart, the liver and the spleen could be confirmed by co-labeling of the ADRP signal by antibody staining in GFP-expressing cells. Similar to the pattern shown in the lung, there was only partial co-expression of the lineage label GFP and ADRP staining in the heart, the liver and the spleen, suggesting that in these organs the major population of cells labeled at P1, are not lipofibroblasts by P14. The expression of mCherry in the postnatal organs the heart, the liver and the spleen demonstrated a pattern as expected since mCherry also co-localized with ADRP only in some cells. However, in the spleen, co-localization of ADRP and mCherry appeared the least evident. This might be due to the accumulation of immune system cells in the spleen which internalize parts of lipid droplets from degraded cells. When lineage tracing of $ADRP^+$ cells was performed throughout development, a decrease in their population over time was revealed. Especially, when mice were injected with tamoxifen in the late stages of alveolarization or later, there were less labeled double-positive cells for GFP and ADRP.

4.4 Depletion of lipofibroblasts using Plin2$^{tm1.1(Cre/ERT2)Mort}$DTA mice

Since the present study demonstrated that the previously generated Cre driver line indeed targeted lipofibroblasts, the Plin2$^{tm1.1(Cre/ERT2)Mort}$ mouse line was used in combination with DTA mice to induce depletion of ADRP^{+} cells during early postnatal alveolarization at P1. Sufficient depletion of lipofibroblasts was successfully accomplished. The amount of lipofibroblasts (mCherry^{+} cells) decreased by ≈50% upon DTA expression in Plin2$^{tm1.1(Cre/ERT2)Mort}$DTA mice comparing with the amount of lipofibroblasts in control lungs when the analysis took place at P8. Also at P14 lipofibroblasts were successfully depleted by ≈59% comparing with non-depleted lungs. The effects of lipofibroblast depletion on lung structure were evaluated with histochemical staining against elastin fibers and nuclei. Dramatic changes in the pulmonary phenotype were observed. At P14 there was observed a complete disruption of alveolarization, resulting in condensed tissue areas next to emphysema-like immature air sacs. Even though in previous studies and data from the PDGFRα characterization (21, 75) it was found that PDGFRα^{+} and αSMA^{+} cells drive secondary septation, it was here evident that lipofibroblasts play a crucial role in lung development. Perhaps a pool of lipofibroblasts as early as in P1, that is not deriving from PDGFRα^{+} (27) cells, might be responsible for the proper function of some further αSMA^{+} cells or is contributing to pathways related to their differentiation and proper localization (Figure 33). Furthermore, lipofibroblasts have been demonstrated to support alveolar epithelial type 2 cell function metabolically *in vitro* and *in vivo* (10, 103, 104). Loss of lipofibroblasts at P1 might cause disruption of a proper function of the epithelial system leading to reduced growth and less secretion of growth factors from the epithelial to the mesenchymal compartment. Furthermore a protective role of lipofibroblasts has been demonstrated in the BPD model, supporting the idea of lipofibroblasts being crucial players during alveolarization (61, 66, 83, 84, 86). Lipofibroblasts further have been demonstrated to participate in alveolarization (87) and to transdifferentiate into myofibroblasts during nicotine exposure *in vitro* (85). Furthermore, lipofibroblasts have been demonstrated to be involved in the development and resolution of pulmonary fibrosis (28). These data again support the idea that lipofibroblasts serve as a crucial component of the cellular system driving development and remodeling of the pulmonary structure. Despite previous evidence (26, 28, 86) of the lipofibroblast existence in the human lung, there is still controversial discussion about it (4, 99). The data presented in this study add value to this underrated fibroblast population, as an important cell-type in neonate lung development and prove that lipofibroblasts are necessary for a proper development of lung structure during alveolarization.

4.5 Considerations and outlook

Despite the clear evidence of MSC markers in PDGFRα^{+} cells demonstrated here, there is still a lot to investigate about fibroblasts in the terms of their plasticity and differentiation. In a study by McGowan et al., lung fibroblasts with different levels of *Pdgfrα* gene expression, also expressed different levels of MSC markers (60). A technical issue that might have influenced the results in this study is that the nuclear expression of the reporter gene GFP in the PDGFRα^{GFP} knock-in mice combined with the mostly extracellular expression of markers for MSC might prevent the recognition of a co-expression within the same cell. Future FACS analyses might validate the findings of the immunohistochemistry results presented here. Another important limitation was that, using reporter genes, the reporter proteins might have a different half life time than the endogenous proteins. Thus the spatiotemporal appearance of the reporter gene might not fully reflect the features of the endogenous protein (endogenous PDGFRα expression compared to GFP expression in PDGFRα^{GFP} mice and endogenous ADRP expression compared to mCherry expression in Plin2$^{tm1.1(Cre/ERT2)Mort}$ mice). When using the CreERT2 stop loxP system, recombination might not be completed, and the tamoxifen availability and half-life might have caused a prolonged recombination period compared to the chosen time-points of induction as shown from the Cre activity study in Plin2$^{tm1.1(Cre/ERT2)Mort}$mTmG mice. Finally, the promoter system of the stop loxP reporter mice might have a different expression than the endogenous promoter and thus might change the abundance of the labeled cells. Further studies are needed to elucidate possible differentiation of myofibroblasts and lipofibroblasts back to PDGFRα^{+} progenitor cells during regeneration. I*n vivo* targeting of these changes might reveal new cellular and molecular target candidates for the development of new therapeutic concepts for pulmonary diseases. Since a proper function of the previously generated Plin2$^{tm1.1(Cre/ERT2)Mort}$ mice has been demonstrated by the present study, this line now is available for future studies, targeting and modulating lipofibroblast in animal disease models or to isolate lipofibroblasts during lungdevelopment, disease and regeneration to uncover the molecular signatures underlying lipofibroblast function using molecular screening approaches such as miRNome, transcriptome, metabolom or epigenome.

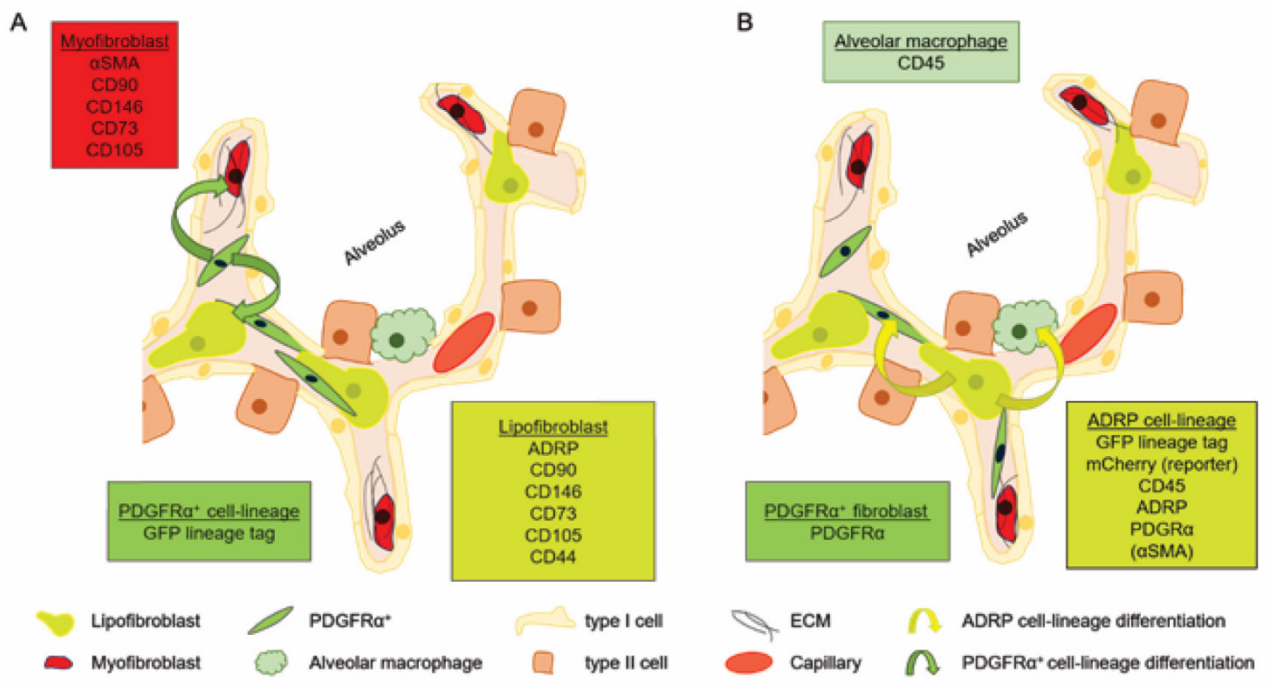

Figure 33 Differentiation of platelet-derived growth factor receptor α^+ fibroblasts and lipofibroblasts during alveolarization.

(A) The cell-lineage of platelet-derived growth factor receptor α^+ (PDGFRα^+) cells (green) can give rise to a part of myofibroblasts and lipofibroblasts during alveolarization (green arrows). Cells deriving from PDGFRα^+ fibroblasts are expressing the mesenchymal stem cell markers CD73, CD146, CD90, CD105 and CD44. (B) Cells of the adipose differentiation related protein$^+$ (ADRP)$^+$ cell-lineage can give rise to PDGFRα^+ cells, CD45$^+$ cells and peribronchial αSMA$^+$ cells (yellow arrows). Type I cell (type I epithelial cell). Type II cell (type II epithelial cell). ECM: extracellular matrix.

5 Summary

The aim of the present study was to characterize pulmonary fibroblast subtypes regarding differentiation and localization during alveolarization and to reveal the impact of fibroblast function on alveolarization. A further aim was to validate and characterize a previously generated Cre driver mouse line to target lipofibroblasts and the further usage of this mouse line to target lipofibroblasts *in vivo*. To address these aims, using *in vivo* tools of the CreERT2 stop loxP system and reporter genes, the present study demonstrated that platelet-derived growth factor receptor α^+ (PDGFRα^+) cells of the early postnatal period could give rise to myofibroblasts and lipofibroblasts during alveolarization. Furthermore, markers of mesenchymal stem cells were detected in generated myo- and lipo-fibroblasts, supporting the progenitor cell character of PDGFRα^+ cells. Consequently, the depletion of early postnatal PDGFRα^+ cells caused a disruption of alveolarization resulting in an abnormal lung structure. This proves the need of PDGFRα^+ cells for proper alveolarization. The present study further validated and characterized the inducible function to target lipofibroblasts of a recently generated Plin2$^{tm1.1(Cre/ERT2)Mort}$ mouse line. Using this functional validated mouse line the present study revealed the spatiotemporal mode of differentiation of lipofibroblasts during alveolarization by labeling and characterizing cells of the ADRP cell-lineage. Finally using the Plin2$^{tm1.1(Cre/ERT2)Mort}$ mouse line it was demonstrated for the first time, that the early postnatal ADRP cell-lineage (lipofibroblast lineage) is essential for appropriate alveolarization. Data of the present study give new insights into the differentiation and function of fibroblast subtypes during alveolarization and provide a new tool to target and manipulate lipofibroblasts *in vivo* by validating the previously generated Cre driver line. The study makes a new contribution to the identification of cellular and molecular targets for the development of new therapeutic strategies for pulmonary structural diseases since the induction of alveolarization in the diseased lung represents a desirable therapeutic approach.

6 Zusammenfassung

Ziel der vorliegenden Arbeit war die Charakterisierung pulmonaler Fibroblasten Subtypen in Bezug auf Differenzierung und Lokalisation während der Alveolarisierung sowie die Aufdeckung des Einflusses der Fibroblastenfunktion auf die Alveolarisierung. Ein weiteres Ziel stellte die Validierung und Charakterisierung einer kürzlich generierten Cre Treiber Mauslinie zur Manipulation von Lipofibroblasten und deren weiterer Gebrauch zur Manipulation von Lipofibroblasten *in vivo* dar. Um diese Ziele zu erreichen wurde mittels *in vivo* Methoden des CreERT2 stop loxP Systems und Reporter Genen gezeigt, dass platelet-derived growth factor receptor α^+ (PDGFRα^+) Zellen der frühen postnatalen Phase Myofibroblasten und Lipofibroblasten in der Alveolarisierung generieren können. Desweitern wurde gezeigt, dass so generierte Myofibroblasten und Lipofibroblasten Marker für mesenchymale Stammzellen exprimieren, als weiteren Hinweis für einen Vorläuferzellcharakter der PDGFRα^+ Zellen. Folgerichtig führte die Depletion früh postnataler PDGFRα^+ Zellen zu einem Abbruch der Alveolarisierung und abnormaler Lungenstruktur. Dieser Effekt beweist die Notwendigkeit PDGFRα^+ Zellen für eine regelrechte Alveolarisierung. Des Weiteren wurde in der vorliegenden Arbeit die induzierbare Funktion einer kürzlich generierten Mauslinie, der Plin2$^{tm1.1(Cre/ERT2)Mort}$ Mauslinie, Lipofibroblasten zu modulieren validiert und charakterisiert. Mit Hilfe dieser funktionell validierten Mauslinie zeigte die vorliegende Arbeit die zeitlich und räumlich abhängige Art der Differenzierung von Lipofibroblasten in der Alveolarisierung durch Markieren und Charakterisieren von Zellen der ADRP Zellabstammungslinie. Schließlich wurde mittels der Plin2$^{tm1.1(Cre/ERT2)Mort}$ Maus Linie erstmalig gezeigt, dass die früh postnatale ADRP Zellabstammunglinie (Lipofibrobalstenabstammungslinie) essentiell für eine adäquate Alveolarisierung ist. Die Daten der vorliegenden Arbeit geben neue Einsichten in die Differenzierung und Funktion von Fibroblasten Subtypen während der Alveolarisierung und liefert durch die Validierung der kürzlich generierten Cre Treiber Mauslinie ein neues Werkzeug, um Lipofibroblasten *in vivo* zu manipulieren. Die vorliegende Arbeit leistet einen neuen Beitrag zur Identifizierung zellulärer und molekularer Zielkandidaten für die Entwicklung neuer therapeutischer Konzepte für strukturelle Lungenerkrankungen, da das Anregen der Alveolarisierung in der erkrankten Lunge einen wünschenswerten therapeutischen Ansatz darstellt.

7 Appendix

7.1 Appendix I: Abbreviations

A555: Alexa 555

A647: Alexa 647

A680: Alexa 680

ADRP: Adipose differentiation related protein

B: Bronchus

bp: Base pair

BSA: Bovine serum albumin

CD: Cluster of Differentiation

cDNA: Complementary DNA

COPD: Chronic obstructive pulmonary disease

ΔCt: Delta (threshold cycle)

°C: Degrees Celsius

DAPI: 4', 6-Diamidino-2-phenylindole dihydrochloride

ddH_2O: Double distilled water

DMEM: Dulbecco's modified Eagle medium

DNA: Deoxyribonucleic acid

dNTP: Deoxyribonucleoside triphosphates

E: Embryonic day

EDTA: Ethylenediaminetetraacetic acid

EMT: epithelial to mesenchymal transition

EpCAM: Epithelial cell adhesion molecule

ER: Estrogen receptor

FACS: Fluorescence-activated cell sorting

FCS: Fetal calf serum

For: Forward

g: Grams

g: Acceleration caused by gravity

GAPDH: Glyceraldehyde 3-phosphate dehydrogenase

GFP: Green fluorescent protein

h: Hour

HEPES: 2-[4-(2-Hydroxyethyl) piperazin-1-yl] ethanesulfonic acid

i.p.: Intraperitoneal

IPF: Idiopathic pulmonary fibrosis

IgG: Immunglobulin G

M: Molar

mCherry: Membrane Cherry

mg: Milligram

min: Minute

ml: Milliliter

mM: Milimolar

mm: Millimeter

mRNA: Messenger RNA

ms: Mouse

MSC: Mesenchymal stem cell

mT: membraneTomato

µg: Microgram

µl: Microliter

µm: Micrometer

NaCl: Sodium chloride

NGS: Normal goat serum

nm: Nanometer

o.n.: Over night

P: Postnatal

PBS: Phosphate-buffered saline

PCR: Polymerase chain reaction

PDGFα: Platelet-derived growth factor α

PDGFRα: Platelet derived growth factor receptor α

PECAM: Platelet endothelial cell adhesion molecule

PFA: Paraformaldehyde

pH: Potential hydrogen

PPARγ: Peroxisome proliferator-activated receptor γ

PTHrP: Parathyroid hormone-related protein

qPCR: Quantitative polymerase chain reaction

rb: Rabbit

Rev: Reverse

RNA: Ribonucleic acid

rpm: Revolutions per minute

RT: Room temperature

rt: Rat

SDS: Sodium dodecyl sulfate

s: second

SPC: Surfactant protein C

αSMA: α-smooth muscle actin

TAE: Tris-Acetate-EDTA-Puffer

TEMED: N, N, N', N'-tetramethylethylenediamine

v/v: Volume by volume

VEGF: Vascular endothelial growth factor

w/v: Mass by volume

WT: Wild type

7.2 Appendix II: Literature

1. **Abdollahi A, Li M, Ping G, Plathow C, Domhan S, Kiessling F, Lee LB, McMahon G, Gröne H-J, Lipson KE, and Huber PE**. Inhibition of platelet-derived growth factor signaling attenuates pulmonary fibrosis. *The Journal of Experimental Medicine* 201: 925-935, 2005.
2. **Abremski K, and Hoess R**. Bacteriophage P1 site-specific recombination. Purification and properties of the Cre recombinase protein. *Journal of Biological Chemistry* 259: 1509-1514, 1984.
3. **Ackermann M, Houdek JP, Gibney BC, Ysasi A, Wagner W, Belle J, Schittny JC, Enzmann F, Tsuda A, Mentzer SJ, and Konerding MA**. Sprouting and intussusceptive angiogenesis in postpneumonectomy lung growth: mechanisms of alveolar neovascularization. *Angiogenesis* 17: 541-551, 2014.
4. **Ahlbrecht K, and McGowan SE**. In search of the elusive lipofibroblast in human lungs. *American Journal of Physiology - Lung Cellular and Molecular Physiology* 307: L605-608, 2014.
5. **Andrae J, Gallini R, and Betsholtz C**. Role of platelet-derived growth factors in physiology and medicine. *Genes & Development* 22: 1276-1312, 2008.
6. **Ataliotis P, Symes K, Chou MM, Ho L, and Mercola M**. PDGF signalling is required for gastrulation of Xenopus laevis. *Development* 121: 3099, 1995.
7. **Avery ME, and Mead J**. Surface properties in relation to atelectasis and hyaline membrane disease. *AMA Journal of Diseases of Children* 97: 517-523, 1959.
8. **Bagnato G, and Harari S**. Cellular interactions in the pathogenesis of interstitial lung diseases. *European Respiratory Review* 24: 102-114, 2015.
9. **Bando M**. Pirfenidone: Clinical trials and clinical practice in patients with idiopathic pulmonary fibrosis. *Respiratory Investigation* 54: 298-304, 2016.
10. **Barkauskas CE, Cronce MJ, Rackley CR, Bowie EJ, Keene DR, Stripp BR, Randell SH, Noble PW, and Hogan BLM**. Type 2 alveolar cells are stem cells in adult lung. *The Journal of Clinical Investigation* 123: 3025-3036, 2013.
11. **Behr J, Kreuter M, Hoeper MM, Wirtz H, Klotsche J, Koschel D, Andreas S, Claussen M, Grohé C, Wilkens H, Randerath W, Skowasch D, Meyer FJ, Kirschner J, Gläser S, Herth FJF, Welte T, Huber RM, Neurohr C, Schwaiblmair M, Kohlhäufl M, Höffken G, Held M, Koch A, Bahmer T, and Pittrow D**. Management of patients with idiopathic pulmonary fibrosis in clinical practice: the insights-IPF registry. *European Respiratory Journal* 46: 186-196, 2015.
12. **Betsholtz C, Lindblom P, Bjarnegard M, Enge M, Gerhardt H, and Lindahl P**. Role of platelet-derived growth factor in mesangium development and vasculopathies: lessons from platelet-derived growth factor and platelet-derived growth factor receptor mutations in mice. *Current Opinion in Nephrology and Hypertension* 13: 45-52, 2004.
13. **Bland RD, Mokres LM, Ertsey R, Jacobson BE, Jiang S, Rabinovitch M, Xu L, Shinwell ES, Zhang F, and Beasley MA**. Mechanical ventilation with 40% oxygen reduces pulmonary expression of genes that regulate lung development and impairs alveolar septation in newborn mice. *American Journal of Physiology - Lung Cellular and Molecular Physiology* 293: L1099-L1110, 2007.
14. **Boström H, Gritli-Linde A, and Betsholtz C**. PDGF-a/PDGF alpha-receptor signaling is required for lung growth and the formation of alveoli but not for early lung branching morphogenesis. *Developmental Dynamics* 223: 155-162, 2002.
15. **Bostrom H, Willetts K, Pekny M, Leveen P, Lindahl P, Hedstrand H, Pekna M, Hellstrom M, Gebre-Medhin S, Schalling M, Nilsson M, Kurland S, Tornell J, Heath JK, and**

Betsholtz C. PDGF-A signaling is a critical event in lung alveolar myofibroblast development and alveogenesis. *Cell* 85: 863-873, 1996.
16. **Branchfield K, Li R, Lungova V, Verheyden JM, McCulley D, and Sun X**. A three-dimensional study of alveologenesis in mouse lung. *Developmental Biology* 409: 429-441, 2016.
17. **Brody JS, and Vaccaro C**. Postnatal formation of alveoli: interstitial events and physiologic consequences. In: *Federation Proceedings* 1979, p. 215-223.
18. **Burri PH**. Fetal and postnatal development of the lung. *Annual Review of Physiology* 46: 617-628, 1984.
19. **Burri PH**. Structural Aspects of Postnatal Lung Development – Alveolar Formation and Growth. *Neonatology* 89: 313-322, 2006.
20. **Chao C-M, Moiseenko A, Zimmer K-P, and Bellusci S**. Alveologenesis: key cellular players and fibroblast growth factor 10 signaling. *Molecular and Cellular Pediatrics* 3: 17, 2016.
21. **Chen L, Acciani T, Le Cras T, Lutzko C, and Perl A-KT**. Dynamic regulation of platelet-derived growth factor receptor α expression in alveolar fibroblasts during realveolarization. *American Journal of Respiratory Cell and Molecular Biology* 47: 517-527, 2012.
22. **Chierakul N, Phanphongsiri S, Chuaychoo B, Muangman N, and Totanarungroj K**. Relationship between emphysema quantification and COPD severity. *Journal of the Medical Association of Thailand = Chotmaihet thangphaet* 97: 1290-1295, 2014.
23. **Cook MJ**. *The anatomy of the laboratory mouse*. Academic Press, 1965
24. **Darby I, Skalli O, and Gabbiani G**. a-Smooth muscle actin is transiently expressed by myofibroblasts during experimental wound healing. *Laboratory Investigation* 63: 21-29, 1990.
25. **Desmouliere A, Geinoz A, Gabbiani F, and Gabbiani G**. TGF-β1 induces α-smooth muscle actin expression in granulation tissue myofibroblasts and in quiescent and growing cultured fibroblasts. *Journal of Cell Biology* 122: 103-111, 1993.
26. **Deutsch GH, and Young LR**. Lipofibroblast Phenotype in Pulmonary Interstitial Glycogenosis. *American Journal of Respiratory and Critical Care Medicine* 193: 694-696, 2016.
27. **El Agha E, Herold S, Al Alam D, Quantius J, MacKenzie B, Carraro G, Moiseenko A, Chao C-M, Minoo P, and Seeger W**. Fgf10-positive cells represent a progenitor cell population during lung development and postnatally. *Development* 141: 296-306, 2014.
28. **El Agha E, Moiseenko A, Kheirollahi V, De Langhe S, Crnkovic S, Kwapiszewska G, Kosanovic D, Schwind F, Schermuly RT, and Henneke I**. Two-way conversion between lipogenic and myogenic fibroblastic phenotypes marks the progression and resolution of lung fibrosis. *Cell Stem Cell* 20: 261-273. e263, 2017.
29. **Endale M, Ahlfeld S, Bao E, Chen X, Green J, Bess Z, Weirauch MT, Xu Y, and Perl AK**. Temporal, spatial, and phenotypical changes of PDGFRα expressing fibroblasts during late lung development. *Developmental Biology* 425: 161-175, 2017.
29. **Farmer CG**. Evolution of the vertebrate cardio-pulmonary system. *Annual Review of Physiology* 61: 573-592, 1999.
30. **Feil S, Valtcheva N, and Feil R**. Inducible Cre mice. In: *Gene Knockout Protocols: Second Edition*, edited by Wurst W, and Kühn R. Totowa, NJ: Humana Press, 2009, p. 343-363.
31. **Feingold KR, Kazemi MR, Magra AL, McDonald CM, Chui LG, Shigenaga JK, Patzek SM, Chan ZW, Londos C, and Grunfeld C**. ADRP/ADFP and Mal1 expression are increased in macrophages treated with TLR agonists. *Atherosclerosis* 209: 81-88, 2010.
32. **Gaillard D, and Puchelle E**. Differentiation and maturation of airway epithelial cells: role of extracellular matrix and growth factors. In: *Lung Development*, edited by Gaultier C, Bourbon JR, and Post M. New York, NY: Springer New York, 1999, p. 46-76.

33. **Gouveia L, Betsholtz C, and Andrae J**. Expression analysis of platelet-derived growth factor receptor alpha and its ligands in the developing mouse lung. *Physiological Reports* 5: e13092, 2017.
35. **Green J, Endale M, Auer H, and Perl AK**. Diversity of interstitial lung fibroblasts is regulated by platelet-derived growth factor receptor alpha kinase activity. *American Journal of Respiratroy Cell and Molecular Biology* 54: 532-545, 2016.
36. **Hagood JS, Miller PJ, Lasky JA, Tousson A, Guo B, Fuller GM, and McIntosh JC**. Differential expression of platelet-derived growth factor-α receptor by Thy-1− and Thy-1+ lung fibroblasts. *American Journal of Physiology-Lung Cellular and Molecular Physiology* 277: L218-L224, 1999.
37. **Hamilton TG, Klinghoffer RA, Corrin PD, and Soriano P**. Evolutionary divergence of platelet-derived growth factor alpha receptor signaling mechanisms. *Molecular and Cellular Biology* 23: 4013-4025, 2003.
38. **Heldin C-H, and Westermark B**. Mechanism of action and in vivo role of platelet-derived growth factor. *Physiological Reviews* 79: 1283, 1999.
39. **Hinz B, and Gabbiani G**. Fibrosis: recent advances in myofibroblast biology and new therapeutic perspectives. *F1000 Biology Reports* 2: 78, 2010.
40. **Hinz B, Phan SH, Thannickal VJ, Galli A, Bochaton-Piallat M-L, and Gabbiani G**. The myofibroblast: one function, multiple origins. *The American Journal of Pathology* 170: 1807-1816, 2007.
41. **Hinz B, Phan SH, Thannickal VJ, Prunotto M, Desmoulière A, Varga J, De Wever O, Mareel M, and Gabbiani G**. Recent developments in myofibroblast biology: paradigms for connective tissue remodeling. *The American Journal of Pathology* 180: 1340-1355, 2012.
42. **Hughes G, Toellner H, Morris H, Leonard C, and Chaudhuri N**. Real world experiences: pirfenidone and nintedanib are effective and well tolerated treatments for idiopathic pulmonary fibrosis. *Journal of Clinical Medicine* 5: 78, 2016.
43. **Imamura M, Inoguchi T, Ikuyama S, Taniguchi S, Kobayashi K, Nakashima N, and Nawata H**. ADRP stimulates lipid accumulation and lipid droplet formation in murine fibroblasts. *American Journal of Physiology Endocrinology and Metabolism* 283: E775-783, 2002.
44. **Jiang HP, Harris SE, and Serrero G**. Molecular cloning of a differentiation-related mRNA in the adipogenic cell line 1246. *Cell growth & differentiation : the molecular biology journal of the American Association for Cancer Research* 3: 21-30, 1992.
45. **Jiang HP, and Serrero G**. Isolation and characterization of a full-length cDNA coding for an adipose differentiation-related protein. *Proceedings of the National Academy of Sciences of the United States of America* 89: 7856-7860, 1992.
44. **Jiang HP, Harris SE, and Serrero G**. Molecular cloning of a differentiation-related mRNA in the adipogenic cell line 1246. *Cell Growth & Differentiation : the Molecular Biology Journal of the American Association for Cancer Research* 3: 21-30, 1992.
45. **Jiang HP, and Serrero G**. Isolation and characterization of a full-length cDNA coding for an adipose differentiation-related protein. *Proceedings of the National Academy of Sciences of the United States of America* 89: 7856-7860, 1992.
46. **Kaplan NB, Grant MM, and Brody JS**. The lipid interstitial cell of the pulmonary alveolus: age and species differences 1, 2. *American Review of Respiratory Disease* 132: 1307-1312, 1985.
47. **Kim DS, Collard HR, and Talmadge E. King J**. Classification and Natural History of the Idiopathic Interstitial Pneumonias. *Proceedings of the American Thoracic Society* 3: 285-292, 2006.

48. **Kimura J, and Deutsch GH**. Key mechanisms of early lung development. *Pediatric and Developmental Pathology* 10: 335-347, 2007.
49. **Ko MSH**. Embryogenomics: developmental biology meets genomics. *Trends in Biotechnology* 19: 511-518.
50. **Koumas L, Smith TJ, Feldon S, Blumberg N, and Phipps RP**. Thy-1 Expression in Human Fibroblast Subsets Defines Myofibroblastic or Lipofibroblastic Phenotypes. *The American Journal of Pathology* 163: 1291-1300, 2003.
51. **Kuhn 3rd C**. Cytochemistry of pulmonary alveolar epithelial cells. *The American Journal of Pathology* 53: 809, 1968.
52. **Leslie K, King TE, and Low R**. Smooth muscle actin is expressed by air space fibroblast-like cells in idiopathic pulmonary fibrosis and hypersensitivity pneumonitis. *Chest Journal* 99: 47S-48S, 1991.
53. **Leslie KO, Mitchell J, and Low R**. Lung myofibroblasts. *Cell Motility and the Cytoskeleton* 22: 92-98, 1992.
54. **Li C, Li M, Li S, Xing Y, Yang C-Y, Li A, Borok Z, De Langhe S, and Minoo P**. Progenitors of Secondary Crest Myofibroblasts Are Developmentally Committed in Early Lung Mesoderm. *Stem Cells* 33: 999-1012, 2015.
55. **Li X, Ye J, Zhou L, Gu W, Fisher EA, and Li P**. Opposing roles of cell death-inducing DFF45-like effector B and perilipin 2 in controlling hepatic VLDL lipidation. *Journal of lipid research* 53: 1877-1889, 2012.
56. **Lindahl P, Karlsson L, Hellstrom M, Gebre-Medhin S, Willetts K, Heath JK, and Betsholtz C**. Alveogenesis failure in PDGF-A-deficient mice is coupled to lack of distal spreading of alveolar smooth muscle cell progenitors during lung development. *Development* 124: 3943-3953, 1997.
57. **Londos C, Sztalryd C, Tansey JT, and Kimmel AR**. Role of PAT proteins in lipid metabolism. *Biochimie* 87: 45-49, 2005.
58. **Madurga A, Mižíková I, Ruiz-Camp J, and Morty RE**. Recent advances in late lung development and the pathogenesis of bronchopulmonary dysplasia. *American Journal of Physiology - Lung Cellular and Molecular Physiology* 305: L893-L905, 2013.
59. **Maeda Y, Davé V, and Whitsett JA**. Transcriptional Control of Lung Morphogenesis. *Physiological Reviews* 87: 219-244, 2007.
60. **Mak KM, Ren C, Ponomarenko A, Cao Q, and Lieber CS**. Adipose differentiation-related protein is a reliable lipid droplet marker in alcoholic fatty liver of rats. *Alcoholism: Clinical and Experimental Research* 32: 683-689, 2008.
61. **Maksvytis H, Vaccaro C, and Brody J**. Isolation and characterization of the lipid-containing interstitial cell from the developing rat lung. *Laboratory Investigation; a Journal of Technical Methods and Pathology* 45: 248-259, 1981.
62. **McCulley D, Wienhold M, and Sun X**. The pulmonary mesenchyme directs lung development. *Current Opinion in Genetics & Development* 32: 98-105, 2015.
63. **McDonald JA**. Lung growth and development. 100: 2008.
64. **McGowan SE, Grossmann RE, Kimani PW, and Holmes AJ**. Platelet-derived growth factor receptor-alpha-expressing cells localize to the alveolar entry ring and have characteristics of myofibroblasts during pulmonary alveolar septal formation. *The Anatomical Record: Advances in Integrative Anatomy and Evolutionary Biology* 291: 1649-1661, 2008.
65. **McGowan SE, Harvey CS, and Jackson SK**. Retinoids, retinoic acid receptors, and cytoplasmic retinoid binding proteins in perinatal rat lung fibroblasts. *American Journal of Physiology - Lung Cellular and Molecular Physiology* 269: L463-L472, 1995.

66. **McGowan SE, Jackson SK, Doro MM, and Olson PJ**. Peroxisome proliferators alter lipid acquisition and elastin gene expression in neonatal rat lung fibroblasts. *American Journal of Physiology - Lung Cellular and Molecular Physiology* 273: L1249-L1257, 1997.
67. **McGowan SE, and McCoy DM**. Platelet-derived growth factor-A regulates lung fibroblast S-phase entry through p27(kip1) and FoxO3a. *Respiratory Research* 14: 68-68, 2013.
68. **McGowan SE, and McCoy DM**. Regulation of fibroblast lipid storage and myofibroblast phenotypes during alveolar septation in mice. *American Journal of Physiology - Lung Cellular and Molecular Physiology* 307: L618-L631, 2014.
69. **McGowan SE, and Torday JS**. The pulmonary lipofibroblast (lipid interstitial cell) and its contributions to alveolar development. *Annual Review of Physiology* 59: 43-62, 1997.
70. **Metzger D, and Chambon P**. Site-and time-specific gene targeting in the mouse. *Methods* 24: 71-80, 2001.
71. **Muzumdar MD, Tasic B, Miyamichi K, Li L, and Luo L**. A global double-fluorescent Cre reporter mouse. G*enesis* 45: 593-605, 2007.
72. **Nagy A**. Cre recombinase: the universal reagent for genome tailoring. *Genesis* 26: 99-109, 2000.
73. **Narayanan M, Owers-Bradley J, Beardsmore CS, Mada M, Ball I, Garipov R, Panesar KS, Kuehni CE, Spycher BD, Williams SE, and Silverman M**. Alveolarization continues during childhood and adolescence: new evidence from helium-3 magnetic resonance. *American Journal of Respiratory and Critical Care Medicine* 185: 186-191, 2012.
74. **Nicola T, Hagood JS, James ML, MacEwen MW, Williams TA, Hewitt MM, Schwiebert L, Bulger A, Oparil S, and Chen Y-F**. Loss of Thy-1 inhibits alveolar development in the newborn mouse lung. *American Journal of Physiology-Lung Cellular and Molecular Physiology* 296: L738-L750, 2009.
75. **Ntokou A, Klein F, Dontireddy D, Becker S, Bellusci S, Richardson WD, Szibor M, Braun T, Morty RE, Seeger W, Voswinckel R, and Ahlbrecht K**. Characterization of the platelet-derived growth factor receptor-α-positive cell-lineage during murine late lung development. *American Journal of Physiology - Lung Cellular and Molecular Physiology* 309: L942-L958, 2015.
76. **O'Hare KH, and Sheridan MN**. Electron microscopic observations on the morphogenesis of the albino rat lung, with special reference to pulmonary epithelial cells. *American Journal of Anatomy* 127: 181-205, 1970.
77. **O'Reilly M, and Thébaud B**. Animal models of bronchopulmonary dysplasia. The term rat models. *American Journal of Physiology - Lung Cellular and Molecular Physiology* 307: L948-L958, 2014.
78. **Ornitz DM, and Itoh N**. The fibroblast growth factor signaling pathway. *Wiley Interdisciplinary Reviews: Developmental Biology* 4: 215-266, 2015.
79. **Padela S, Cabacungan J, Shek S, Belcastro R, Yi M, Jankov RP, and Tanswell AK**. Hepatocyte growth factor is required for alveologenesis in the neonatal rat. *American Journal of Respiratory and Critical Care Medicine* 172: 907-914, 2005.
80. **Padela S, Yi M, Cabacungan J, Shek S, Belcastro R, Masood A, Jankov RP, and Tanswell AK**. A critical role for fibroblast growth factor-7 during early alveolar formation in the neonatal rat. *Pediatric Research* 63: 232-238, 2008.
81. **Perl A-KT, and Gale E**. FGF signaling is required for myofibroblast differentiation during alveolar regeneration. *American Journal of Physiology-Lung Cellular and Molecular Physiology* 297: L299-L308, 2009.

82. **Popova AP, Bentley JK, Cui TX, Richardson MN, Linn MJ, Lei J, Chen Q, Goldsmith AM, Pryhuber GS, and Hershenson MB**. Reduced platelet-derived growth factor receptor expression is a primary feature of human bronchopulmonary dysplasia. *American Journal of Physiology - Lung Cellular and Molecular Physiology* 307: L231-L239, 2014.
83. **Rehan V, and Torday J**. Hyperoxia augments pulmonary lipofibroblast-to-myofibroblast transdifferentiation. *Cell Biochemistry and Biophysics* 38: 239-249, 2003.
84. **Rehan VK, Sakurai R, Corral J, Krebs M, Ibe B, Ihida-Stansbury K, and Torday JS**. Antenatally administered PPAR-gamma agonist rosiglitazone prevents hyperoxia-induced neonatal rat lung injury. *American Journal of Physiology - Lung cellular and Molecular Physiology* 299: L672-680, 2010.
85. **Rehan VK, Sakurai R, Wang Y, Santos J, Huynh K, and Torday JS**. Reversal of nicotine-induced alveolar lipofibroblast-to-myofibroblast transdifferentiation by stimulants of parathyroid hormone-related protein signaling. *Lung* 185: 151-159, 2007.
86. **Rehan VK, Sugano S, Wang Y, Santos J, Romero S, Dasgupta C, Keane MP, Stahlman MT, and Torday JS**. Evidence for the presence of lipofibroblasts in human lung. *Experimental Lung Research* 32: 379-393, 2006.
87. **Rehan VK, and Torday JS**. PPARγ signaling mediates the evolution, development, homeostasis, and repair of the lung. *PPAR Research* 2012: 289867, 2012.
88. **Rehan VK, Wang Y, Patel S, Santos J, and Torday JS**. Rosiglitazone, a peroxisome proliferator-activated receptor-γ agonist, prevents hyperoxia-induced neonatal rat lung injury in vivo. *Pediatric Pulmonology* 41: 558-569, 2006.
89. **Roesch K, Jadhav AP, Trimarchi JM, Stadler MB, Roska B, Sun BB, and Cepko CL**. The transcriptome of retinal Müller glial cells. *Journal of Comparative Neurology* 509: 225-238, 2008.
90. **Rudnick D**. Developmental capacities of the chick lung in chorioallantoic grafts. *Journal of Experimental Zoology* 66: 125-153, 1933.
91. **Sanders YY, Kumbla P, and Hagood JS**. Enhanced myofibroblastic differentiation and survival in Thy-1(−) lung fibroblasts. *American Journal of Respiratory Cell and Molecular Biology* 36: 226-235, 2007.
92. **Schultz CJ, Torres E, Londos C, and Torday JS**. Role of adipocyte differentiation-related protein in surfactant phospholipid synthesis by type II cells. *American Journal of Physiology - Lung Cellular and Molecular Physiology* 283: L288-L296, 2002.
93. **Shannon JM, and Hyatt BA**. Epithelial-mesenchymal interactions in the developing lung. *Annual Review of Physiology* 66: 625-645, 2004.
94. **Silva DMG, Nardiello C, Pozarska A, and Morty RE**. Recent advances in the mechanisms of lung alveolarization and the pathogenesis of bronchopulmonary dysplasia. *American Journal of Physiology - Lung Cellular and Molecular Physiology* 309: L1239-L1272, 2015.
95. **Skalli O, Ropraz P, Trzeciak A, Benzonana G, Gillessen D, and Gabbiani G**. A monoclonal antibody against alpha-smooth muscle actin: a new probe for smooth muscle differentiation. *The Journal of Cell Biology* 103: 2787-2796, 1986.
96. **Smith BT**. Lung maturation in the fetal rat: acceleration by injection of fibroblast-pneumonocyte factor. *Science* 204: 1094-1095, 1979.
97. **Spooner BS, and Wessells NK**. Mammalian lung development: Interactions in primordium formation and bronchial morphogenesis. *Journal of Experimental Zoology* 175: 445-454, 1970.

98. **Su AI, Wiltshire T, Batalov S, Lapp H, Ching KA, Block D, Zhang J, Soden R, Hayakawa M, Kreiman G, Cooke MP, Walker JR, and Hogenesch JB**. A gene atlas of the mouse and human protein-encoding transcriptomes. *Proceedings of the National Academy of Sciences of the United States of America* 101: 6062-6067, 2004.
99. **Tahedl D, Wirkes A, Tschanz SA, Ochs M, and Muhlfeld C**. How common is the lipid body-containing interstitial cell in the mammalian lung? *American Journal of Physiology Lung Cellular and Molecular Physiology* 307: L386-394, 2014.
100. **Tallquist M, and Kazlauskas A**. PDGF signaling in cells and mice. *Cytokine & Growth Factor Reviews* 15: 205-213, 2004.
101. **Torday J, Hua J, and Slavin R**. Metabolism and fate of neutral lipids of fetal lung fibroblast origin. *Biochimica et Biophysica Acta (BBA) - Lipids and Lipid Metabolism* 1254: 198-206, 1995.
102. **Torday JS, and Rehan VK**. Developmental cell/molecular biologic approach to the etiology and treatment of bronchopulmonary dysplasia. *Pediatric Research* 62: 2-7, 2007.
103. **Torday JS, and Rehan VK**. Stretch-stimulated surfactant synthesis is coordinated by the paracrine actions of PTHrP and leptin. *American Journal of Physiology - Lung Cellular and Molecular Physiology* 283: L130-L135, 2002.
104. **Torday JS, Sun H, Wang L, and Torres E**. Leptin mediates the parathyroid hormone-related protein (PTHrP) paracrine stimulation of fetal lung maturation. *American Journal of Physiology Lung Cellular and Molecular Physiology* 282: L405-L410, 2002.
105. **Townsley MI**. Structure and composition of pulmonary arteries, capillaries and veins. *Comprehensive Physiology* 2: 675-709, 2012.
106. **Tschanz SA, Salm LA, Roth-Kleiner M, Barre SF, Burri PH, and Schittny JC**. Rat lungs show a biphasic formation of new alveoli during postnatal development. *Journal of Applied Physiology (1985)* 117: 89-95, 2014.
107. **Ullah I, Subbarao Raghavendra B, and Rho Gyu J**. Human mesenchymal stem cells - current trends and future prospective. *Bioscience Reports* 35: e00191, 2015.
108. **Vaccaro C, and Brody JS**. Ultrastructure of developing alveoli. I. The role of the interstitial fibroblast. *The Anatomical Record* 192: 467-479, 1978.
109. **Varisco BM, Ambalavanan N, Whitsett JA, and Hagood JS**. Thy-1 signals through pparγ to promote lipofibroblast differentiation in the developing lung. *American Journal of Respiratory Cell and Molecular Biology* 46: 765-772, 2012.
110. **Voehringer D, Liang H-E, and Locksley RM**. Homeostasis and effector function of lymphopenia-induced 'memory-like' T cells in constitutively T cell-depleted mice. *Journal of Immunology (Baltimore, Md : 1950)* 180: 4742-4753, 2008.
111. **Vyas-Read S, Wang W, Kato S, Colvocoresses-Dodds J, Fifadara NH, Gauthier TW, Helms MN, Carlton DP, and Brown LAS**. Hyperoxia induces alveolar epithelial-to-mesenchymal cell transition. *American Journal of Physiology-Lung Cellular and Molecular Physiology* 306: L326-L340, 2014.
112. **Warburton D, El-Hashash A, Carraro G, Tiozzo C, Sala F, Rogers O, De Langhe S, Kemp PJ, Riccardi D, Torday J, Bellusci S, Shi W, Lubkin SR, and Jesudason E**. Lung organogenesis. *Current Topics in Developmental Biology* 90: 73-158, 2010.
113. **Weaver M, Batts L, and Hogan BLM**. Tissue interactions pattern the mesenchyme of the embryonic mouse lung. *Developmental Biology* 258: 169-184, 2003.
114. **Whimster WF**. The microanatomy of the alveolar duct system. *Thorax* 25: 141-149, 1970.

115. **Williams MC**. Alveolar type I cells: molecular phenotype and development. *Annual Review of Physiology* 65: 669-695, 2003.
116. **Wilson DB**. Anatomy: A regional atlas of the human body, 2nd Edition. *Head & Neck Surgery* 4: 178-178, 1981.
117. **Wright JR, and Clements JA**. Metabolism and turnover of lung surfactant. *The American Review of Respiratory Disease* 136: 426-444, 1987.
118. **Yamada M, Kurihara H, Kinoshita K, and Sakai T**. Temporal expression of alpha–smooth muscle actin and drebrin in septal interstitial cells during alveolar maturation. *Journal of Histochemistry & Cytochemistry* 53: 735-744, 2005.
119. **Zhou Y, Hagood JS, and Murphy-Ullrich JE**. Thy-1 expression regulates the ability of rat lung fibroblasts to activate transforming growth factor-β in response to fibrogenic stimuli. *The American Journal of Pathology* 165: 659-669, 2004.

7.3 Appendix III: Controls

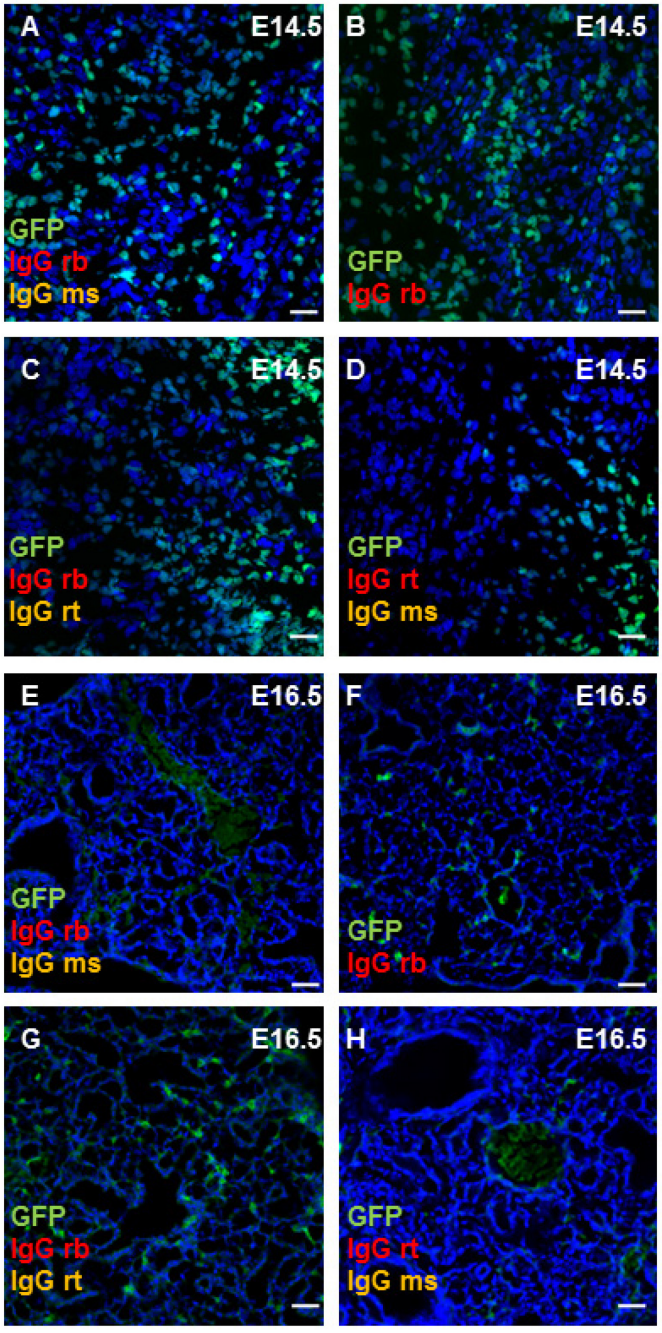

Figure 34 Isotype controls for PDGFR^{GFP} mice for embryonic day 14.5 and 16.5.

(A-H) Lung tissue of PDGFRα^{GFP} mice was stained for IgG control antibodies against rabbit (rb), rat (rt), and mouse (ms) at embryonic day (E) 14.5 and E16.5, followed by secondary antibody staining (A-C and E-G) A555 anti-rabbit (red). (A, D, E, H) A647 anti-mouse (orange). (C, G) A647 anti-rat (orange). (D, H) A555 anti-rat (red). A 4',-6-diamidino-2-phenylindole dihydrochloride nuclear stain (blue) was used. Green fluorescent protein^{+} (GFP^{+}) cells were detected at all stages but no signal was detected for the isotype staining. Scale bar = 50 µm.

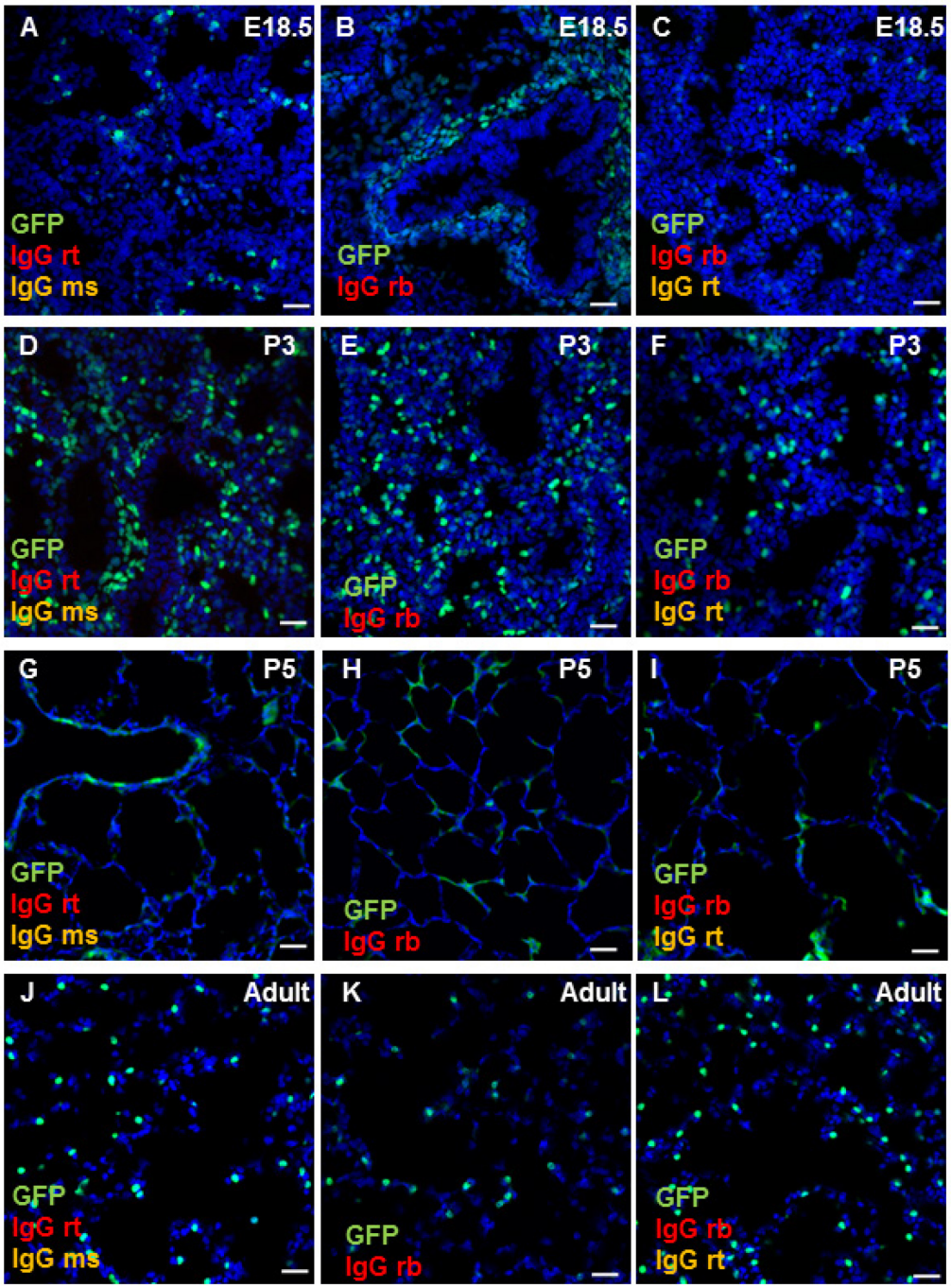

Figure 35 Isotype controls for PDGFR^{GFP} mice for embryonic day 18.5, postnatal day 3 and 5, and adult stage.

(A-L) Lung tissue of PDGFRα^{GFP} mice was stained for IgG control antibodies against rabbit (rb), rat (rt), and mouse (ms) at embryonic day (E) 18.5 and postnatal day (P) 3, P5 and adult stage, followed by secondary antibody staining (B, C, E, F, H, I, K, L) A555-anti-rabbit (red). (A, D, G, J) A647 anti-mouse (orange). (C, F, I, L) A647 anti-rat (orange). (A, D, G, J) A555 anti-rat (red). A 4', 6-diamidino-2-phenylindole dihydrochloride nuclear stain (blue) was used. Green fluorescent protein^{+} (GFP^{+}) cells (green) were detected at all stages but no signal was detected for the isotype staining. Scale bar = 50 µm.

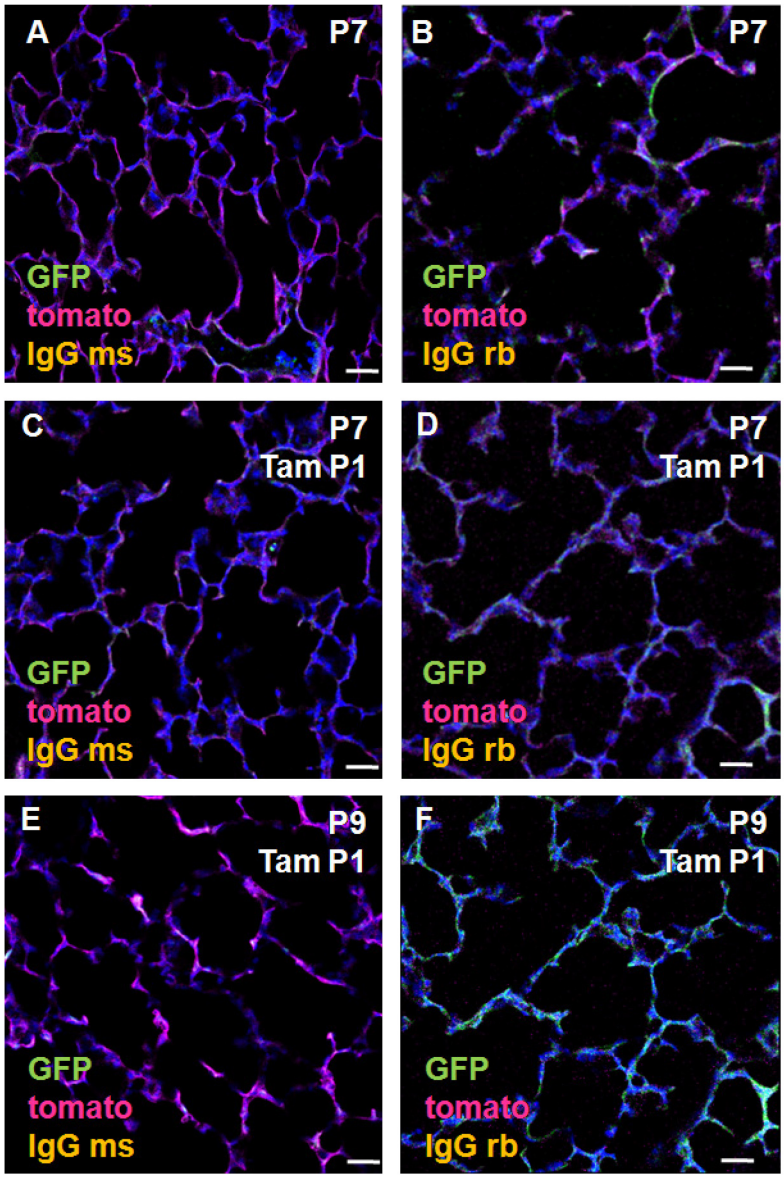

Figure 36 Isotype controls for PDGFRα^{Cre}mTmG and PDGFRα^{CreER}mTmG mice for postnatal day 7 and 9.

(A-B) Lung tissue of PDGFRα^{Cre}mTmG was stained for IgG control antibodies against rabbit (rb), and mouse (ms) at postnatal day (P) 7. (C-F) Lung tissue of PDGFRα^{CreER}mTmG was stained for the same IgG control antibodies at P7 and P9 after tamoxifen (Tam) injection at P1. Tissues were subsequently stained with A647 anti-rabbit or A647 anti-mouse (orange) antibodies. A 4', 6-diamidino-2-phenylindole dihydrochloride nuclear stain (blue) was used. Green fluorescent protein^{+} (GFP^{+}) cells (green) as well as tomato^{+} (magenda) were detected at all stages but no signal was detected for the isotype staining. Scale bar = 50 μm.

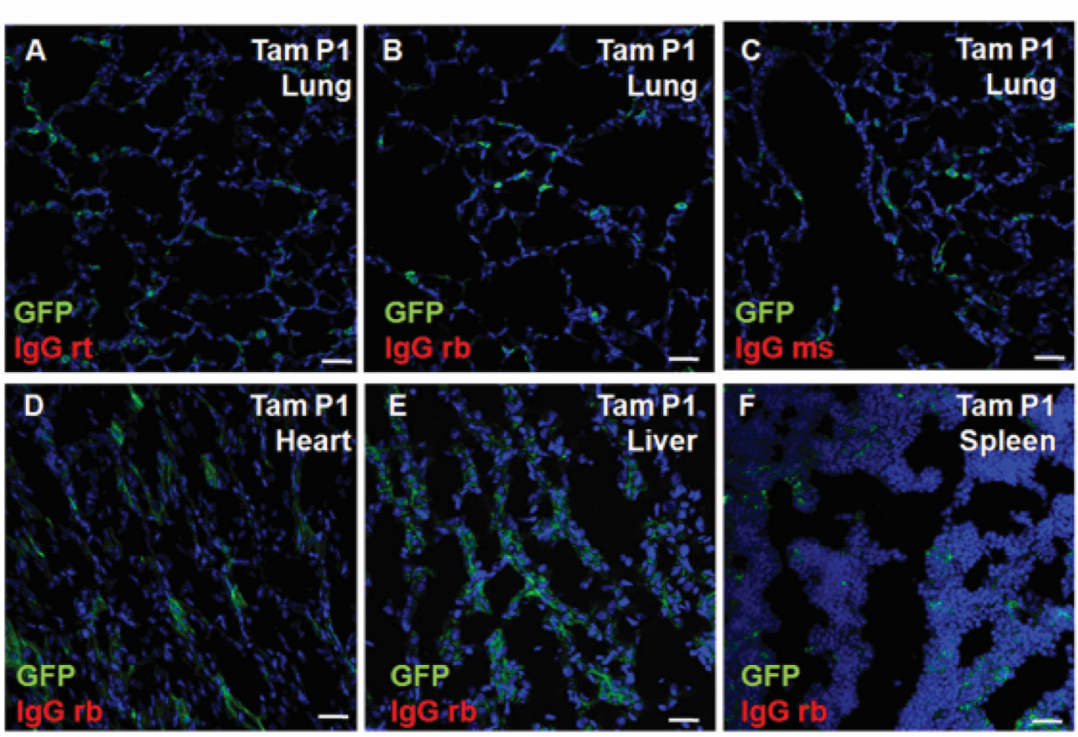

Figure 37 Isotype controls for Plin2$^{tm1.1(Cre/ERT2)Mort}$mTmG for postnatal day 14.

(A-F) Tissues of Plin2$^{tm1.1(Cre/ERT2)Mort}$mTmG was stained for IgG control antibody against rat (rt), rabbit (rb), and , mouse (ms) at postnatal day (P) 14, after tamoxifen (Tam) injection at P1. Tissues were subsequently stained with A647 anti-rat, A647 anti-rabbit, or A647 anti-mouse (red) antibodies. A 4', 6-diamidino-2-phenylindole dihydrochloride nuclear stain (blue) was used. Green fluorescent protein^{+} (GFP^{+}) cells (green) were detected at all tissues, marking adipose differentiation related protein (ADRP) expression but no signal was detected for the isotype staining. Scale bar = 50 μm.

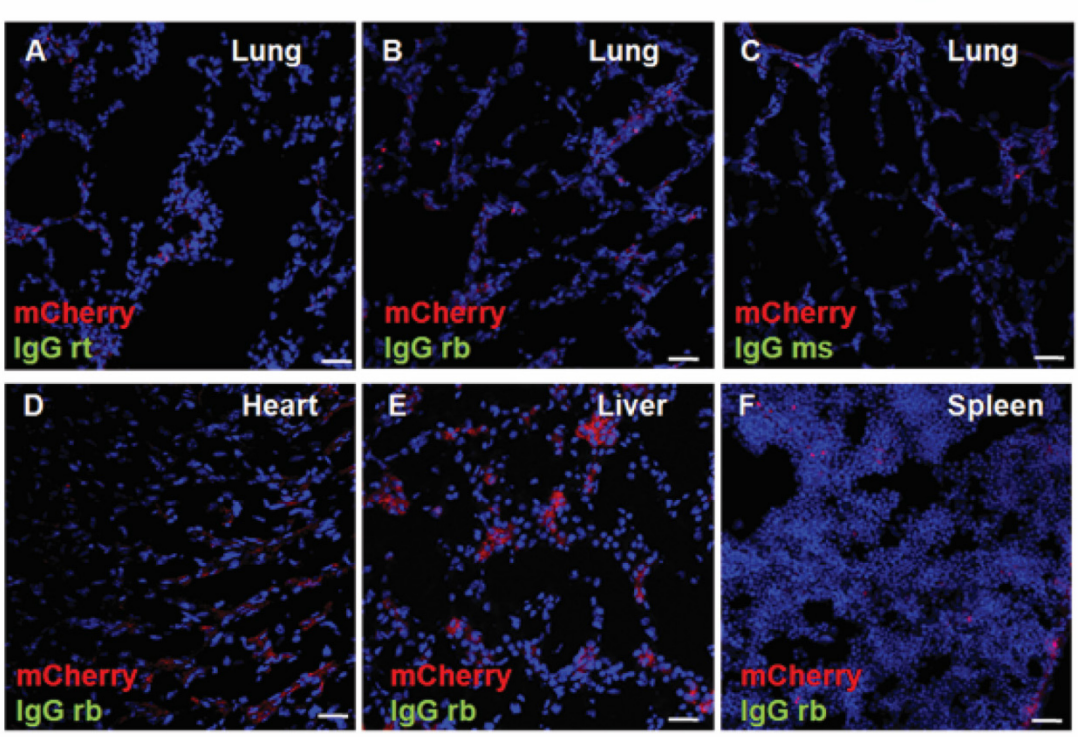

Figure 38 Isotype controls for Plin2$^{tm1.1(Cre/ERT2)Mort}$ for postnatal day 14.

(A-F) Tissues of Plin2$^{tm1.1(Cre/ERT2)Mort}$ mice was stained for IgG control antibody against rat (rt), rabbit (rb), and , mouse (ms) at postnatal day (P) 14. Tissues were subsequently stained with A647 anti-rat, A647 anti-rabbit, or A647 anti-mouse (green) antibodies. A 4', 6-diamidino-2-phenylindole dihydrochloride nuclear stain (blue) was used. Membrane Cherry^{+} (mCherry^{+}) cells (red) were detected at all tissues, marking adipose differentiation related protein (ADRP) expression but no signal was detected for the isotype staining. Scale bar = 50 μm.

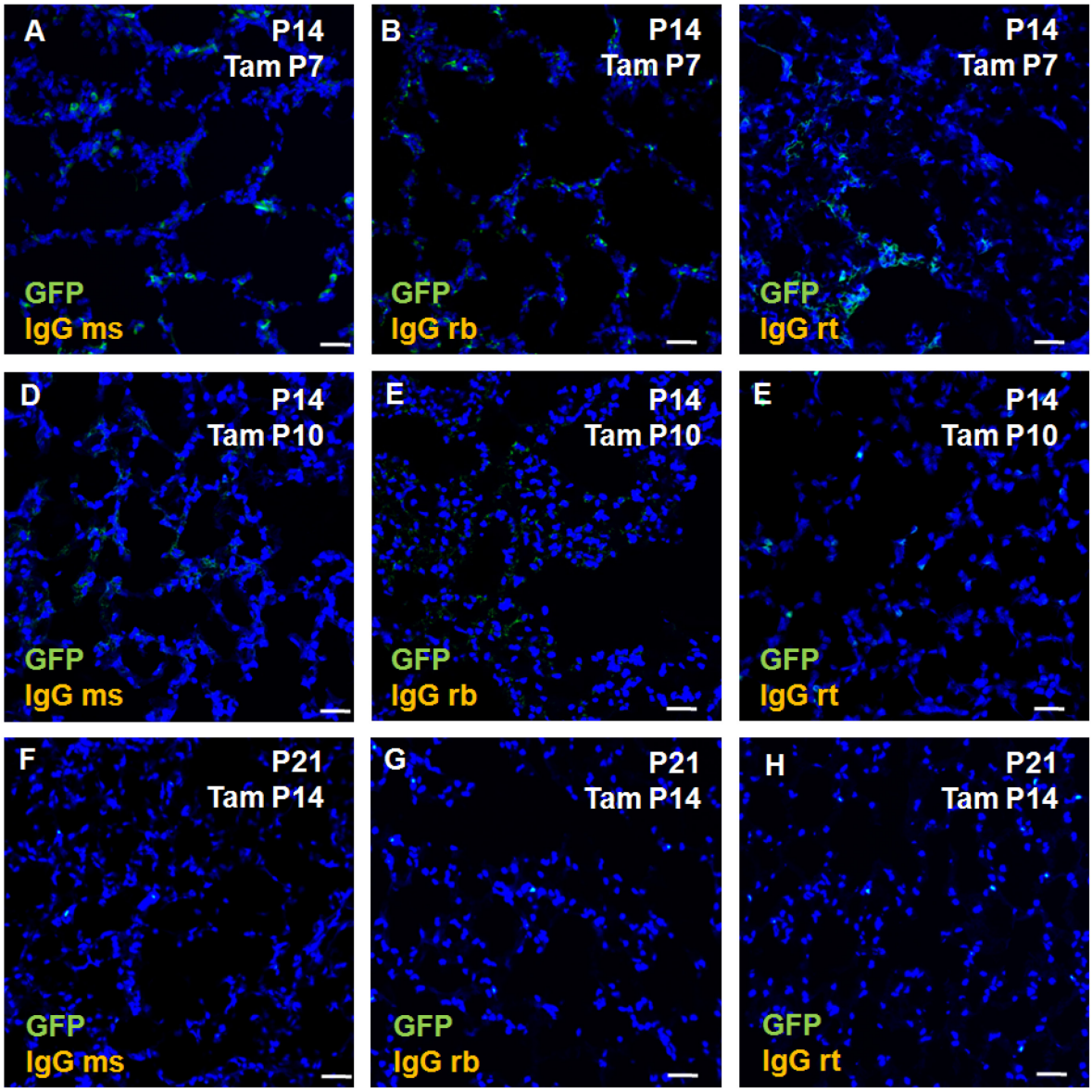

Figure 39 Isotype controls for Plin2$^{tm1.1(Cre/ERT2)Mort}$mTmG for lineage tracing at postnatal day 7, 10 and 14.

(A-F) Tissues of Plin2$^{tm1.1(Cre/ERT2)Mort}$mTmG mice was stained for IgG control antibody against mouse (ms), rabbit (rb), and, rat (rt) at postnatal day (P) 17, P10 and P14. Tissues were subsequently stained with A647 anti-mouse, A647 anti-rabbit, or A647 anti-rat (orange) antibodies. A 4', 6-diamidino-2-phenylindole dihydrochloride nuclear stain (blue) was used. Green fluorescent protein^{+} (GFP^{+}) cells (green) were detected at all tissues, marking adipose differentiation related protein (ADRP) expression but no signal was detected for the isotype staining. Scale bar = 50 µm.

7.4 Appendix IV: Figures

7.5 Appendix IV: Tables

Eidesstattliche Erklärung

Ich erkläre: Ich habe die vorgelegte Dissertation selbständig, ohne unerlaubte fremde Hilfe und nur mit den Hilfen angefertigt, die ich in der Dissertation angegeben habe. Alle Textstellen, die wörtlich oder sinngemäß aus veröffentlichten oder nicht veröffentlichten Schriften entnommen sind, und alle Angaben, die auf mündlichen Auskünften beruhen, sind als solche kenntlich gemacht. Bei den von mir durchgeführten und in der Dissertation erwähnten Untersuchungen habe ich die Grundsätze guter wissenschaftlicher Praxis, wie sie in der „Satzung der Justus-Liebig-Universität Gießen zur Sicherung guter wissenschaftlicher Praxis“ niedergelegt sind, eingehalten

Ort, Datum

Unterschrift

Acknowledgements

It was a bit more than three years ago when my doctoral studies started and besides the scientific insights that I gained, I had the chance to meet wonderful people who supported me all the way.

First I would like to thank Prof. Dr. med. Werner Seeger for giving me the opportunity to work on this project, to attend to the international graduate program Molecular Biology and Medicine of the Lung (MBML), and that for preventing any negative effects of some unfortunate events at the very beginning of my PhD studies.

In addition, I would like to thank Prof. Dr. Adriaan Dorresteijn for so kindly accepting to be the Director of my thesis.

It takes great effort to be a patient mentor and an inspiring supervisor and Dr. Rory Morty and Dr. Katrin Ahlbrecht managed to fulfill this role in the most admirable manner. I would like to thank them both for always standing by my side during my PhD training, for never losing their trust on me, and for leading me on transforming the stressful moments into productive work. They will be always two figures that I appreciate and look up to.

In addition I would like to thank my MBML tutors, Dr. Florian Veit, Dr. Dorothea Peters and Dr.Elie el Agha for supporting my educational training.

I would like to express my gratitude to all my lab colleagues for making every day joyful and also for sharing their knowledge and experience, the technical assistants and animal care takers, especially Diana, Kevin and Christina. I would like to thank Dr. Friederike Klein and Dr. Peter Rauschkolb for sharing with me their knowledge at the beginning of the project, as well as my senior lab members and MBML tutors Ivana, Tanya and Anita for teaching me about different techniques and also for the cheerful time at work.

Some of my colleagues though, managed to take a special place in my heart, and therefore I would like to thank Alberto, Claudio and Jordi for making our work place feel like home. Thank you Alberto, for making me understand that there is a calmer and wiser way of facing life. Thank you Claudio for being an exceptional colleague and for your friendship, I will cherish it the rest of my life. Thank you Jordi, for the breaks we shared under the sun and for all the bright and joy that you always brought with you at lab.

I would like to thank all my MBML classmates for being a group of marvelous people and the time we had together, during the academic program but also outside of it. Elsa, Ivonne, Luciana, David, Dijana, Despoina, Aleksandar, Irina, Paulina and Mira, I would like to thank you for your scientific help and mostly for your friendship, I will keep all our lovely memories always with me.

Last, but not least I would like to thank my family and particularly my brothers and my husband, for tolerating my absence all those years, for cheering me up during complicate times and for making every day beautiful.